Long-Term Atmospheric Measurement and Interpretation of Radiatively Active Trace Gases

October 2020 – September 2021

Annual Report

Alistair Manning[1], Simon O'Doherty[2], Dickon Young[3], Alison Redington[1], Daniel Say[2], Joseph Pitt[2], Tim Arnold[4,5], Chris Rennick[4], Matt Rigby[2], Adam Wisher[2], Angelina Wenger[2], and Peter Simmonds[6]

[1] *Met Office, Fitzroy Road, Exeter, EX1 3PB, United Kingdom*
[2] *Atmospheric Chemistry Research Group, University of Bristol, Cantock's Close, Bristol, BS8 1TS, United Kingdom*
[3] *Terra Modus Consultants Ltd, Bwthyn y Ffynnon, Cwmfelin Boeth, Whitland, SA34 0RS, United Kingdom*
[4] *National Physical Laboratory, Hampton Road, Teddington, TW11 0LW, United Kingdom*
[5] *School of GeoSciences, University of Edinburgh, Edinburgh, EH9 3FE, United Kingdom*
[6] *International Science Consultants, 39 Avon Castle Drive, Ringwood, BH24 2BB, United Kingdom*

February 17, 2022

Photo of Winnats Pass courtesy of @grantrichie/Unsplash

Contents

1 Executive Summary

The work described in this report has two key aims:

- Estimate the global trends in the atmospheric concentrations of all of the key greenhouse gases.
- Provide independent estimates of UK emissions of all non-CO_2 greenhouse gases through the use of atmospheric observations, and for these to be directly compared to the official UK inventory.

Below are the key findings for each of the groups of gases investigated, more comprehensive details are provided in the later chapters.

1.1 Key Results

- **Methane (CH_4)**
  CH_4 has an accelerating upward global background mole fraction, currently increasing by $\sim$ 16 ppb yr^{-1} (Figure 13b) in the Northern Hemisphere (NH). UK estimates of CH_4 in the GHGI and InTEM are in good agreement from 2012 (Figure 1a). Since 2012, the GHGI UK CH_4 estimate has declined by 1.95% per year, in the same period the InTEM estimate has declined by 2.08% per year, thus supporting the change in the inventory estimate (Lunt et al. 2021). However, InTEM shows little change in emissions from 1990-2012 whereas the GHGI has fallen by more than 50% since 1990 (Figure 14a).

- **Nitrous Oxide (N_2O)**
  UK InTEM estimates 2013-2019 are, on average, $\sim$ 20% higher than the GHGI (Figure 1b). The UK emissions have a very strong seasonal cycle (amplitude of $\sim$ 80 Gg). Peak emissions in May-Aug, minima in Jan-Feb (Figure 17 c&d). Improvements in the N_2O observation instrumentation in 2018 and 2019 has reduced the InTEM emission uncertainty.

- **Carbon Dioxide (CO_2)**
  Global CO_2 reached a level of 415.48 ppm in June 2021. Since 1992, the CO_2 global background mole fraction has increased at an average rate of $\sim$ 2 ppm yr^{-1}, but this rate has increased slightly since 2012.

- **Hydrofluorocarbons (HFCs)**
  An update to the GHGI HFC emission model in 2021 has led to a reduction in the reported UK emissions of HFCs across all years (Figure 1c). The InTEM HFC estimates are consistently lower than the GHGI 2008-2019. The least good agreement is in 2019 where the reported

total HFC is $\sim$ 12.5 Tg CO_2-eq yr^{-1} compared to the InTEM estimate of $\sim$ 8.0 Tg CO_2-eq yr^{-1}. The InTEM 1-year estimate for 2021 indicates an increase of $\sim$ 1.0 Tg CO_2-eq yr^{-1} compared with the 2020 value (provisional finding). UK emissions of HFCs comparing the GHGI with InTEM was published in August this year (Manning et al. 2021).

- **Perfluorocarbons (PFCs)**

  InTEM estimates are initially higher than the GHGI values (2005-2010) but in more recent years the total UK PFC estimates have compared well and are largely level (Figure 1d).

- **InTEM comparison with GHGI**

  Figure 2 shows the results of subtracting the GHGI from the InTEM emission estimates for the UK for each of the gas groups. It shows that InTEM is statistically similar to the GHGI for CH_4, PFC and SF_6, for HFCs the GHGI is statistically above InTEM and for N_2O the GHGI is statistically below InTEM. The combination of all gases for the GHGI and InTEM, Figure 2f, shows that overall the two estimates are statistically similar with 2019 showing the greatest difference.

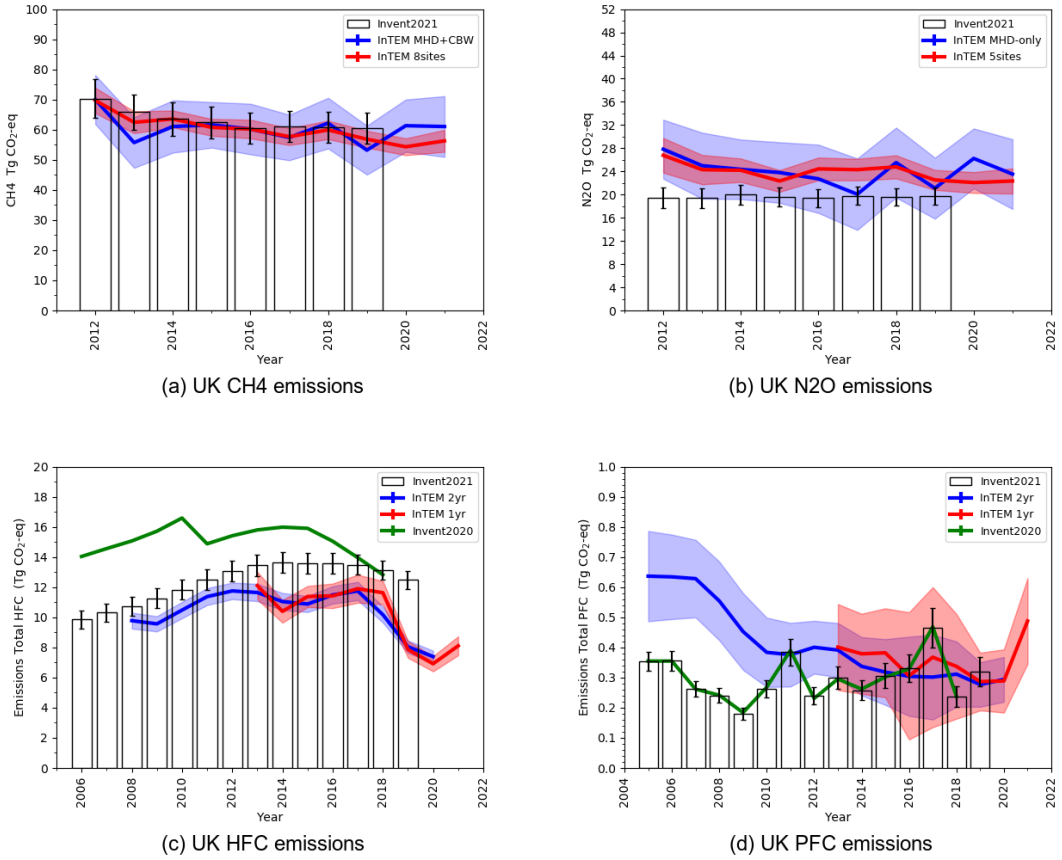

Figure 1: UK emission estimates (Tg CO_2-eq yr^{-1}) from the GHGI reported in 2021 (black) and InTEM (blue and red) (a) CH_4 (b) N_2O (c) Total HFC and (d) Total PFC. The uncertainty bars represent 1-σ. The green lines in (c) and (d) represent the GHGI reported in 2020. The blue InTEM lines represent estimates with fewer observation sites and/or longer inversion time windows.

- **Hydrofluoroolefins (HFOs) and Hydrochlorofluoroolefins (HCFOs)**

  HFOs and HCFOs are rapidly replacing hydrofluorocarbons as refrigerant gases due to their short atmospheric lifetimes and low global warming potentials (GWP). Atmospheric measurements of these gases at a number of AGAGE observation sites including Mace Head and Tacolneston show that emissions of these gases to the atmosphere are increasing (Figure 50) (Vollmer et al. 2015). Potential by-products of HFO degradation are of environmental concern, for example Trifluoroacetic acid (TFA) (Solomon et al. 2016; Behringer et al. 2021) and HFC-23 (Campbell et al. 2021).

- **Bilsdale tall tower observatory**

  There was a major fire at the Bilsdale telecommunications tower on 10^{th} August this year which caused extensive damage to the tower and infrastructure, rendering the structure out of service and leaving up to a million people without a TV or radio signal. North Yorkshire Fire and Rescue Service reported that eight pumps and crews had been sent to tackle the

blaze and firefighters said the fire included the tower itself. Access to the site was granted by on 27^{th} September, and all of the atmospheric measurement equipment was salvaged from the site and returned to the University of Bristol for testing. The tower was demolished through controlled demolition on 6^{th} October. It is proposed that the sampling equipment (housed in the University of Bristol mobile laboratory) be returned to a temporary mast at Bilsdale in March/April 2022.

The impact of losing BSD from the DECC network is shown in Figure 3. The spatial resolution of the CH_4 InTEM results from July 2021, with BSD observations, compared to September 2021, without BSD observations, is significantly reduced in the north of England.

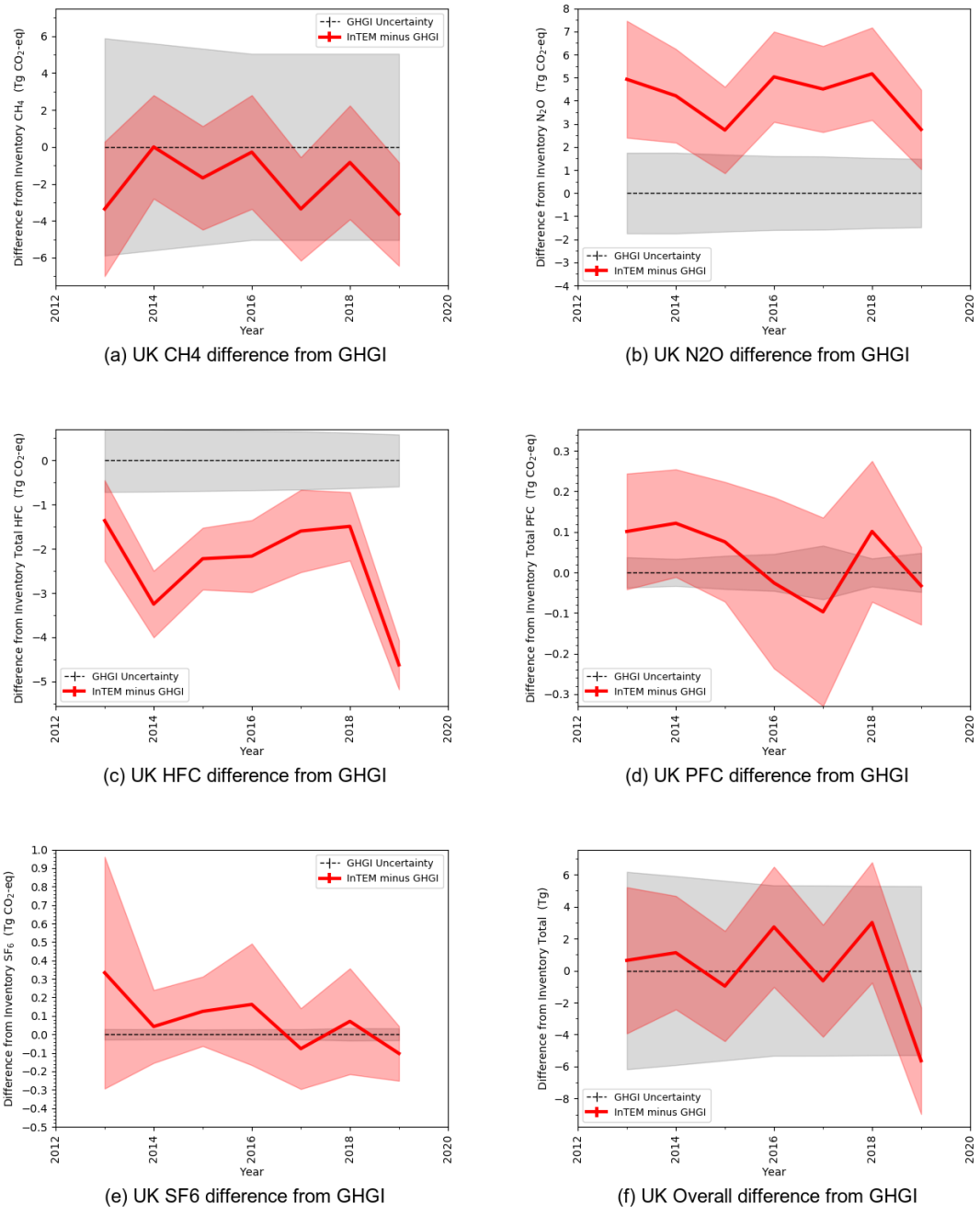

Figure 2: Difference between InTEM UK emission estimates and the 2021 GHGI 2013-2019 (Tg CO_2-eq yr^{-1}). GHGI uncertainty (grey) and InTEM minus GHGI estimates (red). Dashed black line marks the normalised GHGI data. (a) CH_4 (b) N_2O (c) Total HFC and (d) Total PFC (e) SF_6 (f) Summation of the difference of each reported GHG. The uncertainty bars represent 1-σ.

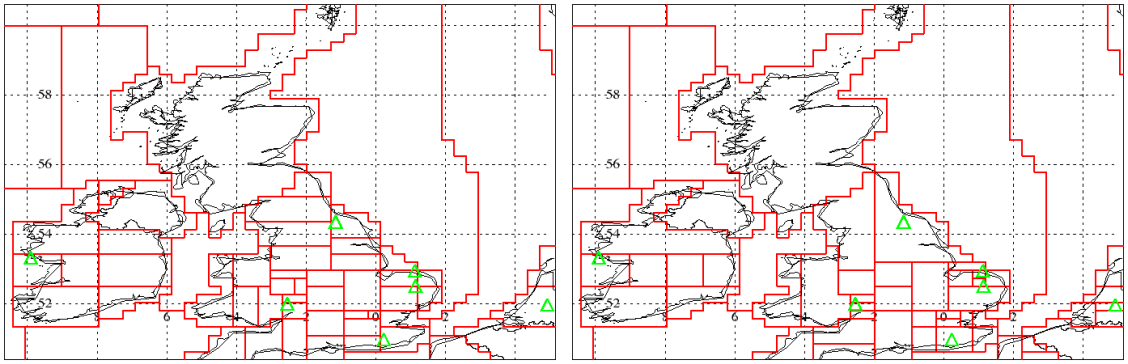

Figure 3: Spatial grid resolution achieved in InTEM with (July 2021) and without (September 2021) CH_4 observations from BSD. The green triangles show the locations of the network of observations available in 2021.

1.2 Significant Developments

- **Radon and Meteorology Observations**

  Radon instruments have been deployed to and are fully operational at four sites in the UK, and routine meteorological observations are now being made at two of the UK DECC stations. Both these developments will help improve InTEM model uncertainty quantification in future years.

- **CH_4 Isotope measurements**

  High-frequency CH_4 isotope measurements are now available from the Heathfield tower, these will help identify the different CH_4 emission source categories affecting the station.

- **Modelled Uncertainty**

  The uncertainty applied to each model time-period and observation within InTEM has been improved for those gases where the frequency and magnitude of pollution events are small.

- **UK HFC paper published**

  A scientific paper on the comparison between the InTEM and inventory estimates for UK HFCs has been published in the journal, Atmospheric Chemistry and Physics, Manning et al. 2021.

2 Introduction

Monitoring the atmospheric concentrations of gases is important for policy makers in assessing the impact of national and international policies related to the atmospheric environment. The effects of control measures on the principle greenhouse gases: carbon dioxide (CO_2), methane (CH_4), nitrous oxide (N_2O), hydrofluorocarbons (HFC), perfluorocarbons (PFC), nitrogen trifluoride (NF_3) and sulphur hexafluoride (SF_6), are now observable. Likewise, measures introduced under the Montreal Protocol to protect the stratospheric ozone layer are also being observed in the atmosphere.

This project has two principle aims:

- Estimate the background atmospheric mole fractions of the principle greenhouse and ozone-depleting gases from the UK and wider network of observations.
- Estimate the UK emissions of the principle greenhouse gases using the UK network of observations and compare these to the reported inventory.

Since 1987, high frequency, real time measurements of the principal halocarbons and radiatively active trace gases have been made as part of the Global Atmospheric Gases Experiment (GAGE) and Advanced Global Atmospheric Gases Experiment (AGAGE) at Mace Head, County Galway, Ireland. For much of the time, the Mace Head measurement station (MHD), which is situated on the Atlantic coast, monitors clean westerly air that has travelled across the North Atlantic Ocean. However, when the winds are easterly, MHD receives substantial regional scale pollution in air that has travelled from the populated and industrial regions of Europe. The site is therefore uniquely situated to record trace gas concentrations associated with both the Northern Hemisphere (NH) background levels and with the more polluted air arising from European emissions.

Building on the success of using the MHD observations in addressing the two principle aims of the project, the UK has developed a network of observation stations called the UK Deriving Emissions related to Climate Change (UK DECC) network. Along with MHD, it consists of four tall tower stations: Ridge Hill (RGL), Herefordshire; Tacolneston (TAC), Norfolk; Bilsdale (BSD), North Yorkshire (originally Angus (TTA), Angus, Scotland); and Heathfield (HFD), West Sussex. RGL became operational in February 2012 and TAC in July 2012. TTA began operating for the network in April 2012 but was decommissioned and replaced with BSD in September 2015 (BSD began operation in January 2014 under the NERC GAUGE programme). HFD began operation in November 2013 under the NERC GAUGE programme but became fully part of the network in September 2018. The expanded network makes it possible to resolve emissions on a higher resolution, both spatially and temporally, across the UK.

The UK DECC network measures, to very high precision, all of the principle greenhouse gases in the

inventory as well as many ozone-depleting gases. The Inversion Technique for Emission Modelling (InTEM) has been developed to use these observations to estimate both mid-latitude NH mole fraction trends and UK emissions of each gas. The atmospheric measurements and resulting emission estimates of greenhouse gases provide an important independent cross-check for the national GreenHouse Gas Inventory (GHGI) of emissions submitted annually to the United Nations Framework Convention on Climate Change (UNFCCC). The GHGI are estimated through in-country submissions of Activity Data and Emission Factors that are, in some cases, very uncertain. The comparisons between the GHGI and InTEM estimates enable BEIS to be more informed in their inventory improvement programme and is also considered good practice by the Intergovernmental Panel on Climate Change (IPCC).

The UK is one of only three countries worldwide (Switzerland and Australia are the others) that currently routinely verify their reported inventory emissions as part of their annual UNFCCC submission of emissions. The UK is the only country to do so for all of the principle GHG gases and has done so since 2003.

The report first describes the performance of the instrumentation over the last year and then shows the global trends in each of the gases. This is followed by a brief descrption of InTEM before an in-depth analysis of the InTEM results are compared to the GHGI for each gas in turn; CH_4, N_2O, HFCs, PFCs, SF_6 and finally NF_3. In addition, global trends and UK emission estimates of a whole range of other gases of relevance to climate change and/or stratospheric ozone-depletion are presented, e.g. CFCs, HCFCs, H_2, other bromine and chlorine containing gases and the newly emerging HFOs. The report concludes with a list of the recent publications produced by the group and acknowledgements. The nomenclature at the end describes the acronyms used in the report. The tables of UK and NWEU emissions for each of the reported GHG gases are presented in Appendix 1.

3 Instrument Performance

A brief summary of site operations is given below.

3.1 Mace Head

General: There have been a number of instrumental issues at Mace Head over the past 12-months. An increase in retention time variability on the Medusa, reported in the previous annual report remains unresolved despite efforts to pinpoint the cause. The variability impacts the data to a small degree, and efforts are ongoing to resolve this issue.

Medusa GCMS: It has been an eventful period for the Medusa with quite a number of issues. A routine update to the Mass Spectrometer acquisition parameters on 18^{th} Sept 2020 resulted in reduced precision for a number of species. Reducing the number of ions acquired, by eliminating ions of lesser importance, alleviated the issue but the root cause is unclear given that no major changes were implemented. Another ongoing minor issue was the generation of a range of communication alarms requiring the computer to be rebooted. It is not clear if this issue is hardware or software related. A blocked/broken Porabond-Q chromatographic column on 22^{nd} Dec 2020 resulted in a loss of $\sim$ 2 weeks of data. An old column was installed as a temporary replacement while awaiting delivery of a new one. The new column was installed on the 9^{th} Feb 2021. Further column problems presented with the GasPro column developing a leak and snapping during the process of finding the leak. Fortunately this occurred close to the column end and it was possible to cut and refit it quickly. The chromatographic retention time variability experienced by the Medusa remains unresolved despite efforts to pinpoint the cause. We have previously reported a number of actions taken, including replacing the Electronic Pneumatic Control (EPC) unit. During this reporting period, the EPC control board was replaced (1^{st} Jan 2021) by an Agilent engineer, and attempted to have the GC mainboard replaced (1^{st} July 2021). Unfortunately the replacement board came without firmware chips. Extracting chips from the existing mainboard risked breaking both the chips and the chip sockets and, on the advice of the Agilent engineer, a decision was made to not attempt the board replacement. There have been a number of instances of baseplate temperature variability which were resolved by conditioning the Cryotiger refrigeration system; however the baseplate temperature is $\sim$ 2°C higher than previously. The filter in the refrigerant line will be replaced as part of the cooling system annual service in February 2022. If the Cryotiger is coming close to end of it's working life, a decision will be made to replace the unit or install a new Stirling cooler system, similar to those deployed successfully at a number of other AGAGE sites. A new electron multiplier was installed on 21^{st} April 2021. A full set of replacement batteries were installed in the Falcon UPS (Uninterruptible Power Supply) on 6^{th} Sept 2021 due to issues

with UPS shutdowns when power to the site was interrupted.

GCMD: This instrument operated exceptionally well over the past 12-months. All periods of data loss were associated with routine maintenance of the sampling equipment.

Intercomparisons: We continue to cooperate with other groups carrying out in situ real-time tropospheric measurements as well as flask samples in order to produce a harmonised regional and global data set for use by theoreticians. Toward this end, we are currently working with a number of groups to develop best estimates of the differences in absolute calibrations and field site calibrations between them and AGAGE-SIO. Two examples of such collaborations are illustrated below:

- **NOAA/GMD:** This is done by inter-comparisons involving exchanges of tanks (checking absolute calibration), comparisons of hemispheric and global mean trends estimated by the two networks, and examination of differences between the AGAGE and GMD in situ instruments and flask samples at our common sites. To help ensure progress on this and other cooperative endeavours, members of the relevant GMD group (J. Butler, S. Montzka, B. Hall and G. Dutton) regularly attend the semi-annual AGAGE meetings and other joint meetings with GMD personnel are, and will be, held from time to time. An example comparison between AGAGE and NOAA data for CH_4 is shown in Figure 4. Where an excellent agreement between the two networks is demonstrated.

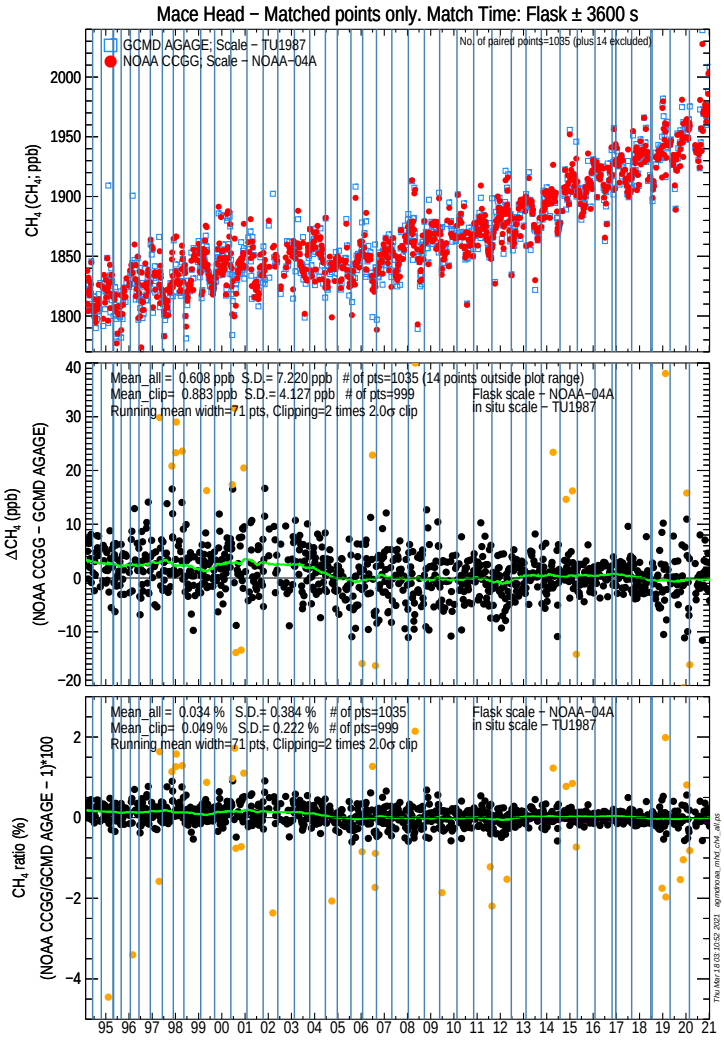

Figure 4: Comparison of CH_4 at Mace Head using NOAA/GMD flask sample compared against the time matched in situ Medusa data. The top plot represents the data matched to within 3 hours, the middle plot is the absolute difference and the lower plot the % difference.

- **WMO/GAW Audit:** Mace Head undergoes a regular 'system and performance' audit by the World Calibration Centre-Empa in agreement with the WMO/GAW quality assurance system (GAW Report No. 258, WCC-Empa Report No. 18/2, 2020). An example bias plot for CH_4 is shown in Figure 5. Mace Head has a dual status of a WMO/GAW research and monitoring 'global' station and an EMEP supersite. At the end of each assessment period a report is produced that summarises the assessment of the Mace Head GAW station, in general, as well as the surface CH_4, CO_2, N_2O, CO and O_3 in particular. This report is distributed to all involved institutes, the Irish GAW Country Contact and the World Meteorological Organization in Geneva. Mace Head was audited in 1996, 1998, 2002, 2005, 2009 and 2018.

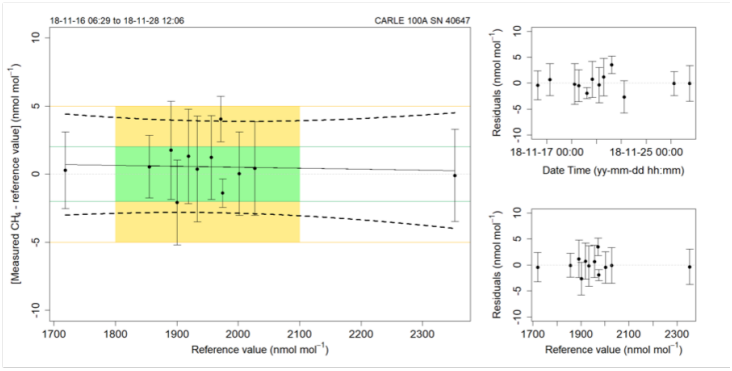

Figure 5: Left: Bias of the CARLE GC/FID instrument with respect to the WMO-X2004A CH_4 reference scale as a function of mole fraction. Each point represents the average of data at a given level from a specific run. The error bars show the standard deviation of individual measurement points. The green and yellow lines correspond to the WMO compatibility and extended compatibility goals, and the green and yellow areas to the mole fraction range relevant for MHD. The dashed lines around the regression lines are the Working-Hotelling 95% confidence bands. Right: Regression residuals (time dependence and mole fraction dependence).

3.2 Tacolneston

General: Routine line pump diaphragm and filter changes took place at regular intervals during the past year. A power cut occurred on 11^{th} March resulting in data outages for all instruments of around a day or less. All three inlet line water traps were replaced on 15^{th} April. The mobile lab (that previously housed the instruments before they were relocated to their current permanent location) was removed from site on 10^{th} June. The sonic anemometers were also realigned on this day, with their previous alignment noted to allow data to be post-corrected. The tower was repainted over a period of 6 weeks beginning on 15^{th} June. Round-robin intercomparison cylinders were analysed on the LGR and Picarro (CRDS) analysers in late June and early July.

LGR: The MD1 pump diaphragm was replaced on 27^{th} October, and the pump was serviced again on 8^{th} December. On 19^{th} January the working standard cylinder was replaced. Three days of data were lost in January due to a software error. The instrument was rebooted on 31^{st} August to address poor stability in the N_2O measurement. Ongoing issues with the stability of cylinder measurements continue to have a small impact on the accuracy of the CO measurements. The prolonged line-conditioning times required for CO measurements necessitate that the LGR instrument measurements of the working standard are preceded by Picarro G2301 measurements of the same standard. As the LGR requires standard measurements twice per day, the frequency of Picarro standard measurements was adjusted to match this in February. This results in increased consumption of standard gas, requiring the standard to be replaced on a frequent basis. The working standard transfer line was replaced on 9^{th} February, and the working standard regulator

was replaced on 2^{nd} March, but no change in gas behaviour was observed. Improving the stability of CO cylinder measurements is an issue that is currently under further investigation.

CRDS (G2301): The 7 micron filters on all inlets were replaced on 13^{th} October 2020 and the 2 micron inlet filter was replaced on 20^{th} October. The MD1 pump was swapped with the Medusa MD1 on 20^{th} October, and this newly installed pump was serviced (including diaphragm replacement) on 8^{th} December. On 19^{th} January the working standard cylinder was replaced. In February around a week of data was lost when the instrument internal computer crashed. On 16^{th} February the working standard measurement frequency was updated to twice per day (see LGR subsection above). In early March several days of data were lost as time synchronisation issues caused repeated software failure. This was resolved remotely by Picarro support. Droplet tests to determine measurement sensitivity to the presence of water vapour in the sample were conducted on 12^{th} and 13^{th} April. Two days data were lost in June due to a software crash.

Medusa GCMS: The Medusa GCMS has performed reasonably well over the reporting period. Sporadic 'steps' in the chromatography, observed throughout the previous reporting period, were resolved with software updates by Jan 2021. Occasional, large retention time shifts for all compounds, observed throughout Apr-Dec 2020, were also resolved by the same update. Beginning on 11^{th} August 2020, two days of data were lost whilst the Cryotiger refrigeration unit was serviced and refilled with coolant. Starting on 1^{st} September, a total of 11 days of data were lost due to failed filaments. On the 3^{rd} December, 8 days of data were lost due to helium supply issues. A further 15 days of data were lost from the 9^{th} March 2021. This was attributed to a power cut on the 11^{th} March and the resultant failure of the TOC unit alongside issues with the Cryotiger unit. Beginning on the 13^{th} April, 7 days of data were lost due to further refilling of coolant in the Cryotiger unit and replacement of the tertiary standard. From the 1^{st} May, 11 days of data were lost due to failure of the EL-160 ethernet-serial converter power supply. A new El-160 and power supply were installed on the 11^{th} May. On 29^{th} May, 1 day of data was lost and from the 18^{th} July, 4 days of data were lost due to filament failures.

3.3 Ridge Hill

General: The sonic anemometers were realigned on 10^{th} December (after noting the previous offsets, so that past wind direction data can be corrected accordingly). The line pumps on the 45 m line failed twice (in January and May), while the 90 m line pump failed once (in July), resulting in short periods ($\sim$ 1 week) of sampling from a single inlet height. A power cut on 28^{th} April led to a single day of data loss due to a malfunctioning uninterruptible power supply. Round-robin intercomparison tanks were analysed on both the Picarro G2301 and the GC-ECD in late May and early June. On 9^{th} July an air conditioning unit was installed at the site to improve the stability of

temperature inside the instrument cabin. A new working standard cylinder was installed on 17^{th} June

CRDS (G2301 and G2401): On 15^{th} October 2020 a Picarro G2401, provided on loan by the ICOS Atmospheric Thematic Centre (ATC), was installed at the site. This instrument was provided to maintain measurement coverage while the regular Ridge Hill Picarro (G2301) was sent to the ICOS ATC for testing (instrument removed on 10^{th} November 2020 after an intercomparison period). The calibration cylinders, which had been sent for re-certification on the WMO scale by the ICOS Central Analytical Laboratory (CAL) in Jena, were returned to site and reinstalled on 2^{nd} November 2020. On 24^{th} February the regular Ridge Hill Picarro (G2301) was reinstalled at the site, and two calibration cylinders were replaced. The loan G2401 Picarro was removed on 8^{th} March. Four days of data were lost in April due to an issue with the instrument hard drive. On 26^{th} August the ICOS shelter test was performed to ensure the compatibility and leak-tightness of the air intake system within the instrument cabin.

GC-ECD: Instrument performance during 2020 was generally good for both N_2O and SF_6. However, in 2021 there have been periods of reduced precision for the N_2O measurement; specifically from the beginning of January to the end of March, and from late July onwards. This reduced precision appears to be associated with instability in both the baseline of the chromatogram and the peak height and area for both species. It is manifested in increased noise on the standard cylinder measurements for N_2O, although it does not appear to adversely impact the measurement of SF_6. The cause of this issue is currently under investigation.

3.4 Bilsdale

General: The Bilsdale site has been out of operation since a large fire occurred on 10^{th} August 2021, causing structural damage to the mast. Electrical power to the site was cut at this time and a 300 m exclusion zone was put in place surrounding the mast. Instrumentation and associated calibration equipment was removed from the site on 27^{th} September. The tower at Bilsdale was demolished through a controlled demolition on 6^{th} October (https://www.itv.com/news/tyne-tees/2021-10-06/314m-fire-damaged-bilsdale-mast-demolished-and-dismantled). Laboratory tests at the University of Bristol confirmed that there was no lasting damage to the optical equipment, and it is proposed to return these instruments to a temporary tower at Bilsdale in March/April 2022.

Prior to the fire, there were few issues at this site. The 108 m line pump failed on 2^{nd} March, and was replaced on the 29^{th} March (in the intervening period only two inlet heights were sampled). Round-robin intercomparison cylinders were analysed on all instruments in June. On 26^{th} July discussions with riggers working on the mast revealed that the 108 m inlet cup had been removed

some time ago; it is not clear why this was done. Some increase in the amount of water entering the line had been observed, but it was being effectively captured by the water trap located at the base of the mast prior to reaching the instruments. All water traps and 40 micron inlet filters were also replaced on 26^{th} July.

CRDS (G2401): In general instrument performance was good and there are no other specific issues to report.

CRDS (G5310): Droplet tests to determine measurement sensitivity to the presence of water vapour in the sample were conducted on 16^{th} and 17^{th} November 2020. In November 2020 buildup of mould in the liquid coolant lines led to instability in the laser temperature and the loss of data for one week. In January 2021 a coolant with mould inhibiting qualities was substituted for the original coolant. The issues associated with the delivery of CO calibration gas described in the Tacolneston site report were also present at Bilsdale. Otherwise there were no major instrument issues to report.

GC-ECD: This instrument has performed well since the last report until the fire; the only issues affecting the measurements are described in the general subsection above.

3.5 Heathfield

General: New aspirated lines were installed at the 100 m level in April 2021 for sampling by an oxygen instrument, maintained by the University of East Anglia. The measurements from this instrument are of potential use for understanding fossil fuel CO_2 emissions. An automated bag sampler has been installed by the Royal Holloway University of London for collection of air samples for off-line methane isotope ratio analysis in their laboratory. These instruments have been installed as part of NPL's involvement in the DARE-UK collaboration. The NPL preconcentrator (Boreas) was installed in May 2021 for measurement of methane isotope ratios in air sampled from the 100 m inlet. Preliminary results from this instrument are described in section 4.5. There was a failure of the main data collection PC at the end of October 2020, which stopped data collection for 7 days. This was fixed by a complete re-installation of the operating system and GCWerks with all original data were restored.

The connections to the tubing from the 100 m inlet were re-plumbed in early November 2020. The Picarro G2401, G5310 and GC-ECD instruments now sample upstream of the new instruments – thus minimising the chance of lab-air contamination arising from issues with the new instruments. The line pump for the 50 m inlet was replaced following a failure in March 2021; now both lines are pumped by the higher flow rate pumps. The 40 micron filter were replaced on both lines in April 2021. The air conditioning installed in 2020 has helped stabilised the laboratory air temperature

and the instruments were able to continue running during warm outdoor temperatures. A new air conditioning system has been installed in the second laboratory, which contains the radon and oxygen instruments.

CRDS (G2401): This instrument has performed well over the last year. The depleted calibration standard replaced in July 2020 (H-358) has been re-analysed by the WMO World Calibration Centre at EMPA, Switzerland. The calibration values have been updated with the mean of the start and end measurements which results in a negligible change in amount fraction for CH_4, CO_2 and N_2O, and a 2.3% increase in the calibration value for CO due to the known drift of this gas during storage in cylinders. The span standards used to determine instrument non-linearity were also re-calibrated; the change to this correction for methane and carbon dioxide was negligible.

CRDS (G5310): This instrument has performed well over the last year. The G5310 is calibrated with the same standard gas as the G2401, so calibration values were also updated with a negligible change in reported amount fraction.

GC-ECD: The performance of this instrument has improved significantly this year following maintenance and cleaning of the valve rotor which has increased the precision from 1 ppb to 0.2 ppb. There was an unexpected period of data loss of 20 days in August 2021 was no flow was recorded by the sample flow controller. This problem was traced to a disconnected pressure sensor in the sample module, which was reconnected and sampling resumed.

4 Improvements, equipment and future potential

4.1 ICOS

The Integrated Carbon Observation System (ICOS) is a research infrastructure that combines three European monitoring networks: measurements of atmospheric composition, measurements of fluxes between the land and the atmosphere, and measurements of fluxes between the ocean and the atmosphere. The Ridge Hill measurement site is currently undergoing the ICOS step 2 labelling process, described in detail by Yver-Kwok et al. (2021), which will enable it to join the ICOS atmospheric measurement network. This part of the labelling process ensures that both measurement and data QA/QC procedures for the site are in alignment with those at other sites across the ICOS network. Once such compatibility has been demonstrated, Ridge Hill can apply to the ICOS general assembly to be recognised as an official ICOS measurement site (step 3 labelling).

Many of the general requirements of the step 2 labelling process were already met by the current measurement infrastructure at Ridge Hill. Additional requirements have included certification of calibration cylinder mole fractions at the ICOS-Central Analytical Laboratories (ICOS-CAL), sending the Ridge Hill Picarro to the ICOS Atmospheric Thematic Center (ATC) for testing, and performing the shelter test as described by Yver-Kwok et al. (2021). Additional sensors will be installed to log the line flow rate and the Picarro flow rate (as required by ICOS specifications). A new long-term target gas will also be installed to ensure continuity in the quality control over a period spanning more than ten years.

Data is now routinely transferred to the central ICOS ATC server, and manual QA/QC is performed on the data weekly, in accordance with ICOS requirements. The site is on track to complete the labelling process at the May 2022 ICOS general assembly meeting.

4.2 Urban monitoring in London

Several projects are aiming to complement the UK-wide DECC network measurements by providing denser coverage of greenhouse gas sensors in London. The LondonGHG project is a pilot scheme that uses a mixture of gold-standard (Picarro) and lower-cost (Licor) instruments at a small number of elevated locations throughout the city. The project will end in September 2022. Measurements are also available from the National Physical Laboratory (NPL, Teddington) and the BT Tower (run by the Centre for Ecology and Hydrology). Through the National Centre for Earth Observation Field Spectroscopy Facility (NCEO FSF), sun-following Fourier transform infrared spectrometer column measurements have been installed at three sites (Bruker EM-27). Instruments have been running for varying lengths of time, with most being established in 2020 or 2021. Continuation of

the measurements beyond 2021 is likely to be on a best-efforts basis.

The following measurement sites were operational in September 2021:

- Thames Barrier (E. London): LondonGHG Picarro and Licor CO_2 and CH_4 observations
- University of Westminster, Harrow campus (N.W. London): LondonGHG Licor CO_2 and CH_4
- St Mary's church, Ealing (W. London): LondonGHG Licor CO_2 and CH_4
- St. Jude on the Hill, Hampsted (N. London): LondonGHG Licor CO_2 and CH_4
- Highfield tower, Romford (N. E. London): LondonGHG Licor CO_2 and CH_4, FSF EM-27 CO_2 and CH_4 column
- BT Tower (Central London): CEH CO_2 and CH_4
- National Physical Laboratory (S. W. London): NPL Picarro CO_2 and CH_4, FSF EM-27 CO_2 and CH_4 column
- University College London, Torrington Place (central London): FSF EM-27 CO_2 and CH_4 column
- Woodgreen Farm: (North of London, outside M25): LondonGHG CO_2 and CH_4.

A preliminary analysis of performance at the Thames Barrier site for NAME and the Cambridge Environmental Research Consultants (CERC) ADMS model was presented in Hoare et al. 2020. It was found that the models were able to simulate the major features in the CH_4 observations at the site. Further work will use these models to derive inverse estimates of CH_4 emissions in London from the LondonGHG, NPL and CEH data.

4.3 Radon network

Radon gas (^{222}Rn) is a decay product of Uranium (^{238}U) and has a half life of 3.82 days. Small amounts of Uranium and its decay products are naturally occurring in all soils. This means all landmasses continuously emit some amount of Radon gas. Radon emissions from the ocean are much smaller than from land, so are often considered negligible. This makes Radon uniquely suitable as a tracer of how much recent contact a parcel of air had with the ground, an example of this is shown in Figure 6. We can exploit that property in multiple ways: For example to validate atmospheric transport models or to help define regional background concentrations of greenhouse gases. There are now 4 sites in the UK measuring, to high accuracy, atmospheric radon concentrations:

- Weybourne, on the coast of North Norfolk, an ICOS site, run by the University of East Anglia, the radon instrument has been operational since 2018, with an inlet height of 11m above ground level (a.g.l).
- Heathfield, part of DECC network, run by the National Physical Laboratory, measures Radon since 2020 with an inlet height of 100m a.g.l.

- Tacolneston, part of the DECC network, run by the University of Bristol, Radon observations started in 2020 from an inlet height 175m a.g.l.
- Ridge Hill, both a DECC network and ICOS site, run by the University of Bristol, Radon measurements started in 2020 from an inlet height of 85m a.g.l.

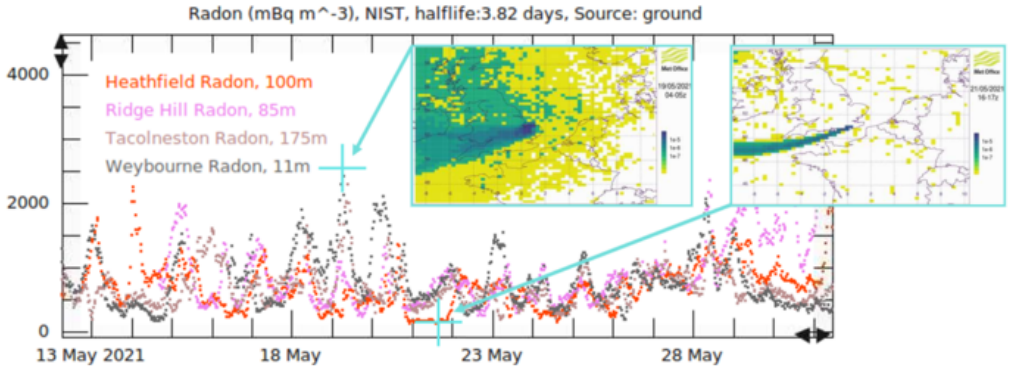

Figure 6: Comparison of Radon observation at all UK sites. The first blue cross on the 19.05.2021 is an example of high Radon because the air mass observed was in contact with a lot of land. The second cross on the 21.05.2021 show a period of time where in Heathfield the air mass observed passed mostly over the ocean which leads to a low radon concentration.

The Tacolneston, Heathfield and Ridge Hill Radon instruments were funded by a NERC capital infrastructure fund. All four sites are taking part in the NERC funded DARE-UK project, aiming to improve national and regional emission estimates. For this we are developing a novel method that combines radon measurements and high-resolution Lagrangian particle dispersion model output to enhance the methods for regional GHG emission estimates. This analysis firstly seeks to identify the bias introduced by errors in meteorology, which are reflected in the atmospheric transport model, and then suggests under which meteorological conditions the inversion models should take special care for deriving emission maps. In order to make the best possible use of the Radon and be confident in judgement calls on whether the transport model used is doing a good job, it is imperative that the Radon data is well calibrated and that the radon emission map used for the modelling comparison is as accurate as possible. As part of the DARE-UK project we have developed a standardised procedure for the radon data-set, which is applicable to any similar radon monitoring station. The process involves calibration of the instrument, deconvolution of data, through to analysis using the high-resolution atmospheric transport model output that accounts for the half-life of radon and a full budget of uncertainties. Performing a deconvolution routine on the radon measurements is an important step when comparing radon with data from other instruments on site. This is because the ANSTO radon detector has a slow temporal response compared to GHG instruments which are fast-response instrument, which introduces an apparent shift to the timestamp of each measurement.

We also joined up with an international consortium in the traceRadon project. TraceRadon aims

to facilitate inter-calibration within the radon community by developing mobile calibration systems and improve existing calibration strategies. One of the main project aims of traceRadon is to create a new spatio-temporal variable Radon emission map. The outcome of this project will provide direct feedback to improve both the Radon observations and the use of Radon in evaluating the performance of the atmospheric transport model.

4.4 Routine observations of meteorology

Continuous meteorological measurements have been added to the UK DECC Network. The measurements started at Ridge Hill and Tacolneston in July 2020. At Ridge Hill, these measurements consist of two sonic anemometers (both at 85 m sampling height), three temperature and relative humidity probes (53 m, 63 m and 85 m sampling heights) and two barometric pressure sensors (85 m sampling height and 1 m height within the ground instrumentation cabin). At Tacolneston, these measurements consist of two sonic anemometers (both at 150 m sampling height), four temperature and relative humidity probes (51 m, 70 m, 150 m and 175 m sampling heights) and two barometric pressure sensors (150 m sampling height and at 1 m height within the ground instrumentation room)

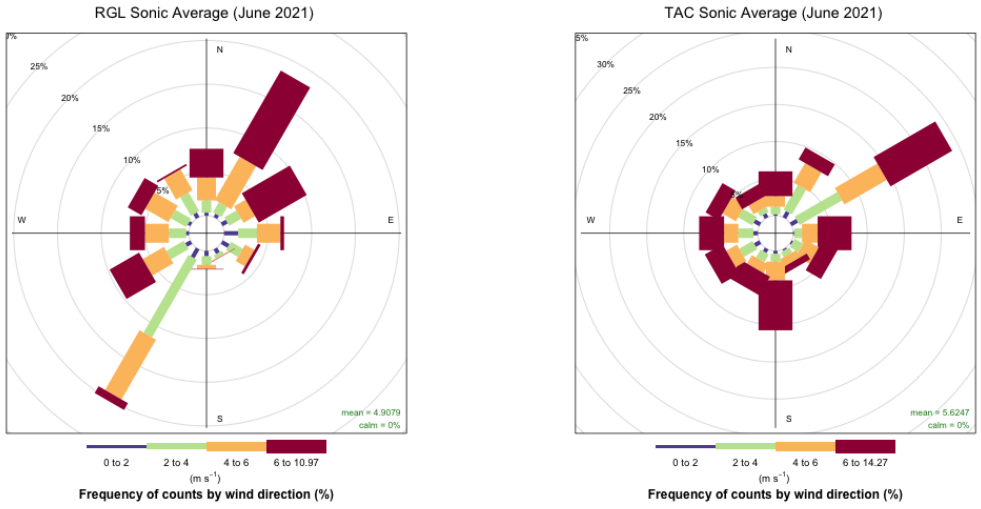

(a) Ridgehill **(b)** Tacolneston

Figure 7: Windrose plots for June 2021.

The information provided by these meteorological measurements will help to better determine the atmospheric stability, supplementing the information already provided through comparison of trace gas observations across the multiple inlet heights. Comparison of these meteorological measurements to their modelled values will be used to identify and remove modelled periods when the modelled meteorology is clearly poor. With the remaining good data, they can be used to quantify the uncertainty attached to each modelled time period and hence improve the quantification

of transport model error within InTEM.

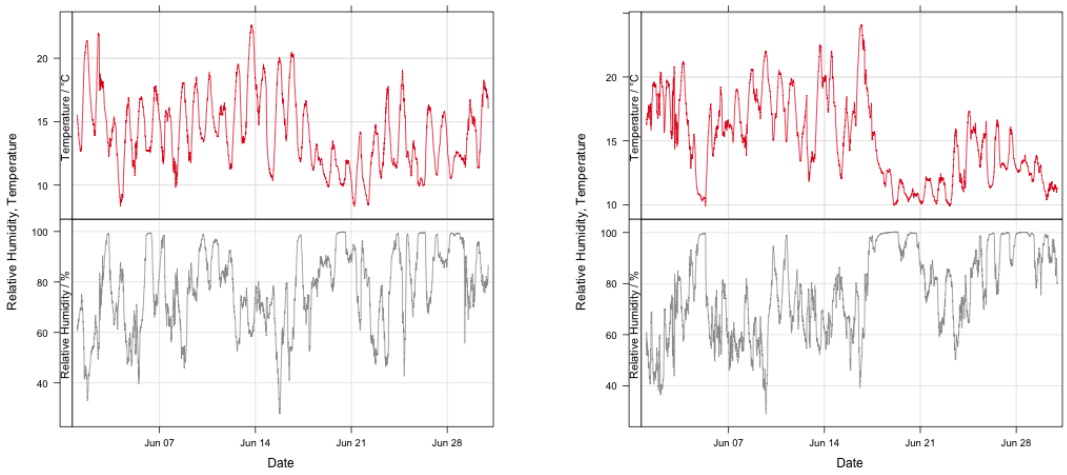

(a) Ridgehill **(b)** Tacolneston

Figure 8: Relative humidity and temperature plots for June 2021.

4.5 Methane stable isotopologues

Methane (CH_4) has several stable isotopologues formed by substituting either the carbon (C) or hydrogen (H) atoms for one of its isotopes. The most common isotopologue is $^{12}CH_4$, comprising around 98.8% of naturally-occurring methane, then $^{13}CH_4$ and $^{12}CH_3D$ form around 1% and 0.06% respectively. The specific proportion in a sample is typically reported as a ratio of the amount of minor to major isotopologue, relative to a standard: $\delta^{13}C = ({}^{13}r/{}^{13}r_{\text{ref}} - 1) \times 1000‰$ and $\delta D = ({}^{2}r/{}^{2}r_{\text{ref}} - 1) \times 1000‰$, where ${}^{13}r = n({}^{13}CH_4)/n({}^{12}CH_4)$ and ${}^{2}r = n({}^{12}CH_3D)/n({}^{12}CH_4)$ are the measured ratios, and ${}^{2}r_{\text{ref}}$ and ${}^{13}r_{\text{ref}}$ are the same ratios for the reference standard. While these three isotopologues are chemically nearly identical, the relative proportion of each depends on the methane formation process, so measurement of $\delta^{13}C$ and δD can provide information for emission source attribution. For example microbial sources, produce methane depleted in $^{13}CH_4$, so that $\delta^{13}C$ is lower for an agricultural source than for a fossil fuel emission source.

A new instrument, named Boreas, has been constructed at NPL that preconcentrates methane from an ambient air sample for analysis by an infrared laser spectrometer. This gives a simultaneous measurement of $\delta^{13}C$, δD, and methane amount fraction with very low uncertainty once every hour. Figure 9 shows a short time series of these measurements for air from the 100 m inlet at Heathfield in the green points. The blue points are measurements of a reference standard cylinder of compressed air filled at Mace Head, which is used to verify instrument performance from the rolling standard deviation of 4 measurements. This precision is shown as the error bars on the green air points. There were a series of pollution events on the 27^{th} June where the isotope ratio

decrease significantly from the baseline value. Analysis of these events indicates the likely source to be microbial-derived methane.

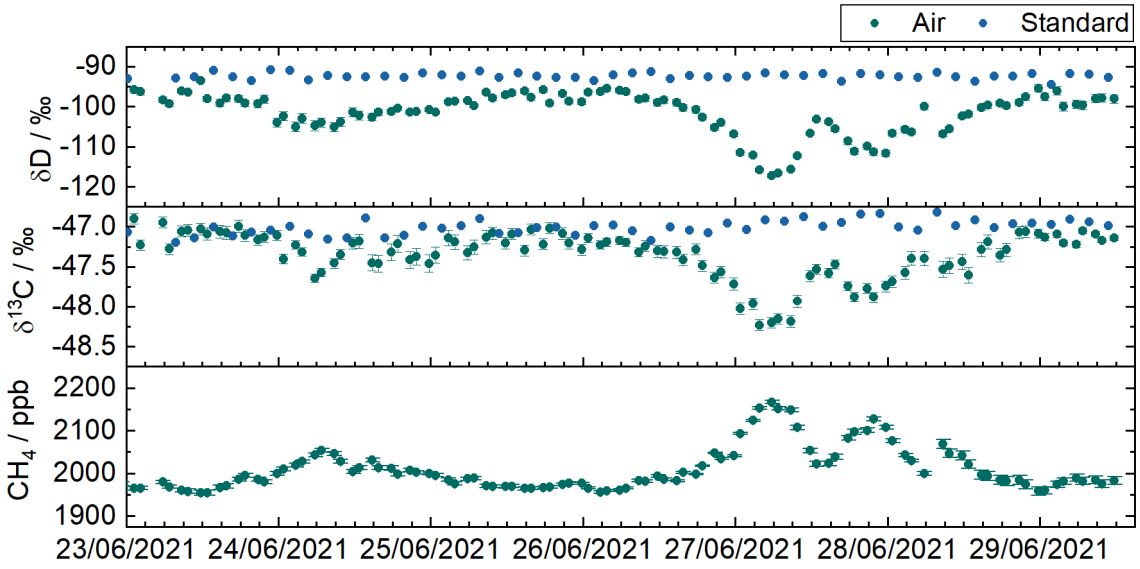

Figure 9: Timeseries of methane isotope ratio δD (top), δ^{13}C (middle) and amount fraction (bottom) measured from the 100 m inlet at Heathfield. Atmospheric measurements are shown in green, reference standard measurements are in blue. The uncertainty is calculated from the rolling standard deviation of four standard measurements and shown as the error bars on the air points.

4.6 Round-robin verification for instrument performance

A round-robin comparison has been in progress during 2021 to evaluate the relative performance of the instruments at each site using a set of cylinders containing natural air spiked with varying levels of CO_2, CH_4, CO and N_2O. SF_6 is also present in these cylinders, but not spiked so cover a much smaller range relative to the pollution events. The air in each cylinder is measured, relative to the local standard and instrumental non-linearity correction, and the measured amount fraction of each species and its standard deviation reported for a set of 5 repeats. The goal within the DECC network is to verify instrument performance and identify any biases between sites or within the network. Currently, the tanks have been analysed at Heathfield, Ridge Hill, Tacolneston and Bilsdale and will be analysed at the other sites. The data presented here are preliminary and give the as-reported values for each species. When the measurements for all sites are complete, the results will be used to identify site-specific issues in calibration and linearity.

The instruments and sites are compared using the method described for verification of the WMO GAW network in Zellweger et al. (2016, 2019). The reported measurements are fitted against the known values for each tank using linear regression. The bias is calculated at the centre of the range defined by the WMO as representative of unpolluted baseline conditions. This bias and

the regression gradient are plotted in figure 10, giving one point for each site or instrument. The shaded diamonds in the figure show the combinations of bias and gradient that satisfy the WMO network compatibility goal for background sites in the dark shading and extended compatibility goal (relevant for sites with higher pollution events) in the lighter shading (WMO 2020). N_2O is measured on both GC-MD and CRDS instruments, with the GC-MD calibrated using standards on the SIO scale. The GC-MD results are reported here on the WMO scale by subtracting 0.44 ppb before plotting. The CRDS instruments measuring CO_2, CO and CH_4 show performance within the extended compatibility goal for all sites and within the more stringent goal for certain instruments. The GC-MD instruments measuring N_2O and SF_6 show more variation in the bias and gradient, and there is an indication of a systematic under-reporting of CH_4 and N_2O, which will be investigated when all site results have been collected.

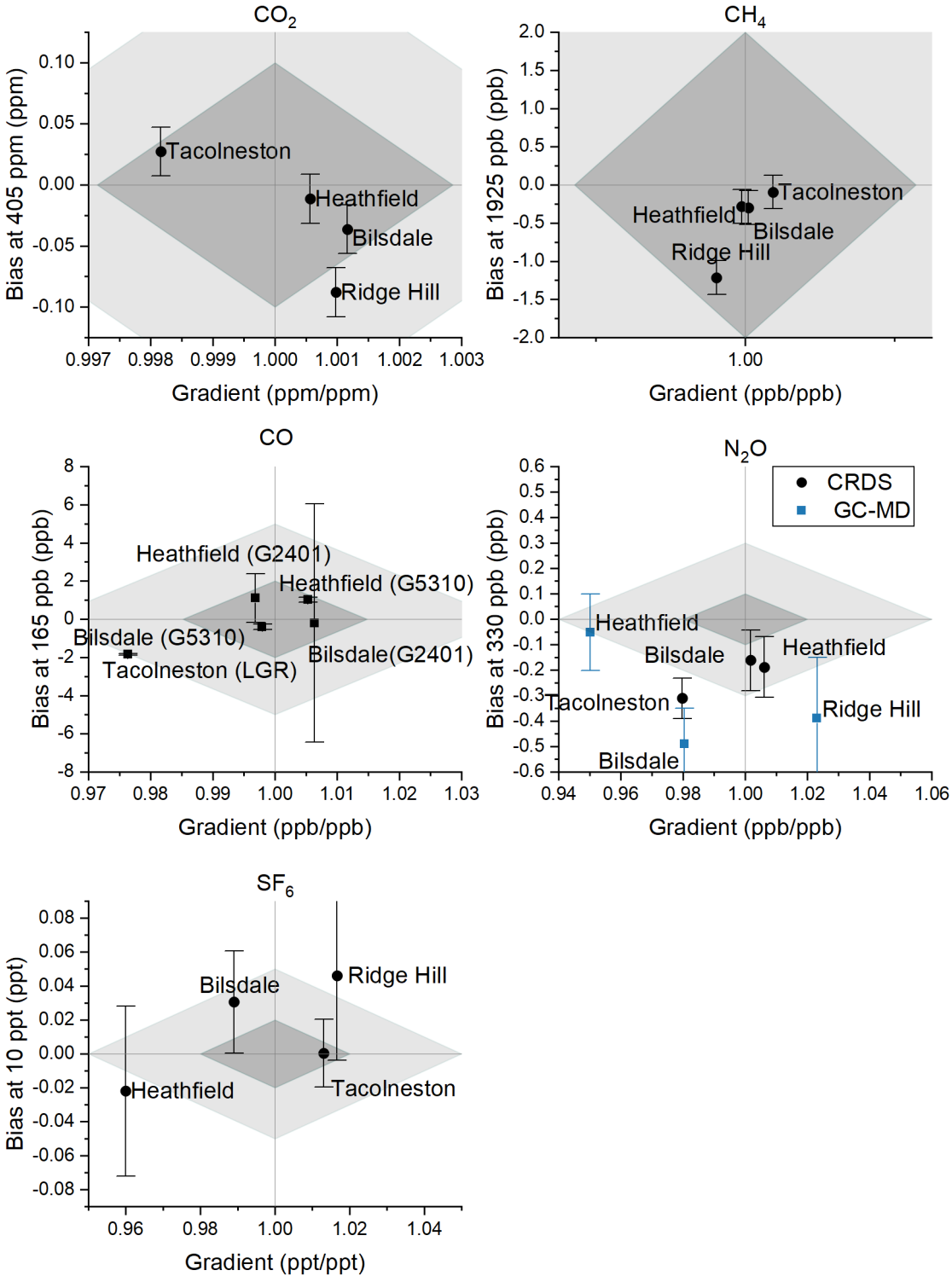

Figure 10: Bias at baseline amount fraction and the gradient from linear regression measured and known values for the set of round-robin standards measured at each site. The error bars represent the repeatability, calculated as the standard deviation of repeated measurements. The shaded areas are the WMO network compatibility goals for well-mixed background air (dark shading) and extended compatibility goal (light shading).

4.7 New technology for hydrogen measurements

Atmospheric mixing ratios of molecular hydrogen (H_2), reported to be stable over the past two decades (Grant et al., 2010), may be altered with the possible introduction of H_2 as an energy carrier. This has provoked increased interest in the H_2 budget as it may result in increased H_2 emissions due to leakages during transport, distribution and usage of the fuel, thereby altering tropospheric and stratospheric chemistry. Without a better understanding of the budget of atmospheric H_2, we will be unable to assess accurately the impact of moving to a hydrogen economy. Field measurements, supported by inverse modelling are needed to resolve the current sources and sinks of H_2. Hydrogen measurements have made at Mace Head atmospheric research station since 1994, using the traditional technology of chromatography combined with Mercuric oxide detection (RGA). This technique suffers from the inherent non-linearity of the RGA reactor bed. In recent years new technology has been demonstrated at Cape Grim observatory in Tasmania. This technology still uses chromatography, but coupled to a Pulsed Discharge Detector (PDD). The results are very promising, with the PDD demonstrating linear response and a factor of 10 improvement in sample precision (Figure 11b).

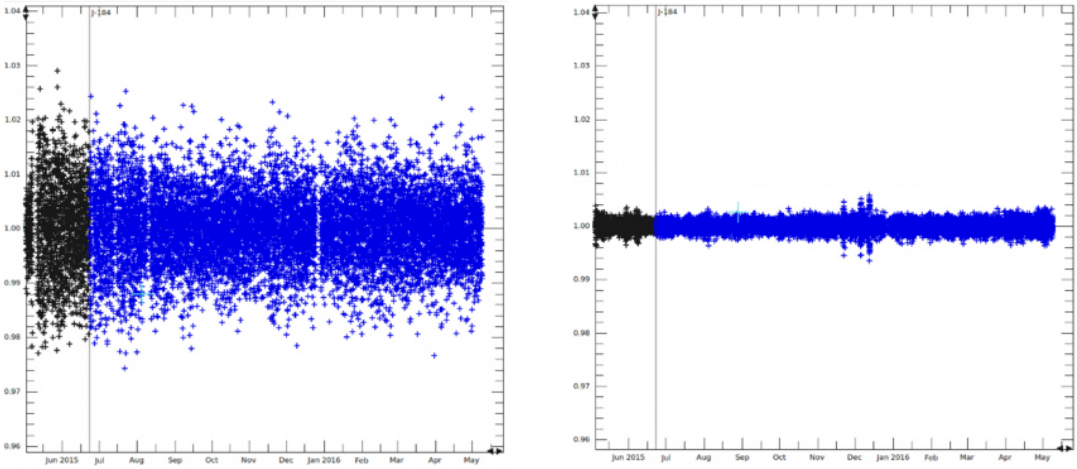

(a) RGA **(b)** PDD

Figure 11: Comparison of sample precision obtained using (a) GC-RGA detection (2%), (b) GC-PDD detection (0.2%).

A PDD detector has been in use alongside an RGA detector at the Cape Grim observatory since 2015, comparisons of the atmospheric data shown in Figure 12 highlight the superior PDD data.

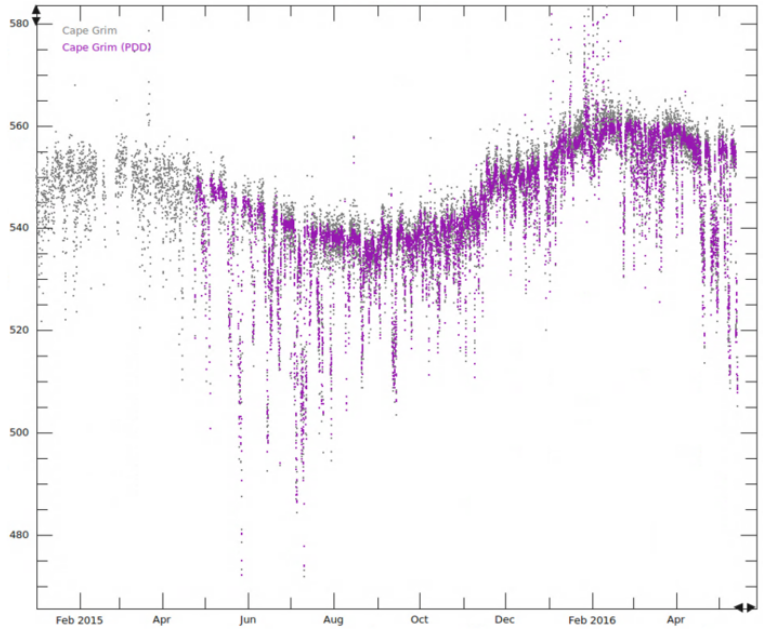

Figure 12: Comparison of H_2 measurements at Cape Grim, Tasmania using PDD (more precise) and RGA (less precise) instrumentation

4.8 Collaborations

The National University of Ireland, Galway (NUIG) and the Irish Environmental Protection Agency (IEPA) have a network of four sites in Ireland operating Picarro cavity ring-down instruments to obtain measurements of CH_4, CO_2 and CO. These sites are situated at Mace Head, County Galway; Carnsore Point, County Wexford; Valencia, County Kerry; and Malin Head, County Donegal. The University of Bristol and the UK Met Office have recently entered into a Memorandum of Understanding (MoU) with NUIG to collaborate and share data between the UK and Irish networks to allow for better understanding of trends and distributions of these gases. There are number of minor operational issues to resolve but it is hoped that these pooled resources will enable better understanding of these gases in the near future.

The University of Bristol have also been actively collaborating with TNO (Netherlands Organisation for Applied Scientific Research) to analyse glass flask samples taken at the Cabauw tall tower in the Netherlands. The analysis is conducted on a Medusa GCMS and Picarro CRDS system in Bristol to provide calibrated measurements of a wide range of GHGs, CH_4, CO_2. This collaboration is also relatively new but it is envisaged that it may help contribute to our emissions estimates over time.

5 Atmospheric Hemispheric Trends

For each gas observed at Mace Head a baseline analysis has been performed. ECMWF (ERA-Interim) meteorology is used from 1989 – 2002 inclusive and Met Office meteorology from 2003 – 2021 inclusive. For each gas, Northern Hemisphere (NH) and Southern Hemisphere (SH) baselines and rates of change (growth) are inferred from the observations at Mace Head, Ireland and Cape Grim, Tasmania, Australia respectively, see Manning et al. 2021 for details of the methodology. Table 1 – Table 4 summarises the annual NH baseline mole fractions for each gas observed and the average and recent rates of change.

Table 1: Mid-latitude Northern Hemisphere mole fractions and trends observed at Mace Head for 1990-2019 (ppt, except for CH_4 and N_2O reported in ppb and CO_2 in ppm). AvAll = Average Atmospheric Growth (ppX yr^{-1}) from 2003 (or from when observations started). Av12m = Growth (ppX yr^{-1}) over last 12 months calculated using a 3-year quadratic fit.

Gas	CH_4	N_2O	CO_2	HFC-125	HFC-134a	HFC-143a	HFC-152a	HFC-23	HFC-32
Unit	ppb	ppb	ppm	ppt	ppt	ppt	ppt	ppt	ppt
1990	1789	309.0							
1991	1809	310.0							
1992	1802	310.0							
1993	1813	311.0	357.0						
1994	1814	312.0	359.0						
1995	1818	312.0	360.0		2.0		1.18		
1996	1822	313.0	363.0		4.0		1.22		
1997	1822	314.0	364.0		6.0		1.36		
1998	1833	315.0	367.0	1.18	10.0		1.77		
1999	1837	315.0	369.0	1.42	13.0		2.18		
2000	1840	317.0	369.0	1.75	17.0		2.48		
2001	1840	317.0	371.0	2.23	21.0		2.87		
2002	1841	318.0	373.0	2.62	25.0		3.36		
2003	1849	319.0	375.0	3.23	30.0		4.09		
2004	1846	319.0	377.0	3.85	35.0	5.47	4.76		1.05
2005	1845	320.0	379.0	4.59	39.0	6.36	5.55		1.57
2006	1845	321.0	382.0	5.38	44.0	7.42	6.70		2.05
2007	1853	322.0	384.0	6.29	48.0	8.39	7.83		2.72
2008	1863	323.0	386.0	7.44	53.0	9.55	8.78	22.54	3.40
2009	1865	323.0	387.0	8.57	58.0	10.65	8.87	23.05	4.08
2010	1870	324.0	390.0	9.99	63.0	11.90	9.37	23.70	5.15
2011	1872	325.0	392.0	11.65	68.0	13.12	9.88	24.65	6.48
2012	1880	326.0	394.0	13.43	73.0	14.50	10.00	25.57	7.71
2013	1885	327.0	397.0	15.46	78.0	15.91	9.95	26.62	9.21
2014	1896	328.0	398.0	17.66	84.0	17.39	9.99	27.85	10.84
2015	1907	329.0	401.0	20.01	89.0	18.75	9.81	28.78	12.83
2016	1919	330.0	404.0	22.62	96.0	20.50	9.92	29.56	15.05
2017	1923	331.0	407.0	25.73	103.0	22.22	9.99	30.68	18.09
2018	1929	332.0	409.0	28.88	108.0	23.73	10.10	31.95	21.25
2019	1939	333.0	411.0	32.24	114.0	25.41	10.57	33.33	25.49
2020	1955	334.0	414.0	35.45	120.0	27.03	10.35	34.48	28.99
AvAll	5.62	0.82	2.11	1.61	4.73	1.36	0.37	1.01	1.79
Av12m	15.85	1.22	2.65	3.34	5.36	1.65	-0.11	1.15	3.70

Table 2: Mid-latitude Northern Hemisphere mole fractions and trends observed at Mace Head for 2004-2019 (ppt). AvAll = Average Atmospheric Growth (ppt yr^{-1}) from 2003 (or from when observations started). Av12m = Growth (ppt yr^{-1}) over last 12 months calculated using a 3-year quadratic fit.

Gas	HFC-227ea	HFC-4310mee	HFC-365mfc	PFC-14	PFC-116	PFC-218	PFC-318	SF_6	NF_3
Unit	ppt	ppt	ppt	ppt	ppt	ppt	ppt	ppt	ppt
2004				74.90	3.646	0.435		5.57	
2005			0.308	75.45	3.723	0.456		5.80	
2006			0.438	76.18	3.811	0.482		6.06	
2007	0.468		0.523	76.86	3.916	0.498		6.31	
2008	0.544		0.608	77.65	3.997	0.516		6.61	
2009	0.626		0.647	78.10	4.063	0.524		6.90	
2010	0.711		0.692	78.73	4.141	0.550		7.17	
2011	0.791	0.226	0.775	79.53	4.239	0.570	1.334	7.47	
2012	0.884	0.239	0.855	80.28	4.300	0.581	1.376	7.77	
2013	0.993	0.248	0.917	81.08	4.381	0.596	1.429	8.10	
2014	1.095	0.260	1.014	81.79	4.468	0.614	1.484	8.44	1.255
2015	1.183	0.274	1.092	82.59	4.553	0.630	1.536	8.77	1.398
2016	1.324	0.279	1.171	83.46	4.619	0.642	1.590	9.09	1.553
2017	1.450	0.285	1.220	84.33	4.728	0.657	1.661	9.44	1.749
2018	1.584	0.284	1.266	85.29	4.816	0.674	1.733	9.78	1.990
2019	1.726	0.301	1.318	86.12	4.910	0.698	1.796	10.14	2.228
2020	1.893	0.311	1.319	87.00	5.001	0.717	1.863	10.46	2.480
AvAll	0.11	0.01	0.06	0.76	0.08	0.02	0.06	0.31	0.21
Av12m	0.17	0.01	0.01	0.87	0.09	0.02	0.07	0.33	0.26

Table 3: Mid-latitude Northern Hemisphere mole fractions and trends observed at Mace Head for 2004-2019 (ppt). AvAll = Average Atmospheric Growth (ppt yr^{-1}) from 2003 (or from when observations started). Av12m= Growth (ppt yr^{-1}) over last 12 months calculated using a 3-year quadratic fit.

Gas	CFC-11	CFC-12	CFC-113	HCFC-124	HCFC-141b	HCFC-142b	HCFC-22	HFC-236fa	HFC-245fa	SO_2F_2	CH_3Cl	CH_2Cl_2
Unit	ppt	ppt	ppt	ppt	ppt	ppt	ppt	ppt	ppt	ppt	ppt	ppt
1990	264.0	496.0	75.29									
1991	266.0	506.0	80.95									
1992	268.0	516.0	84.11									
1993	269.0	521.0	84.98									
1994	268.0	527.0	84.26									
1995	267.0	533.0	84.37		5.14	8.00						34.65
1996	266.0	537.0	84.33		7.30	9.26						36.26
1997	265.0	540.0	83.72		9.68	10.63						36.52
1998	263.0	542.0	83.13	1.142	11.24	11.38					538.0	32.49
1999	261.0	543.0	82.61	1.325	13.22	12.42	145.0				536.0	31.28
2000	260.0	546.0	82.22	1.427	15.08	13.60	151.0				519.0	30.00
2001	259.0	546.0	81.41	1.577	16.23	14.59	158.0				513.0	28.76
2002	257.0	546.0	80.65	1.585	17.56	14.99	163.0				513.0	28.95
2003	255.0	546.0	79.96	1.630	18.53	15.52	169.0				526.0	30.60
2004	253.0	545.0	79.27	1.649	19.13	16.27	174.0				524.0	30.36
2005	251.0	544.0	78.71		19.10	16.92	179.0			1.450	528.0	30.09
2006	248.0	543.0	77.85		19.55	18.02	187.0			1.529	520.0	31.87
2007	246.0	541.0	77.11		20.21	19.22	194.0	0.070	1.062	1.554	530.0	34.34
2008	244.0	538.0	76.74		20.89	20.55	204.0	0.079	1.275	1.609	535.0	35.83
2009	242.0	535.0	75.96		21.26	21.40	211.0	0.079	1.388	1.663	531.0	35.93
2010	240.0	533.0	75.21		21.96	21.91	219.0	0.092	1.545	1.735	529.0	39.62
2011	238.0	530.0	74.54		23.04	22.67	226.0	0.107	1.784	1.822	520.0	38.88
2012	236.0	527.0	73.99		24.13	23.01	230.0	0.118	2.004	1.914	527.0	40.95
2013	235.0	524.0	73.33		24.91	23.27	236.0	0.127	2.210	2.023	534.0	49.68
2014	234.0	522.0	72.75		25.28	23.34	241.0	0.139	2.397	2.132	532.0	48.81
2015	232.0	519.0	71.97		25.63	23.33	245.0	0.146	2.565	2.229	539.0	48.20
2016	231.0	515.0	71.51		25.97	23.38	249.0	0.159	2.790	2.325	542.0	50.25
2017	230.0	512.0	70.98		25.92	23.40	252.0	0.172	3.065	2.445	528.0	58.34
2018	229.0	509.0	70.39		25.60	23.25	254.0	0.188	3.233	2.511	528.0	55.12
2019	227.0	505.0	69.82		25.79	23.19	258.0	0.204	3.551	2.630	522.0	55.74
2020	225.0	501.0	69.37		26.06	22.87	258.0	0.214	3.705	2.717	522.0	58.91
AvAll	-1.24	0.31	-0.13	0.08	0.82	0.59	5.40	0.01	0.20	0.08	-1.00	0.95
Av12m	-2.64	-3.87	-0.48	0.02	0.23	-0.29	0.99	0.01	0.17	0.10	0.72	3.80

Table 4: Mid-latitude Northern Hemisphere mole fractions and trends observed at Mace Head for 2004-2019 (ppt or ppb). AvAll = Average Atmospheric Growth (ppX yr^{-1}) from 2003 (or from when observations started). Av12m = Growth (ppX yr^{-1}) over last 12 months calculated using a 3-year quadratic fit.

Gas	$CHCl_3$	CCl_4	CH_3CCl_3	C_2Cl_4	CH_3Br	Halon-1211	Halon-1301	Halon-2402	CO	H_2	O_3
Unit	ppt	ppt	ppt	ppt	ppt	ppt	ppt	ppt	ppb	ppb	ppb
1990		108.0	150.0								34.52
1991		105.0	152.0								35.75
1992		105.0	149.0								34.85
1993		104.0	139.0								34.78
1994	11.99	104.0	125.0						110.0	507.0	36.44
1995	12.41	103.0	111.0						114.0	508.0	34.93
1996	12.47	101.0	95.0						126.0	515.0	37.60
1997	11.93	100.0	79.0						117.0	506.0	36.81
1998	12.06	99.0	66.0			4.043	2.730		143.0	519.0	39.89
1999	11.57	98.0	55.0		10.96	4.170	2.827		122.0	520.0	41.57
2000	11.25	97.0	47.0		10.43	4.324	2.961		117.0	511.0	40.27
2001	11.26	96.0	39.0	5.026	9.85	4.373	2.993		113.0	507.0	39.55
2002	11.17	95.0	32.0	4.688	9.11	4.395	3.027		117.0	509.0	40.68
2003	11.24	94.0	27.0	4.626	8.87	4.414	3.073		132.0	513.0	40.96
2004	11.30	93.0	23.0	4.283	9.47	4.497	3.109	0.498	120.0	509.0	40.38
2005	11.38	93.0	19.0	3.759	10.23	4.481	3.164	0.495	119.0	513.0	39.91
2006	11.39	91.0	16.0	3.759	9.40	4.457	3.228	0.490	119.0	515.0	41.34
2007	11.31	90.0	13.0	3.522	9.06	4.418	3.225	0.482	116.0	512.0	39.70
2008	11.56	89.0	11.0	3.395	9.11	4.383	3.259	0.474	119.0	514.0	41.09
2009	10.97	88.0	9.0	2.911	8.57	4.320	3.261	0.466	113.0	510.0	40.80
2010	11.95	87.0	8.0	3.042	8.30	4.242	3.303	0.456	121.0	510.0	39.55
2011	11.65	86.0	7.0	2.665	8.34	4.160	3.303	0.451	113.0	517.0	40.07
2012	11.78	85.0	5.0	2.456	8.25	4.073	3.339	0.445	119.0	517.0	40.10
2013	12.89	84.0	5.0	2.413	8.15	3.967	3.386	0.438	115.0	519.0	41.42
2014	13.89	83.0	4.0	2.388	7.64	3.867	3.402	0.429	115.0	517.0	40.18
2015	14.49	82.0	3.0	2.342	7.55	3.751	3.392	0.423	113.0	515.0	40.45
2016	15.15	80.0	3.0	2.298	7.45	3.640	3.386	0.419	111.0	516.0	39.42
2017	15.77	80.0	2.0	2.358	7.35	3.537	3.379	0.412	109.0	519.0	40.43
2018	15.51	79.0	2.0	2.184	7.17	3.427	3.376	0.403	109.0	523.0	40.21
2019	13.93	78.0	2.0	2.250	7.10	3.327	3.393	0.400	109.0	524.0	40.38
2020	13.96	77.0	1.0	2.131	7.14	3.228	3.391	0.398	108.0	523.0	37.84
AvAll	0.06	-1.06	-4.78	-0.14	-0.18	-0.04	0.03	-0.01	-0.15	0.65	0.16
Av12m	-0.01	-1.23	-0.19	-0.09	-0.03	-0.10	-0.00	-0.00	-0.01	0.99	-1.11

6 Regional Emission Estimation

6.1 Introduction

This chapter presents the InTEM inversion results, showing the atmospheric trends and regional emissions of the gases that are measured in the UK DECC network and that are reported to the UNFCCC (United Nations Framework Convention on Climate Change). For each gas, the NH and SH baselines are presented for two AGAGE (Advanced Global Atmospheric Gases Experiment) stations; Mace Head, Ireland in the mid-latitude NH and Cape Grim, Australia in the mid-latitude SH. UK estimated emissions follow where a comparison is made between the InTEM results and the reported UNFCCC inventory values (April 2021 submission). The reported and InTEM estimates for each gas are tabulated and presented in Annex 1 for both the UK (UNFCCC April 2021 submission) and North West Europe (NWEU = IRL + UK + FRA + BEL + NLD + LUX + DEU) (UNFCCC April 2020 submission). It should be noted that the emission estimates for 2021 only use 8 months of provisional observations (Jan - Aug) and should be treated with some caution.

InTEM is briefly presented but for more information the reader is referred to the Methodology report. The uses, atmospheric lifetimes, and global warming potentials for the different gases reported under the UNFCCC are presented in Table 5.

6.2 Summary of InTEM inverse modelling

Each observation in the UK DECC network is comprised of two parts; a time-varying NH baseline mole fraction and a perturbation above baseline. The perturbations above baseline, observed across the UK DECC network, are driven by emissions on regional scales that have yet to be fully mixed on the hemisphere scale and are the principle information used to estimate surface emissions across north-west Europe. A method for estimating emissions from observations, referred to as 'Inversion Technique for Emission Modelling' (InTEM) (Manning et al. 2011; Arnold et al. 2018; Manning et al. 2021), has been developed over many years and is used here to estimate UK and NWEU emissions using the observations from the UK DECC network and other European networks where available.

InTEM links the observation time-series with each 4-hour NAME air history estimate of how surface emissions dilute as they travel to the observation stations. An estimated emission distribution, when combined with the NAME output, can be transformed into a modelled time-series at each of the measurement stations. The modelled and the observed time-series can then be statistically compared. InTEM uses a Bayesian statistical technique with a non-negative least squares solver to find the emission distributions that produces the modelled times-series at each observation station

that has the best statistical match to the observations. The Bayesian method requires the use of a prior emission distribution with associated uncertainties as the starting point for the inversion. The prior information can influence and inform the inversion (posterior) solution. In this work the prior emission information has been chosen to be either land-based but population weighted (HFCs) or spread uniformly across the land (PFCs, SF_6, NF_3) or informed by the NAEI (UK National Atmospheric Emissions Inventory) nested within EDGAR (global prior of emissions) estimate (CH_4 and N_2O). However, to preserve the independence of the inversion results presented here from the prior estimates, the priors were given very large uncertainties thus ensuring the inversion results are dominated by the observations not the prior. For CH_4 and N_2O, where the inversion time window was set to one month, the prior was given more weight but the solutions were still dominated by the observations.

For InTEM to provide robust solutions for every area within the modelled domain, each region needs to significantly contribute to the air concentration at the UK DECC network sites for a reasonable number of time periods. If the signal from an area is only rarely or poorly seen by the network, then its impact on the statistics is minimal and the inversion method will have little skill at determining its true emission. The contributions that different grid boxes make to the air concentration at each station varies from grid to grid. Grid boxes that are distant from the observation site contribute little to the observation, whereas those that are close have a large impact. To balance the contributions from different grid boxes, those that are more distant are grouped together into increasingly larger regions. The grouping cannot extend beyond country or Devolved Administration (DA) boundaries. The country boundaries can extend into the surrounding seas to reflect both emissions from shipping, off-shore installations and river runoff but also because the inversion has geographical uncertainty.

For each greenhouse gas, two sets of inversions are performed, with the inversion time frame being either one calendar year or two calendar years. The 2-year inversions started in the year MHD started observing the gas, the 1-year inversions started in 2013 to coincide with the UK DECC network. Every inversion period is repeated 24 times, each time having 8 randomly chosen blocks of 5-days of observations per year removed from the dataset (equivalent to approximately 10% of the year). Annual emission estimates were made by averaging the inversion results covering the appropriate year. Observations from Jungfraujoch (JFJ, Switzerland) and Monte Cimone (CMN, Italy), Taunus (TOB, Germany), Carnsore Point (CSP, Ireland), Cabauw (CBW, The Netherlands) and Weybourne (WAO, Norfolk, UK) were used where available and complemented those in the UK DECC network. For CH_4, N_2O and SF_6, where observations are available from 5 to 8 sites, the inversion time frames were set to 3- and 1-months. The repeating of each inversion multiple times with the random removal of $\sim 10\%$ of the observations from each inversion improves the estimates of uncertainty.

There are a range of uncertainties in the emissions that are estimated. Uncertainty arises from many factors: errors in the baseline estimate; emissions that vary over time-scales shorter than the inversion time-window e.g. diurnal, seasonal or intermittent; heterogeneous emissions; errors in the transport model (NAME) or the underpinning 3-dimensional meteorology; errors in the observations themselves. The potential magnitudes of these uncertainties have been estimated and are incorporated within InTEM to inform the uncertainty of the modelled results.

At RGL, HFD, TAC and BSD, CH_4 is observed at two or more heights. If, during a 4-hour period the observed CH_4 differs significantly across the heights, it is an indication that the meteorology is particularly complex and therefore the modelled meteorology will have significant uncertainty. At the other stations, where measurements are not made at multiple heights, the assessment of poor modelling is made using the modelled boundary layer height, wind speed and atmospheric stability. Such 4-hour periods are identified at each observation station and are excluded from the inverse modelling.

Estimating the model and observation uncertainty is an important part of InTEM. The observation uncertainty is estimated each day by repeatedly measuring the same tank of air. The standard deviation of these measurements is defined as the observation uncertainty for that day's observations of that gas at that station. For the high frequency (1-minute) Picarro observations the variability over each 4-hour period is defined as the observation uncertainty. The model uncertainty is defined as having two components; a baseline uncertainty and a meteorological uncertainty. The baseline uncertainty is estimated during the fitting of the NH baseline trend to the baseline observations. The meteorological uncertainty is proportional to the magnitude of the pollution event with an imposed minimum of the median pollution event for that gas for that year at that station.

The most significant work over the last year was the publication of the paper on UK HFCs (Manning et al. 2021) and the paper, currently in review, on UK methane emissions (Lunt et al. 2021). Over the last year there have been some minor improvements to the InTEM methodology in the estimation of the hemispheric background levels, model uncertainty, UK land-sea mask, improved NAME modelling and the comprehensive inclusion of observational data from JFJ, CMN, TOB, WAO, CBW and CSP stations, all detailed in Manning et al. 2021.

6.3 Summary of the GHG reported to the UNFCCC

Table 5 describes the principle uses of each of the gases reported to the UNFCCC and observed in the network, their radiative efficiency, atmospheric lifetime and global warming potential in a 100-year framework (GWP_{100}).

Table 5: Principle uses of each of the gases, their radiative efficiency, atmospheric lifetime and global warming potential in a 100-year framework (GWP_{100}) (Chapter 8, Working Group 1, 5th Assessment Report of the IPCC, (Myhre et al. 2013)). The GWP_{100} for the HFCs are taken from the more recent 2018 Ozone Assessment (Montzka et al. 2018)).

Gas	Chemical Formula	Main Use	Radiative Efficiency ($Wm^{-2}ppb^{-1}$)	Atmospheric lifetime (yr)	GWP_{100}
Methane	CH_4	Landfill, farming, energy, wetlands	0.000363	12.4	28
Nitrous Oxide	N_2O	Nylon manufacture, farming	0.00300	121	265
Carbon Dioxide	CO_2	Combustion	0.0000137	indefinite	1
HFC-125	CHF_2CF_3	Refrigeration blend, fire suppression	0.23	28.2	3,450
HFC-134a	CH_2FCF_3	Mobile air conditioner	0.16	13.4	1,360
HFC-143a	CH_3CF_3	Refrigeration blend	0.16	47.1	5,080
HFC-152a	CH_3CHF_2	Aerosol propellant, foam-blowing agent	0.10	1.5	148
HFC-23	CHF_3	Bi-product of manufacture of HCFC-22	0.18	222	12,690
HFC-32	CH_2F_2	Refrigeration blend	0.11	5.2	705
HFC-227ea	CF_3CHFCF_3	Fire suppression, inhalers, foam blowing	0.26	38.9	3,140
HFC-245fa	$C_3H_3F_5$	Blowing and insulation agent	0.24	7.7	880
HFC-43-10mee	$C_5H_2F_{10}$	Electronics industry	0.42	16.1	1,470
HFC-365mfc	$C_4H_5F_5$	Foam blowing	0.22	8.7	810
PFC-14	CF_4	Bi-product alum. production, electronics	0.09	50,000	6,630
PFC-116	C_2F_6	Electronics, bi-product alum. production	0.25	10,000	11,100
PFC-218	C_3F_8	Electronics, bi-product alum. production	0.28	2,600	8,900
PFC-318	C_4F_8	Semiconductor and electronics industries	0.32	3,200	9,540
Sulphur Hexafluoride	SF_6	Circuit breaker in high voltage switchgear	0.57	3,200	23,500
Nitrogen Trifluoride	NF_3	Semiconductor manufacture	0.20	500	16,100

6.4 Methane (CH_4)

Methane (CH_4) is the second most important anthropogenic greenhouse gas behind carbon dioxide due to its radiative properties and atmospheric abundance. It has a Global Warming Potential over 100 years (GWP_{100}) of 28 and its total global radiative forcing attributable to anthropogenic CH_4 emissions is currently about 0.97 W m^{-2} (Myhre et al. 2013). The global background surface dry air mole fraction of atmospheric CH_4 reached 1857 ppb in 2018, approximately 2.6 times greater than its estimated pre-industrial equilibrium value in the mid 18^{th} century (Saunois et al. 2020). This growth is attributable in large part to increased anthropogenic emissions arising primarily from agriculture (e.g., livestock production, rice cultivation, biomass burning), fossil fuel production and use, waste disposal, and alterations to natural methane fluxes due to increased atmospheric CO_2 concentrations and climate change (Ciais et al. 2013). After a brief plateau period around the turn of the 21^{st}century (Cunnold et al. 2002; Dlugokencky et al. 2003), CH_4 mole fractions began rising again globally in 2007 (Rigby et al. 2008; Dlugokencky et al. 2009; Frankenberg et al. 2011; Nisbet et al. 2016) with some of the strongest growth rates occurring from 2014 onward (Nisbet et al. 2019). This increase in CH_4 growth rate was accompanied by a shift in the δ^{13}C-CH_4 isotopic ratios to more negative values, suggesting a change in the global makeup of sources and/or sinks. The drivers responsible for this shift are presently not well-understood, and possibilities include changes in tropical wetland, biomass burning, agriculture, and fossil fuel emissions or changes in the hydroxyl radical sink (e.g. Monteil et al. 2011; Schaefer et al. 2016; Schwietzke et al. 2016; Nisbet et al. 2016; Rigby et al. 2017; Worden et al. 2017; McNorton et al. 2018; Turner et al. 2019; Nisbet et al. 2019; Hmiel et al. 2020). Quantifying the CH_4 budget and understanding how major sources and sinks have been evolving is key to designing emission pathways that limit global warming due to the importance of CH_4 in meeting global climate targets (Ganesan et al. 2019; Nisbet et al. 2019, 2020). In the UK for example, the UK NAEI is prepared with a delay of two years, whereas emissions estimation based on atmospheric observations can be carried out with a delay of at most a few months. This efficiency offers a potential advantage for using atmospheric measurements to track the UK's progress towards greenhouse gas reduction targets (Lunt et al. 2021).

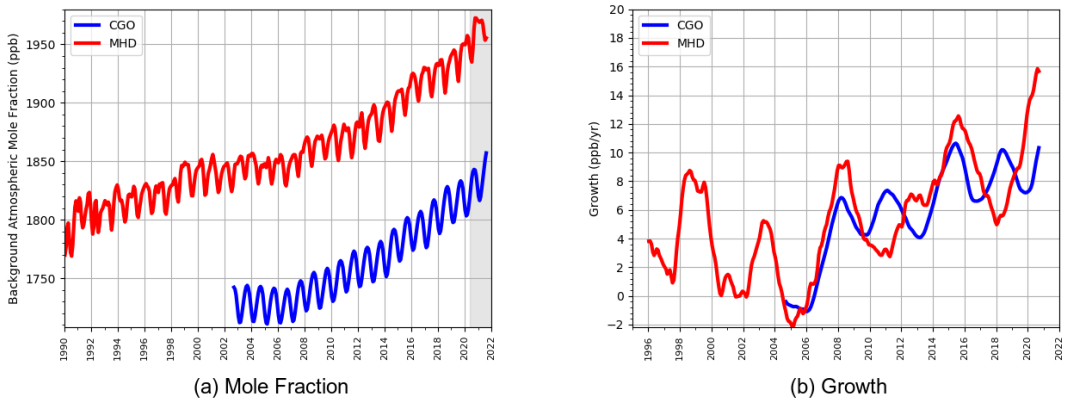

Figure 13: Northern (red) and Southern (blue) Hemisphere atmospheric background levels (left) and rates of increase (right) as observed at the Mace Head, Ireland and Cape Grim, Australia measurement stations. Grey shaded area represents un-ratified provisional data.

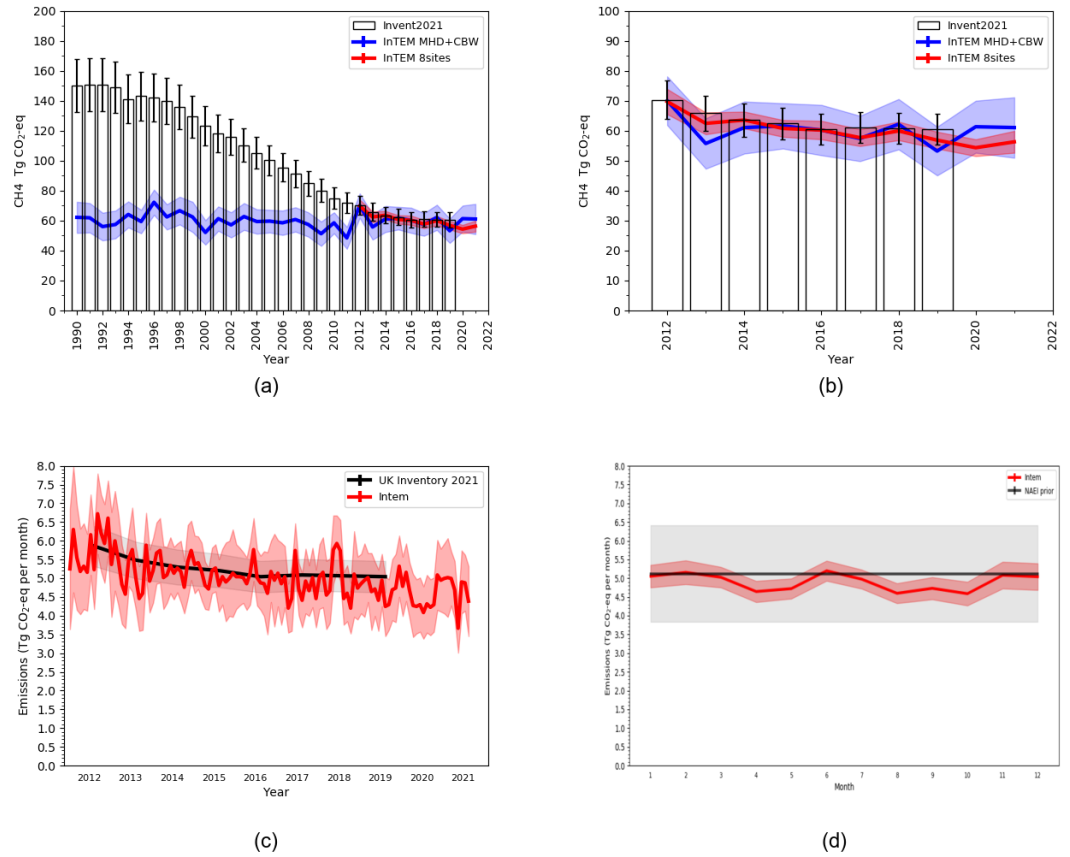

Figure 14: CH_4 UK emission estimates (Gg yr^{-1}) from the UNFCCC GHGI (black) and InTEM (blue 3-mth 2 sites and red 1-mth full network) (a) Annualised comparison 1990-2021; (b) Annualised comparison 2012-2021; (c) Monthly comparison; (d) Average seasonal cycle of emissions. The uncertainty bars represent 1-σ.

Summary of the key findings:

- Accelerating global trend upwards, currently NH increasing by $\sim$ 16 ppb yr^{-1} (Figure 13b).
- NH background has a strong seasonal cycle ($\sim$ 25 ppb).
- UK GHGI and InTEM are in good agreement from 2012 (Figure 14b).
- Since 2012 the inventory has declined by 1.95% per year compared to the 2012-2019 average emission, in the same period the 8-site monthly InTEM inversion declined by 2.08% per year, thus supporting the change in the inventory estimate (Lunt et al. 2021).
- InTEM shows little change in emissions from 1990 whereas the GHGI has fallen by more than 50% since 1990 (Figure 14a).
- Little evidence of a seasonal cycle in UK emissions although there is year to year variability (Figure 14c).
- UK distribution of emissions shows minimal change over the year (Figure 15).

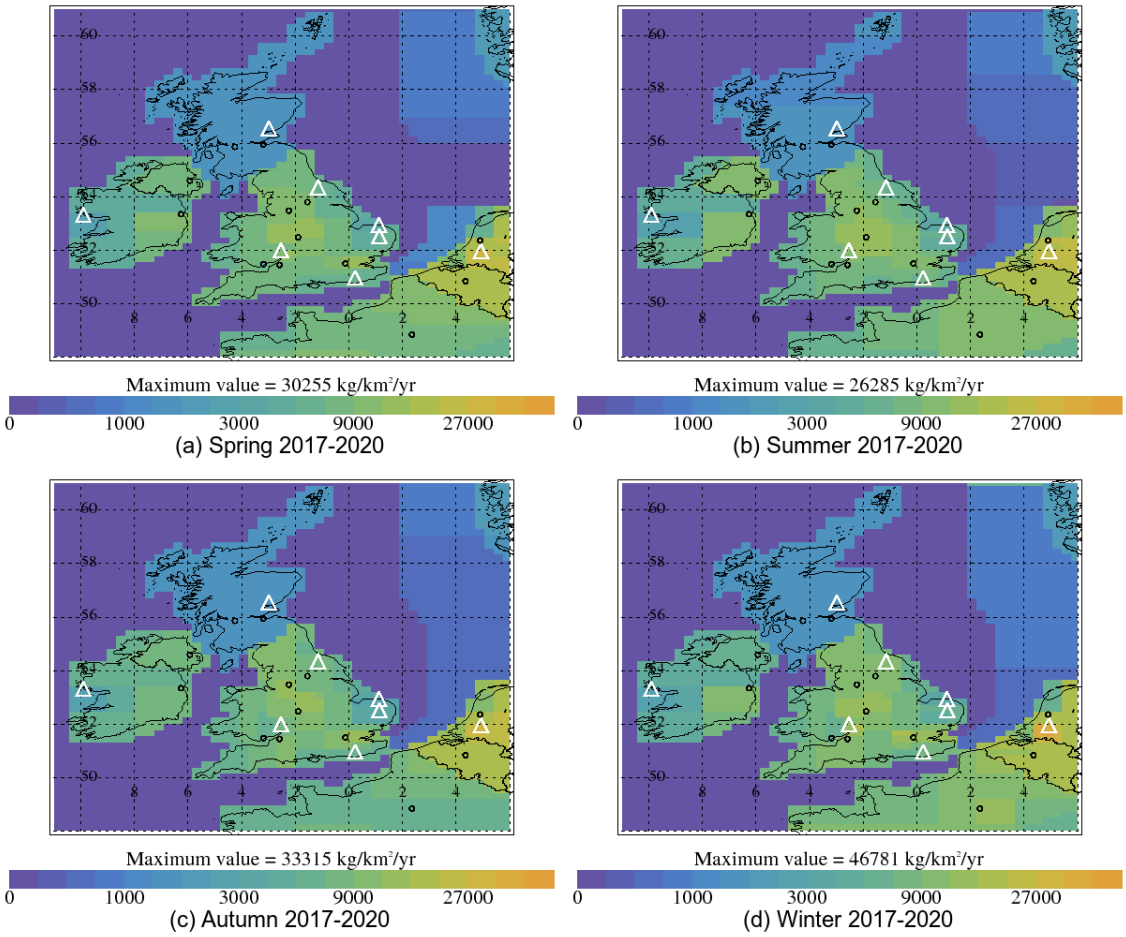

Figure 15: Average seasonal InTEM CH_4 emission estimates (kg km^{-2} yr^{-1}) 2017-2020. Measurement stations are shown as white triangles and major urban areas by circles.

6.5 Nitrous Oxide (N_2O)

Nitrous oxide (N_2O), like carbon dioxide, is a long-lived greenhouse gas that accumulates in the atmosphere. It is the third most important anthropogenic greenhouse gas after CO_2 and CH_4, it has a GWP_{100} of 265, far exceeding that of CO_2, and its emissions weighted by ozone depletion potential currently exceed those of all other substances (Ravishankara et al. 2009). Atmospheric mixing ratios of N_2O have been rising by approximately 0.93 ppb yr^{-1} (WMO 2018), reaching an average level of 334 ppb in 2020. It's long lifetime ($\sim$ 120 years) results in most emitted N_2O reaching the stratosphere, where photooxidation makes it the primary source of stratospheric NOx ("active nitrogen"). NOx is the main natural catalyst of ozone (O_3) destruction (Crutzen 1970). The main loss mechanism for N_2O is destruction in the stratosphere through photolysis and the reaction with O(1D) (Prather et al. 2015). Seasonal cycles in the troposphere are driven by both stratosphere-to-troposphere exchange and by surface emissions. Anthropogenic sources of N_2O account for $\sim$ 40% of all N_2O emissions, with natural sources accounting for the other $\sim$ 60% (Ciais et al. 2013). Natural sources of N_2O are from natural soils, oceans, and atmospheric chemistry. Anthropogenic sources are dominated by agriculture, followed by industrial and fossil fuel sources, biomass burning, rivers and estuaries, atmospheric deposition, and human excreta (Ciais et al. 2013). Emissions of N_2O following fertilizer application can exhibit major temporal and spatial variability because microbial nitrification and denitrification processes that give rise to N_2O formation are strongly dependent on soil moisture, temperature, soil type, and fertilizer application timing. It has been reported that indirect N_2O emissions downstream from the site of fertilizer application could be 2.6 - 9 times larger than is presently accounted for in bottom-up estimates (Griffis et al. 2013; Turner et al. 2015), this may, in part, explain the higher InTEM estimates compared to the GHGI, but this is currently conjecture. In the coming decades, N_2O emissions are expected to increase as a result of the growing demand for food, feed, fibre and energy, and an increase in sources from waste and waste water and industrial processes (Tian et al. 2020). Summary of the key findings:

- The N_2O NH mole fraction is currently increasing by $\sim$ 1.2 ppb yr^{-1} (Figure 16b).
- NH background has a pronounced seasonal cycle (amplitude of $\sim$ 0.8 ppb) (Figure 16a).
- UK InTEM estimates 2013-2019 are, on average, $\sim$ 20% higher than GHGI (Figure 17b).
- UK emissions are spread across country throughout the year (Figure 18).
- UK emissions have a very strong seasonal cycle (amplitude of $\sim$ 80 Gg). Peak emissions in May-Aug, minima in Jan-Feb. 2015 has a suppressed summer maximum (Figure 17c&d).
- Estimating N_2O annual emission in InTEM with just MHD observations has larger uncertainty compared to using all 5 sites but the trend and magnitudes are similar (Figure 17a&b).
- Improvements in the observation instruments has reduced InTEM uncertainty. In 2014-2017 the average InTEM uncertainty was 7.3 Gg yr^{-1} compared to 6.6 in 2019-2020, when 3 sites

were operating the new laser instruments.

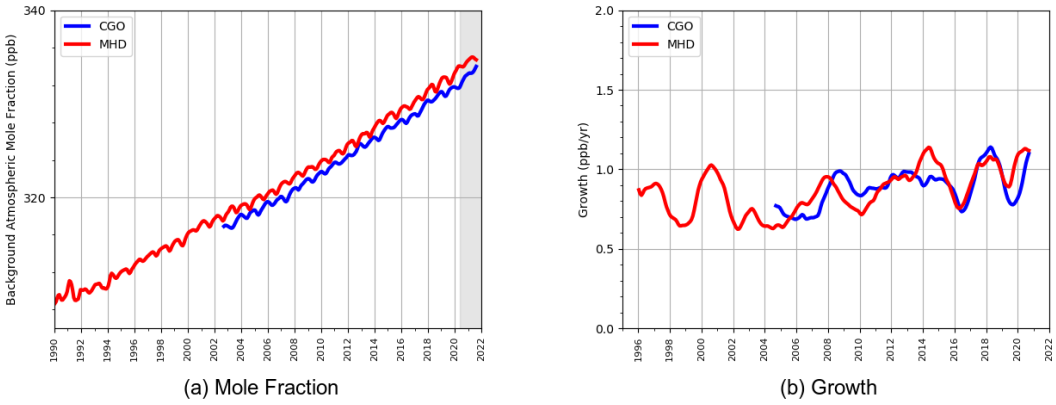

Figure 16: Northern (red) and Southern (blue) Hemisphere atmospheric background levels (left) and rates of increase (right) as observed at the Mace Head, Ireland and Cape Grim, Australia measurement stations. Grey shaded area represents un-ratified provisional data.

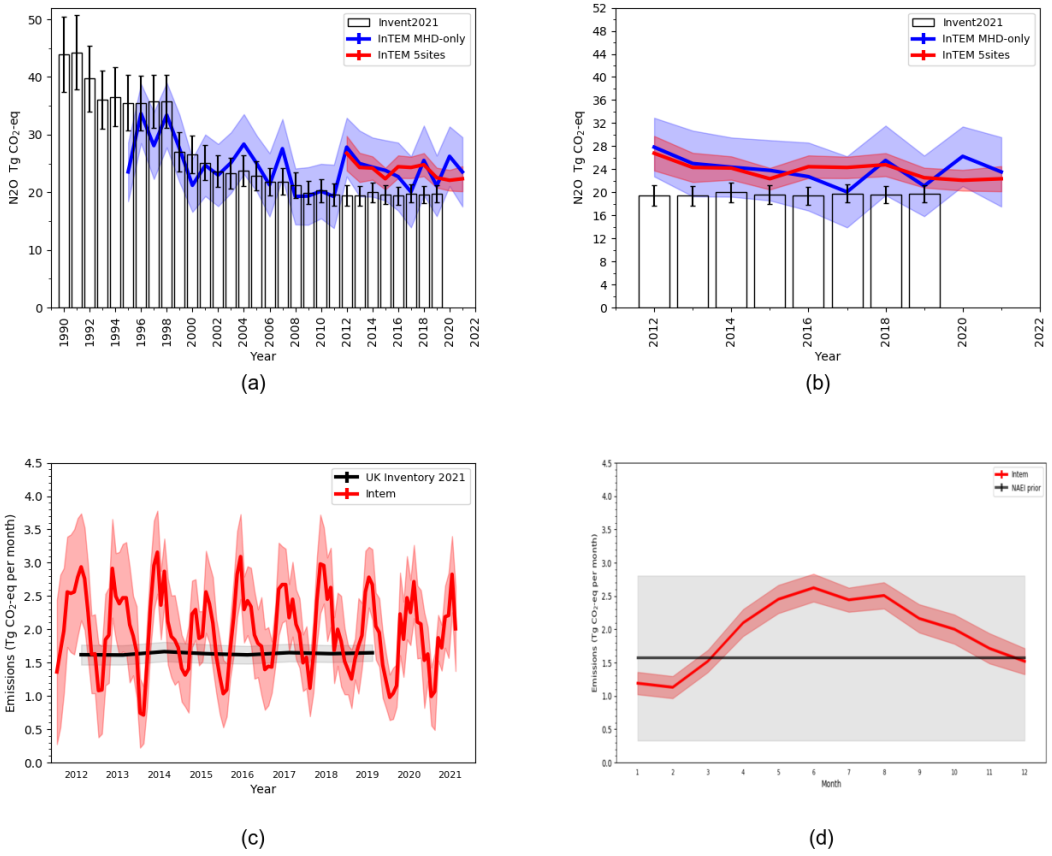

Figure 17: N_2O UK emission estimates (Gg yr^{-1}) from the UNFCCC GHGI (black) and InTEM (blue 3-mth 2 sites and red 1-mth full network) (a) Annualised comparison 1990-2021; (b) Annualised comparison 2012-2021; (c) Monthly comparison; (d) Average seasonal cycle of emissions. The uncertainty bars represent 1-σ.

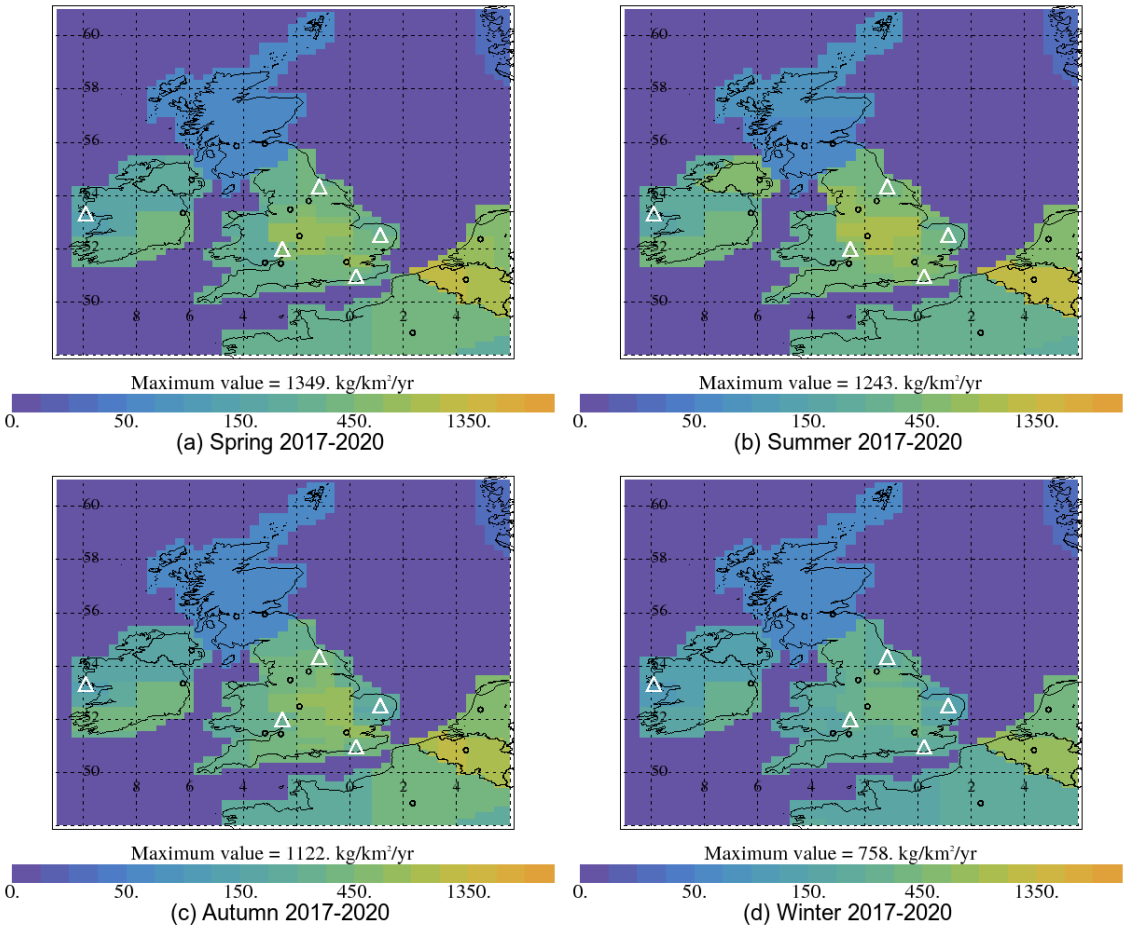

Figure 18: Average seasonal InTEM N_2O emission estimates (kg km^{-2} yr^{-1}) 2017-2020. Measurement stations are shown as white triangles and major urban areas by circles.

6.6 Sulphur Hexafluoride (SF_6)

SF_6 is the most potent GHG of all of the reported gases with a GWP_{100} of 23,500 and a long atmospheric lifetime of 3,200 years (Table 5). The global mole fraction is currently increasing at 0.33 ppt yr^{-1}, up from 0.25 ppt yr^{-1} in 2005 (Figure 19). SF_6 is predominantly used in electrical circuit breakers, heavy-duty gas-insulated switchgear for systems with voltages from 5 - 38 kV, and other switchgear used in the electrical transmission systems to manage high voltages (>38 kV). The electrical power industry uses $\sim$ 80% of all SF_6 produced worldwide. Although the units themselves are hermetically sealed and pressurised, aging equipment, breakdown and disposal, alongside leakage from wear-and-tear will cause this sector to emit SF_6. A minor use of this gas is as a blanketing (i.e. oxygen inhibiting inert gas) agent during magnesium production. Hence there are many sources of SF_6, some of which are quite diffuse.

The UK GHGI shows a steady decrease in emissions after 2001. The InTEM 3-mth inversions

show increasing emissions from 2005-2010 and then a decline thereafter, also matched by the 1-mth inversions (Figure 20a). There is good agreement with the inventory after 2013. The InTEM 1-mth estimates, Figure 20b, shows periodic spikes in emissions. There is evidence of strong emissions from SW Germany in all seasons, Figure 21.

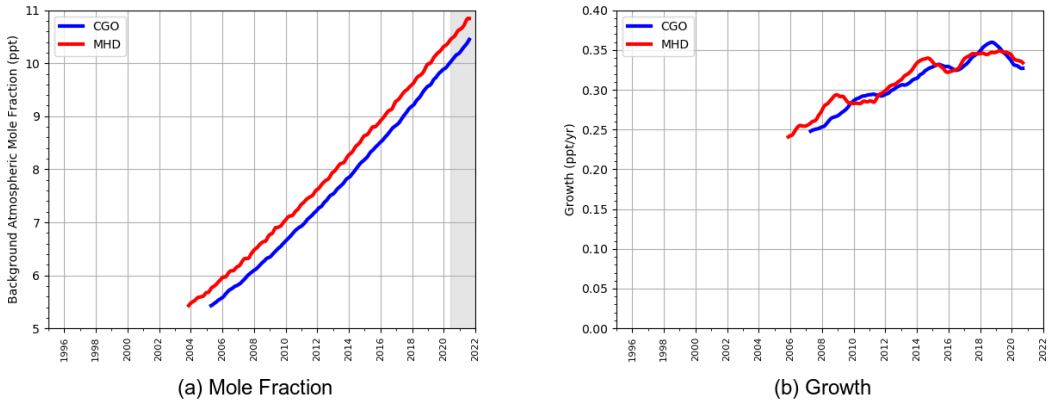

Figure 19: Northern (red) and Southern (blue) Hemisphere atmospheric background levels (left) and rates of increase (right) as observed at the Mace Head, Ireland and Cape Grim, Australia measurement stations. Grey shaded area represents un-ratified provisional data.

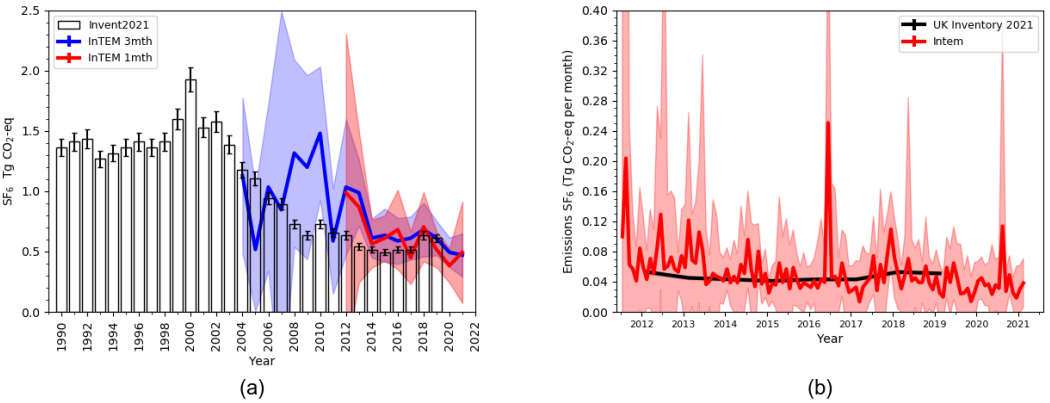

Figure 20: SF_6 UK emission estimates (Gg yr^{-1}) from the UNFCCC GHGI (black) and InTEM (blue 3-mth and red 1-mth) (a) Annualised comparison 1990-2021; (b) Monthly comparison 2012-2021. The uncertainty bars represent 1-σ.

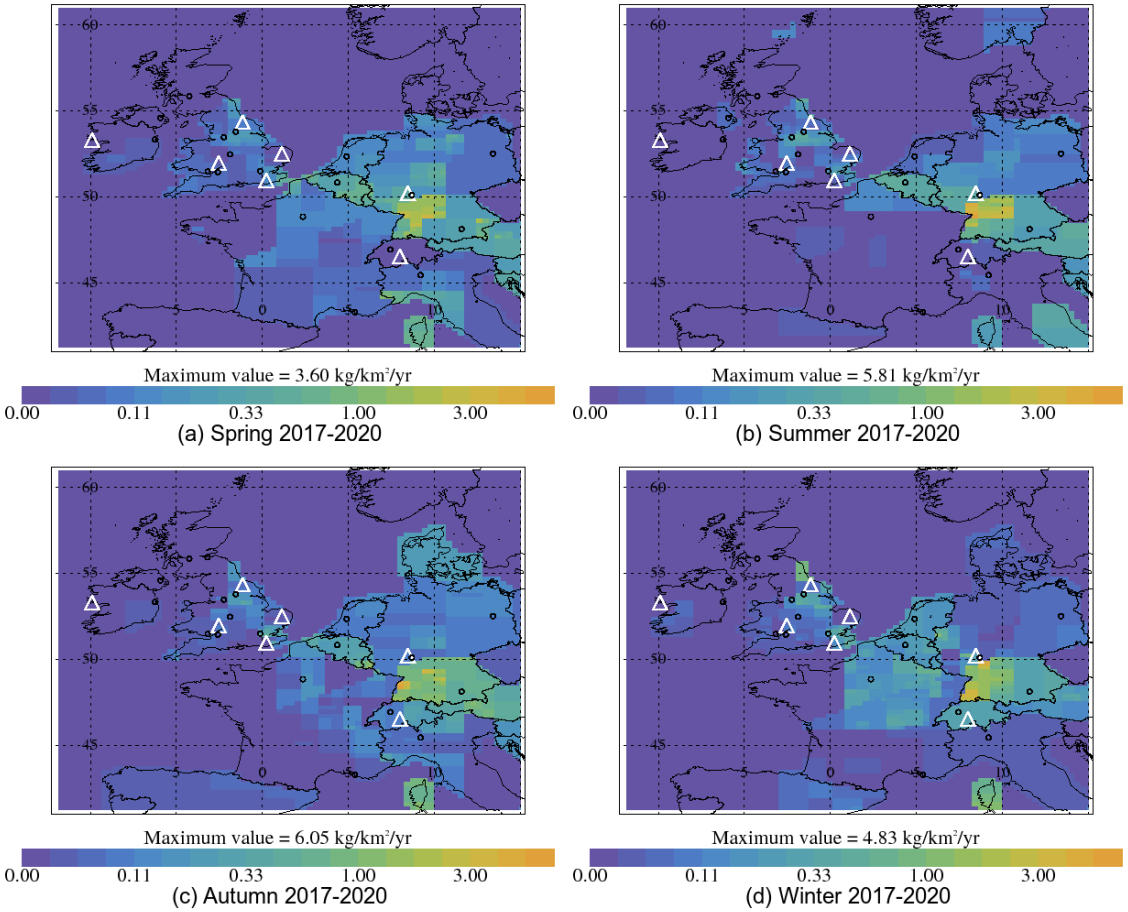

Figure 21: Average seasonal InTEM SF_6 emission estimates (kg km^{-2} yr^{-1}) 2017-2020. Measurement stations are shown as white triangles and major urban areas by circles.

6.7 Carbon Dioxide (CO_2)

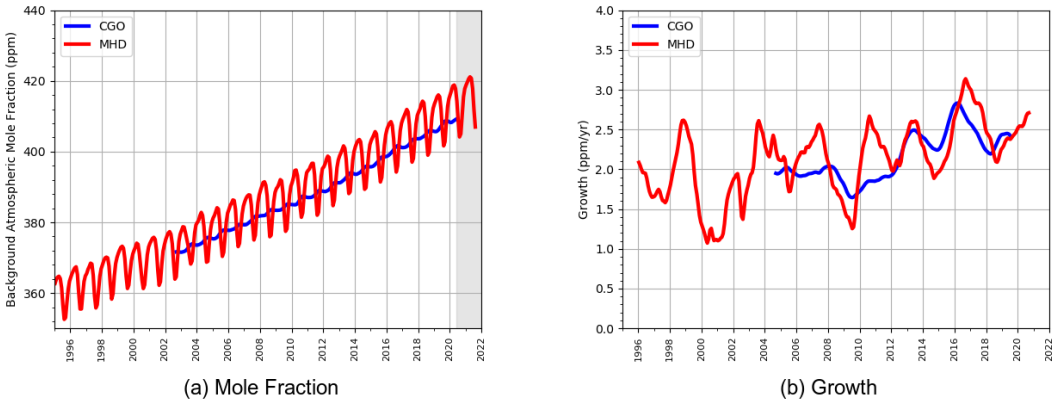

Figure 22: Northern (red) and Southern (blue) Hemisphere atmospheric background levels (left) and rates of increase (right) as observed at the Mace Head, Ireland and Cape Grim, Australia measurement stations. Grey shaded area represents un-ratified provisional data.

CO_2 is the most important greenhouse gas due to its abundance in the atmosphere. Since 1992, its NH background surface dry air mole fraction has increased at an average rate of ~ 2 ppm yr^{-1}, but this rate has increased slightly since 2012.

6.8 Hydrofluorocarbons (HFCs)

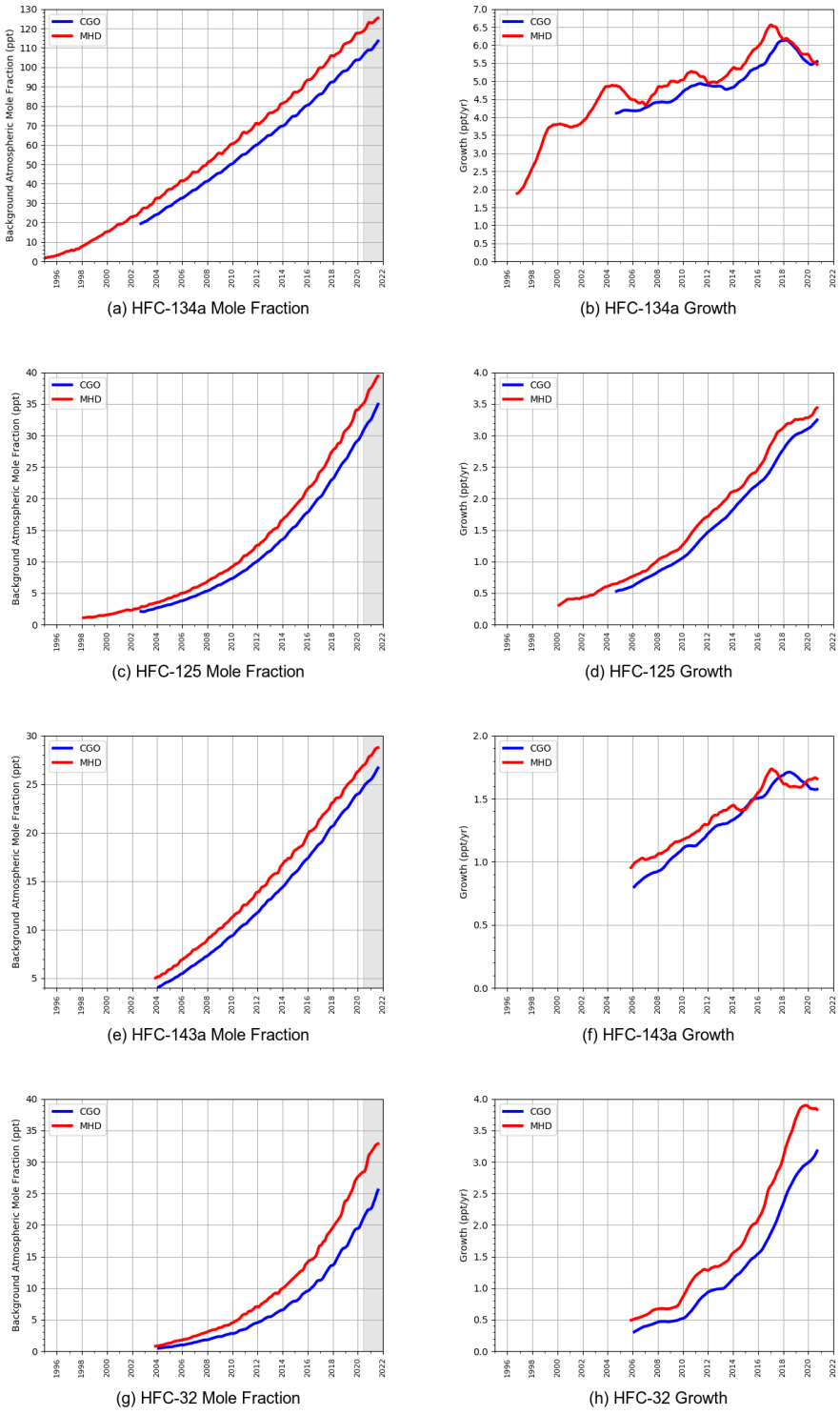

Figure 23: Northern (red) and Southern (blue) Hemisphere atmospheric background levels (left) and rates of increase (right) as observed at the Mace Head, Ireland and Cape Grim, Australia measurement stations. Grey shaded area represents un-ratified provisional data.

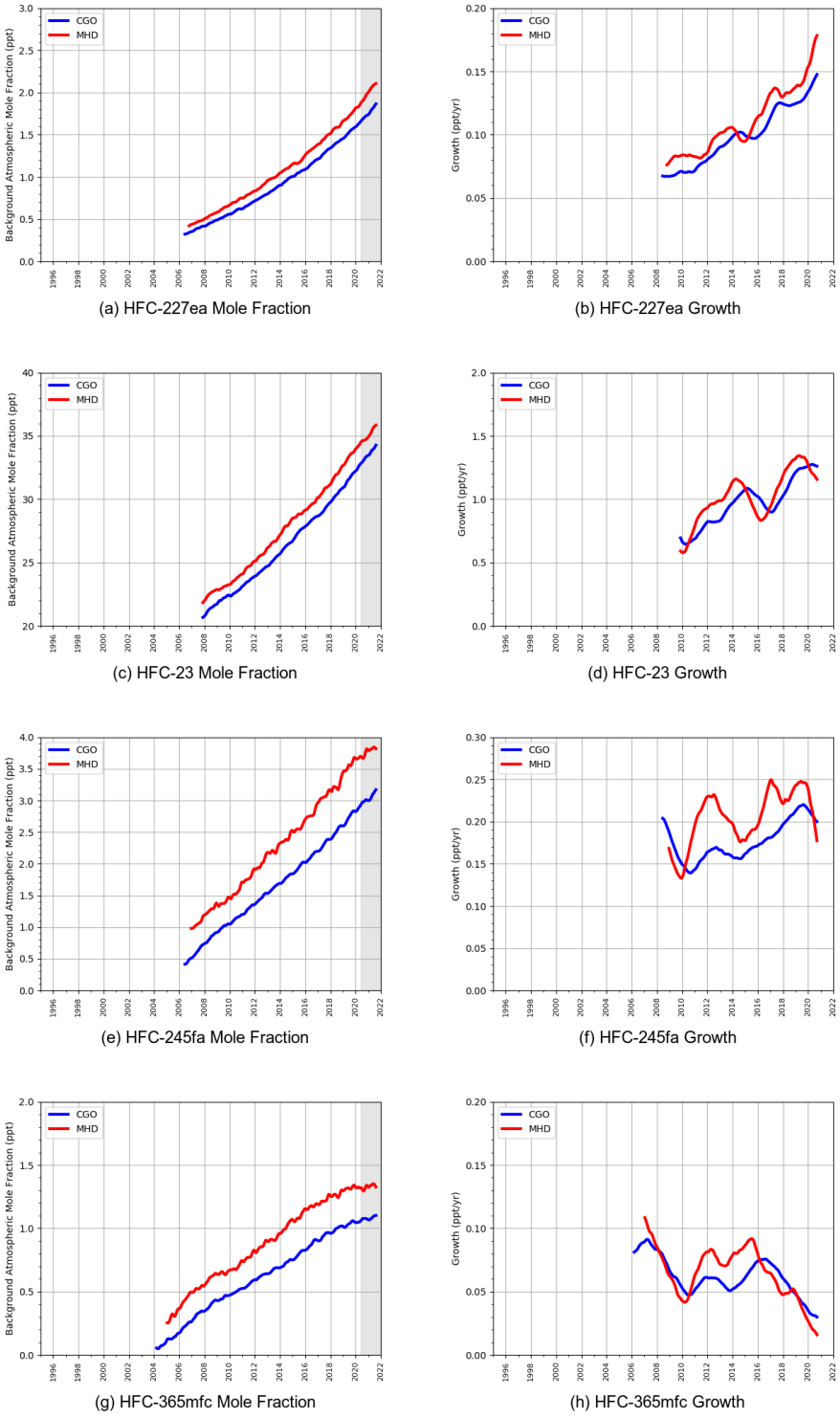

Figure 24: Northern (red) and Southern (blue) Hemisphere atmospheric background levels (left) and rates of increase (right) as observed at the Mace Head, Ireland and Cape Grim, Australia measurement stations. Grey shaded area represents un-ratified provisional data.

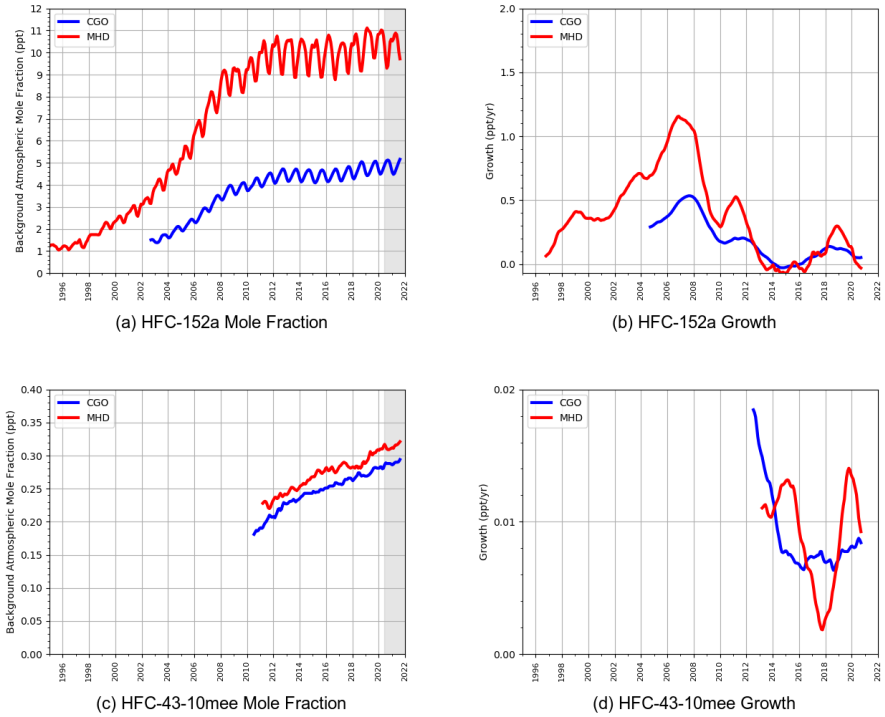

Figure 25: Northern (red) and Southern (blue) Hemisphere atmospheric background levels (left) and rates of increase (right) as observed at the Mace Head, Ireland and Cape Grim, Australia measurement stations. Grey shaded area represents un-ratified provisional data.

The atmospheric mole fractions of all the HFCs reported here (HFC-125, HFC-134a, HFC-143a, HFC-152a, HFC-23, HFC-32, HFC-227ea, HFC-245fa, HFC-365mfc and HFC-43-10mee) are growing in the NH as can been seen in Figures 23, 24 and 25, (left hand panels) and this is replicated in the Southern Hemisphere albeit with a time lag of 1-2 years. These plots show the background mid-latitude NH mole fractions and rates of increase of each of the HFCs measured at Mace Head, Ireland, in red, alongside the same measurements made at Cape Grim, Australia, in blue. Some of the gases, notably HFC-134a, HFC-125, HFC-32 and HFC-227ea, are growing very rapidly in the atmosphere. Others are growing much more slowly e.g. HFC-152a, HFC-43-10mee and HFC-365mfc. HFC-23 is the most important in terms of its impact on the climate as its GWP_{100} is by far the highest at over 12,000. The next most important gases, with GWP_{100}s of 3,000-5,000, are HFC-125, HFC-143a and HFC-227ea and then HFC-134a with a GWP_{100} of 1,300 (Table 5). The mixing ratios of HFC-43-10mee are growing much more slowly, while HFC-152a has shown little overall growth since 2012 and has even recorded a few years of decline. HFC-152a has a strong seasonal cycle and a large inter-hemispheric gradient due to its short lifetime. The growth of HFC-365mfc in the NH has fallen steadily since 2015, which is reflected in the mixing ratio plateauing in the NH in 2020. The overall growth of HFC-32, HFC-125, HFC-143a and HFC-227ea has continued to increase over the measurement period, although HFC-143a and HFC-227ea have had periods

where the annual growth reduced briefly before then increasing in subsequent years. HFC-32 has shown the most rapid increase in growth of all the HFCs, but in 2020, for the first time, the NH annual growth is less than that for the previous year, which could be the first indication of a slow down. HFC-23 and HFC-245fa have, on average, increasing growth but they are not uniformly rising. Figure 23 shows that the growth of HFC-134a, since reaching a peak in 2017 in the NH and 2018 in the SH, has undergone a reduction in annual growth in both hemispheres, implying that the global emissions of this gas are currently falling. The SH annual growth is generally smaller than in the NH and the trend lags behind by 1–2 years.

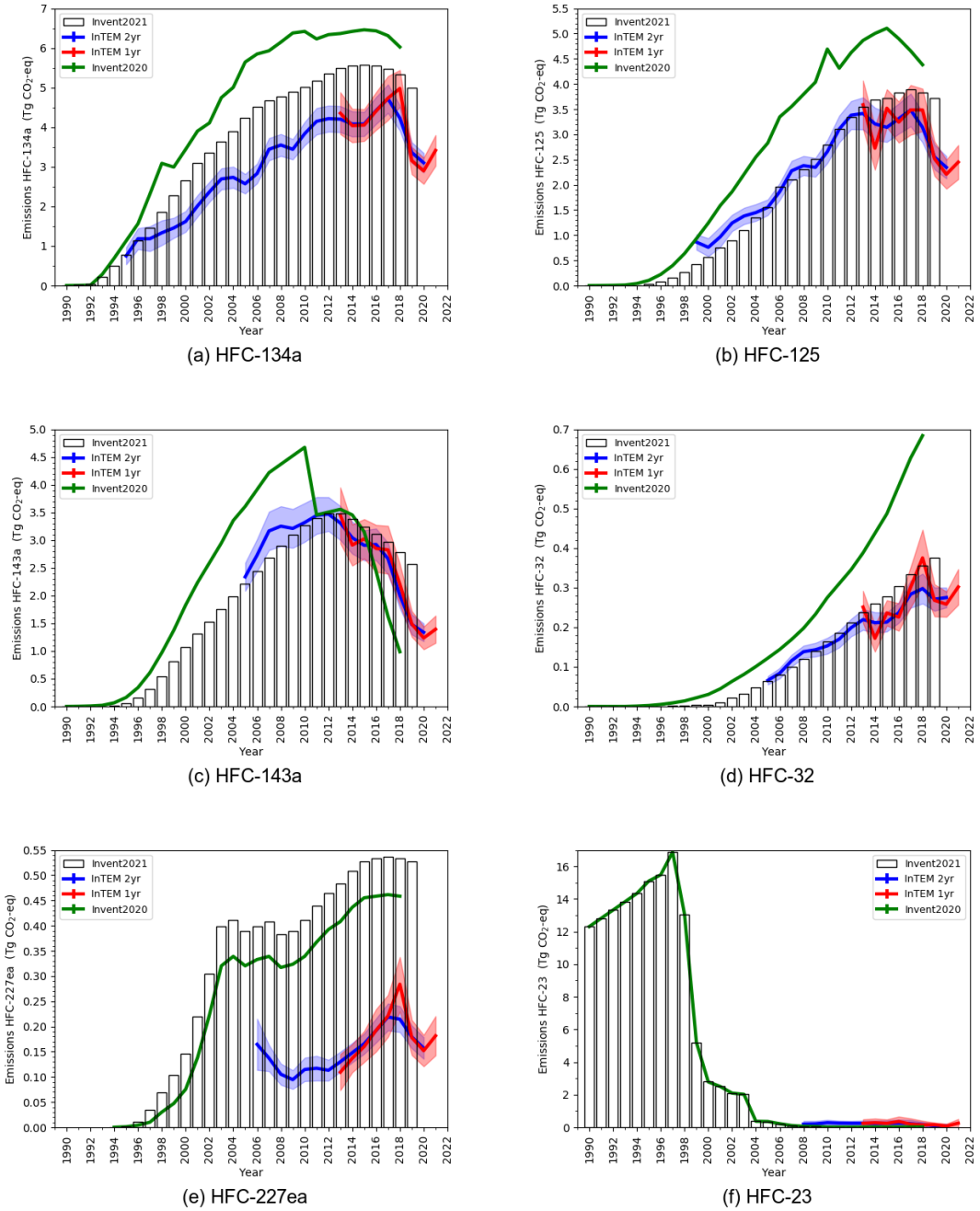

Figure 26: HFC UK emission estimates (Gg yr^{-1} CO_2-eq) from the 2021 UNFCCC inventory (black bars), 2020 UNFCCC inventory (green) and InTEM Annualised 2-year inversion (blue) Annual inversion (red). The shading represents 1-σ.

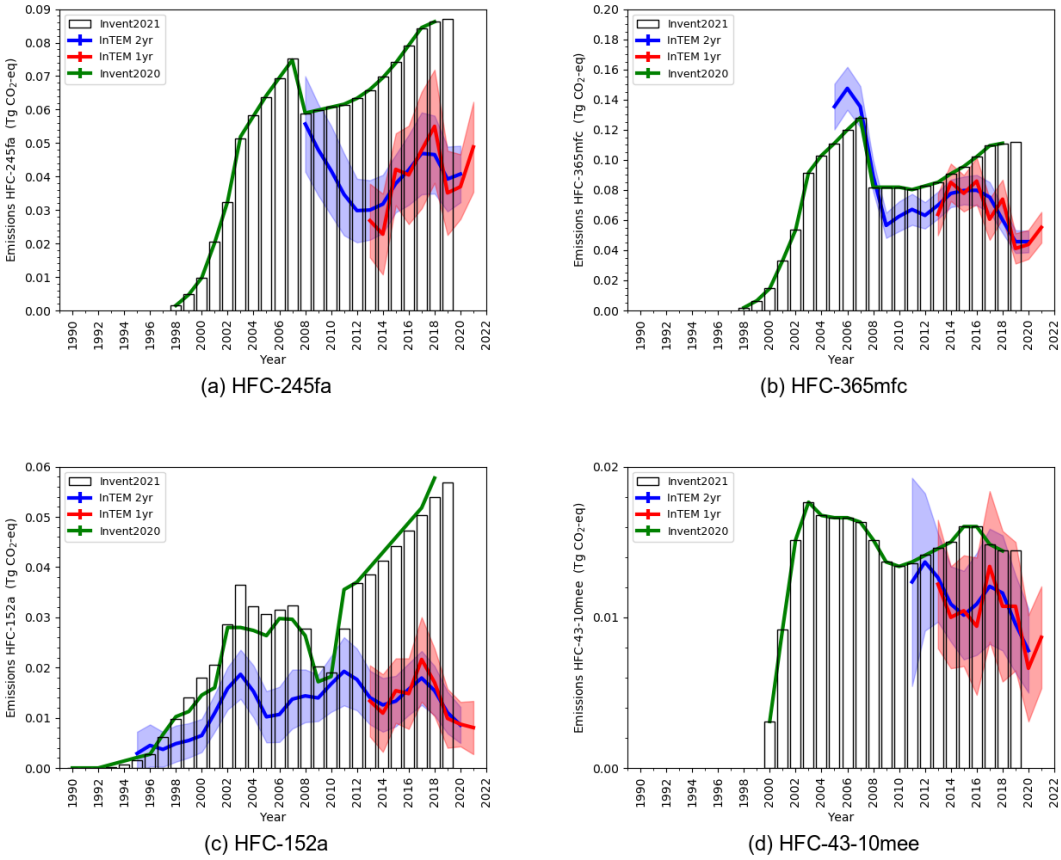

Figure 27: HFC UK emission estimates (Gg yr^{-1} CO_2-eq) from the 2021 UNFCCC inventory (black bars), 2020 UNFCCC inventory (green) and InTEM annualised 2-year inversion (blue) and annual inversion (red). The shading represents 1-σ.

Figures 26 and 27 show the UK InTEM estimated annual emissions up to and including 2021, (annualised 2-year inversion in blue and 1-year inversion in red) and the UK GHG Inventory (GHGI) 2021, as black bars, and UK GHGI 2020, in green, for all reported HFCs. Please note that no uncertainties are published for the individual HFCs in the UK GHGI estimates, only an estimate of total HFC uncertainty which is plotted in Figure 32. InTEM estimates that all of the UK HFC emissions have decreased over the last 2 years from 2018, however they are all (with the exception of HFC-152a) now showing an upturn in 2021. It should be noted however that the emissions for 2021 should be treated as provisional as they are based on only 8 months of provisional measurement data. The InTEM estimate is plotted against the most recent (2021) UK UNFCCC submission estimate whose latest data year is 2019 (black bars). There were significant revisions to the model used to estimate the UK UNFCCC HFC emissions which resulted in some substantial changes compared with the 2020 submission, shown as a green line in each plot. The revision in the refrigeration and air conditioning (RAC) inventory model was motivated by previous InTEM Vs GHGI comparisons and demonstrates the impact and importance of the measurement derived InTEM estimates presented

in this report. Please note that the recently published paper (Manning et al. 2021) shows the 2020 UK UNFCCC data as that was the latest available at the time of submission. There have been significant reductions in the reported GHGI emissions for HFC-134a, HFC-125, HFC-143a and HFC-32 and a slight increase in the emissions for HFC-227ea. The remaining HFC's are largely unchanged. Apart from HFC-227ea, these changes have led to a better agreement with the InTEM emission estimates. The InTEM decline in UK HFC-134a, HFC-143a and HFC-125 emissions is however faster than the GHGI predicts. For HFC-32 the inventory is increasing while InTEM flattens. There is a large disparity between InTEM and the GHGI for HFC-227ea, with InTEM estimating well under half that reported. For HFC-152a, HFC-365mfc and HFC-245fa the recent estimates are diverging when InTEM and the GHGI are compared, with the GHGI increasing and InTEM plateauing or decreasing and the 2019 values being more than 50% less than the GHGI. Emissions of HFC-23 have greatly reduced in the UK since the 1990's (Figure 26) and remained largely flat since 2004. Figure 28 shows the emissions from 2008.

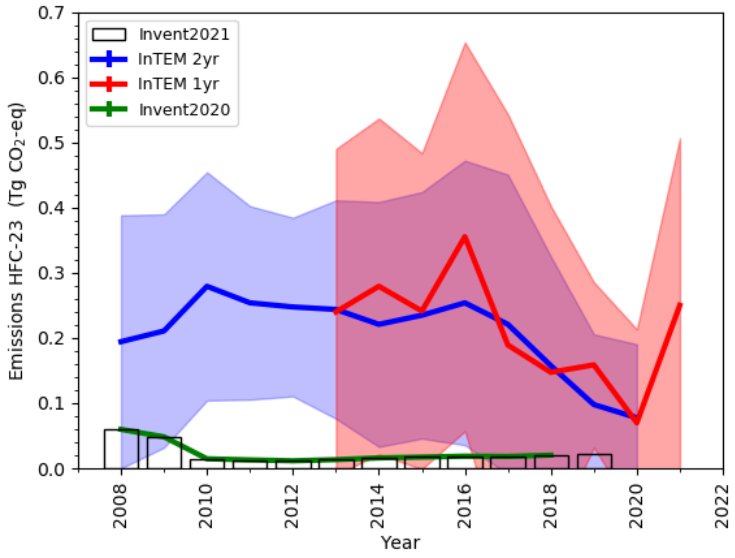

Figure 28: HFC-23 UK emission estimates from 2008 (Gg yr^{-1} CO_2-eq) from 2021 UNFCCC inventory (black bars), 2020 UNFCCC inventory (green) and InTEM annualised 2-year inversion (blue) and annual inversion (red). The shading represents 1-σ.

Figures 29, 30 and 31 show 4-year average InTEM emission maps (2017-2020) for the modelled HFCs. Plots on the left-hand panels show the wider European domain and the right-hand plots are zoomed over the UK (same scale). Please note the scale varies between gases. The maps show that the model predicts the largest emission sources for HFC-134a, HFC-143a, HFC-125, HFC-32 and HFC-152a to be from central and southern regions of the UK, largely following population over this period. HFC-227ea has high emission estimates in the UK, Belgium and the Netherlands. HFC-23 has relatively low emissions over the UK compared with those seen in Germany, the south-

east of France and Northern Italy. Emissions of HFC-23 have greatly reduced in Europe since the 1990's and have remained flat since 2004. HFC-245fa, HFC-365mfc and HFC-43-10mee estimate the largest emissions are coming from Belgium and the Netherlands.

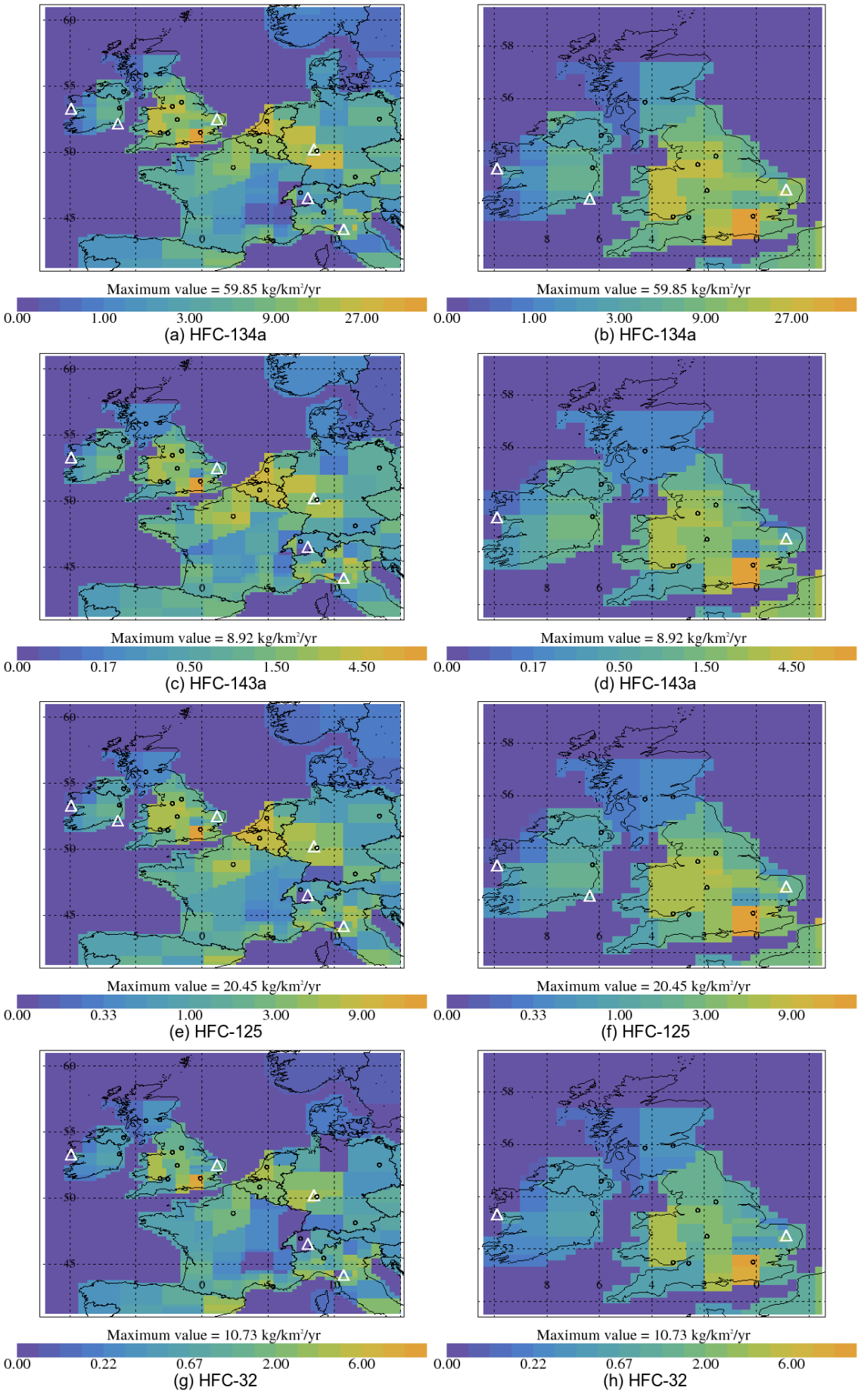

Figure 29: InTEM emission estimates (kg km^{-2} yr^{-1}) for 2017-2020 for NW Europe (left) and the UK and Ireland (right)

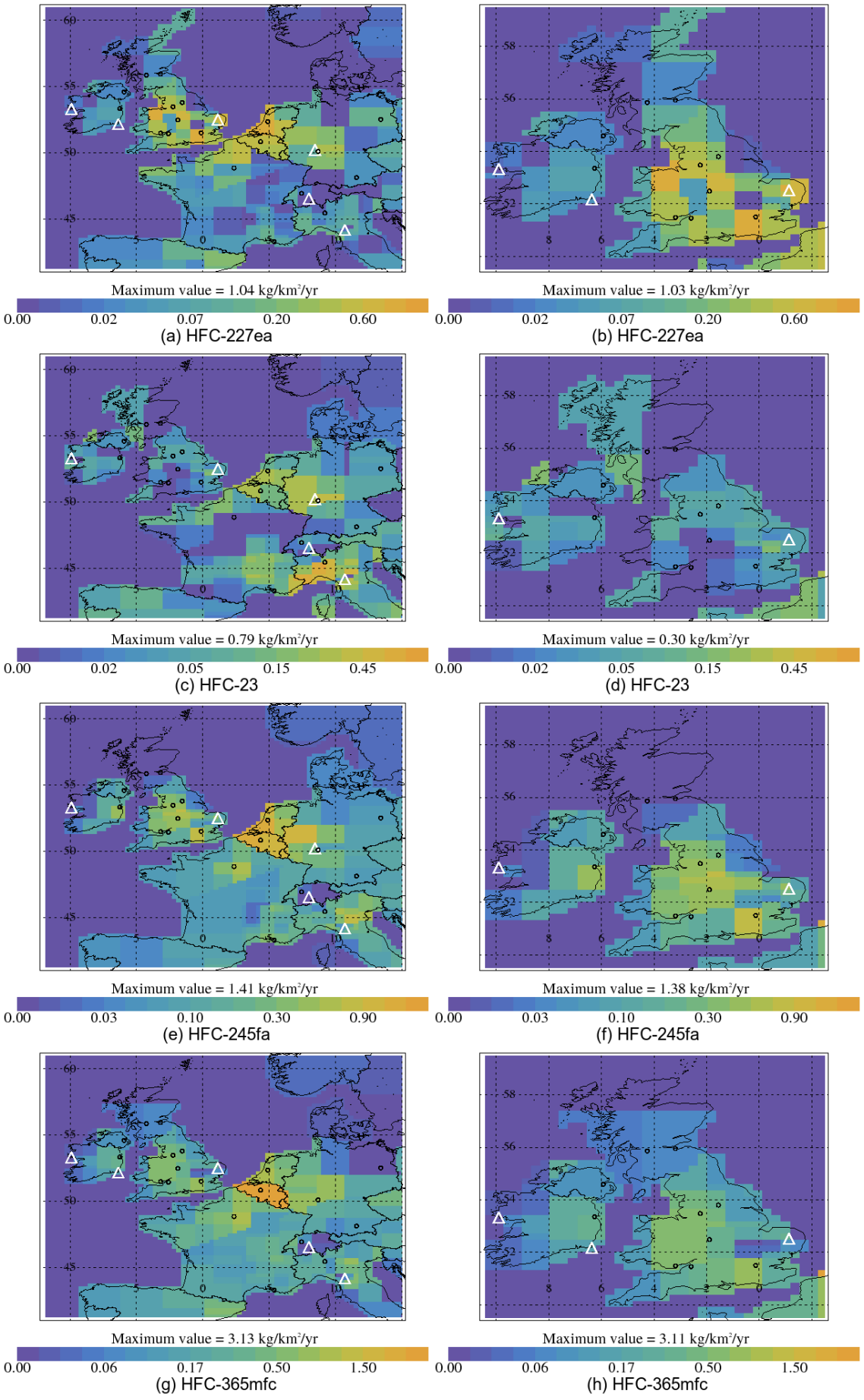

Figure 30: InTEM emission estimates (kg km^{-2} yr^{-1}) for 2017-2020 for NW Europe (left) and the UK and Ireland (right)

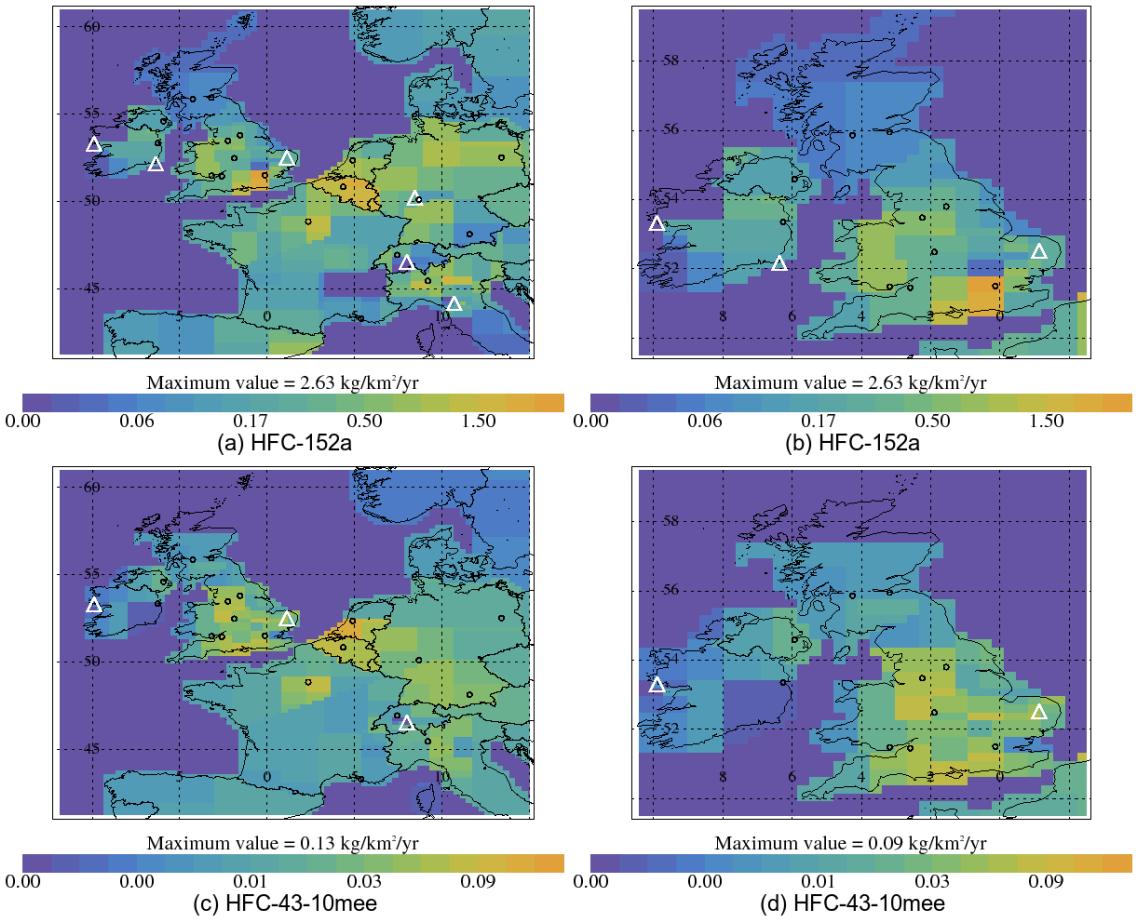

Figure 31: InTEM emission estimates (kg km^{-2} yr^{-1}) for 2017-2020 for NW Europe (left) and the UK and Ireland (right)

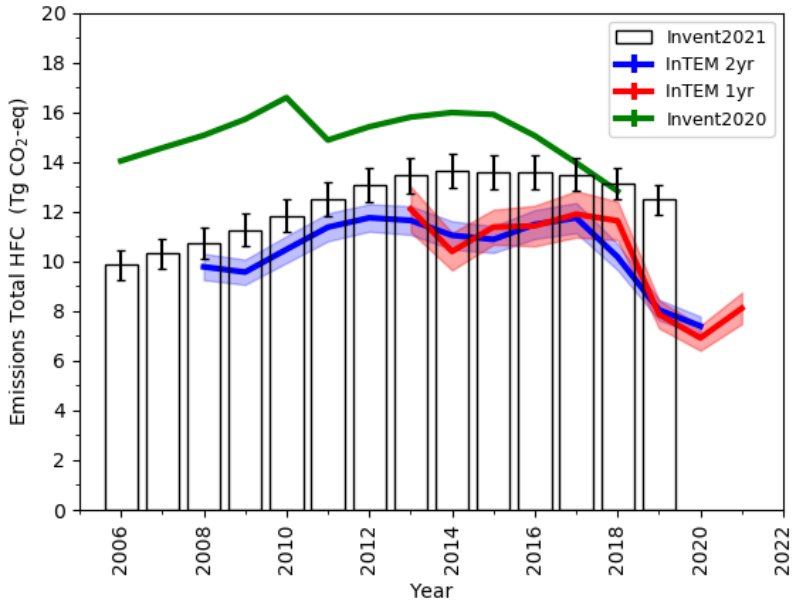

Figure 32: Total UK HFC emission estimates (HFC-125, HFC-134a, HFC-143a, HFC-152a, HFC-23, HFC-32, HFC-227ea, HFC-245fa, HFC-365mfc and HFC-43-10mee) in Tg CO_2-eq yr^{-1} from the UK inventory submitted to the UNFCCC in 2021 (black), 2020 UNFCCC inventory (green), InTEM annualised 2-year inversion (blue) and InTEM 1-year inversion (red). The uncertainty shown represents 1 σ.

All of the HFCs modelled, weighted by their GWP_{100} values, have been combined to estimate a total UK HFC emission estimate in Tg CO_2-eq yr^{-1} (Figure 32). Note that due to the start date of the measurement of HFC-43-10mee, it is only included in the InTEM value from 2011 onwards, however its contribution ($\sim$ 0.01 Tg CO_2-eq yr^{-1}) is close to negligible. The total GHGI HFC emission for the UK reported in April 2021 is shown as black bars. The total GHGI HFC emission for the UK reported in April 2020 (and shown in the 2020 annual contract report) is shown as a green line. There has been a downwards shift in the total HFC emissions between the two reported GHGI inventories of $\sim$ 4 Tg CO_2-eq yr^{-1} in 2006-2010, $\sim$ 2 Tg CO_2-eq yr^{-1} in 2011-2015, with the shift lessening from 2016-2017 to virtually nothing in 2018. This shift in the GHGI has resulted in a much closer agreement with the InTEM total HFC emissions estimates. The InTEM estimates are consistently lower than the GHGI 2008-2019. The closest agreement is from 2008-2012, after which the InTEM estimates decrease for a few years before rising again to a peak in 2017. The GHGI continues to rise until 2014, where it plateaus until it begins to decrease in 2018 and 2019. The least good agreement is in 2019 where the reported total HFC is $\sim$ 12.5 Tg CO_2-eq yr^{-1} compared to the InTEM estimate of $\sim$ 8.0 Tg CO_2-eq yr^{-1}. The InTEM 1-year estimate for 2021 indicates an increase of $\sim$ 1.0 Tg CO_2-eq yr^{-1} compared with the 2020 value, though it is too soon to infer any definite change of trend as this number is only based on 8 months of data and thus should be considered provisional.

6.9 Perfluorocarbons (PFCs)

Globally, atmospheric mole fractions of all the PFC's are increasing. They all have long atmospheric lifetimes and high GWP_{100}s (Table 5). They originate as by-products from the production of aluminium and from the electronic and semi-conductor industries. The NH atmospheric mole fraction of PFC-14, Figure 33, is increasing at an average rate of $\sim$ 0.8 ppt yr^{-1} over the measurement period (2006-2021). There is evidence of a significant drop in growth after the 2008 financial crisis, but it has since increased its growth to a level greater than 0.9 ppt yr^{-1}. On average the global atmospheric mole fraction of PFC-116 is increasing at $\sim$ 0.08 ppt yr^{-1}, PFC-218 at $\sim$ 0.018 ppt yr^{-1} and PFC-318 at $\sim$ 0.059 ppt yr^{-1} (Figure 33).

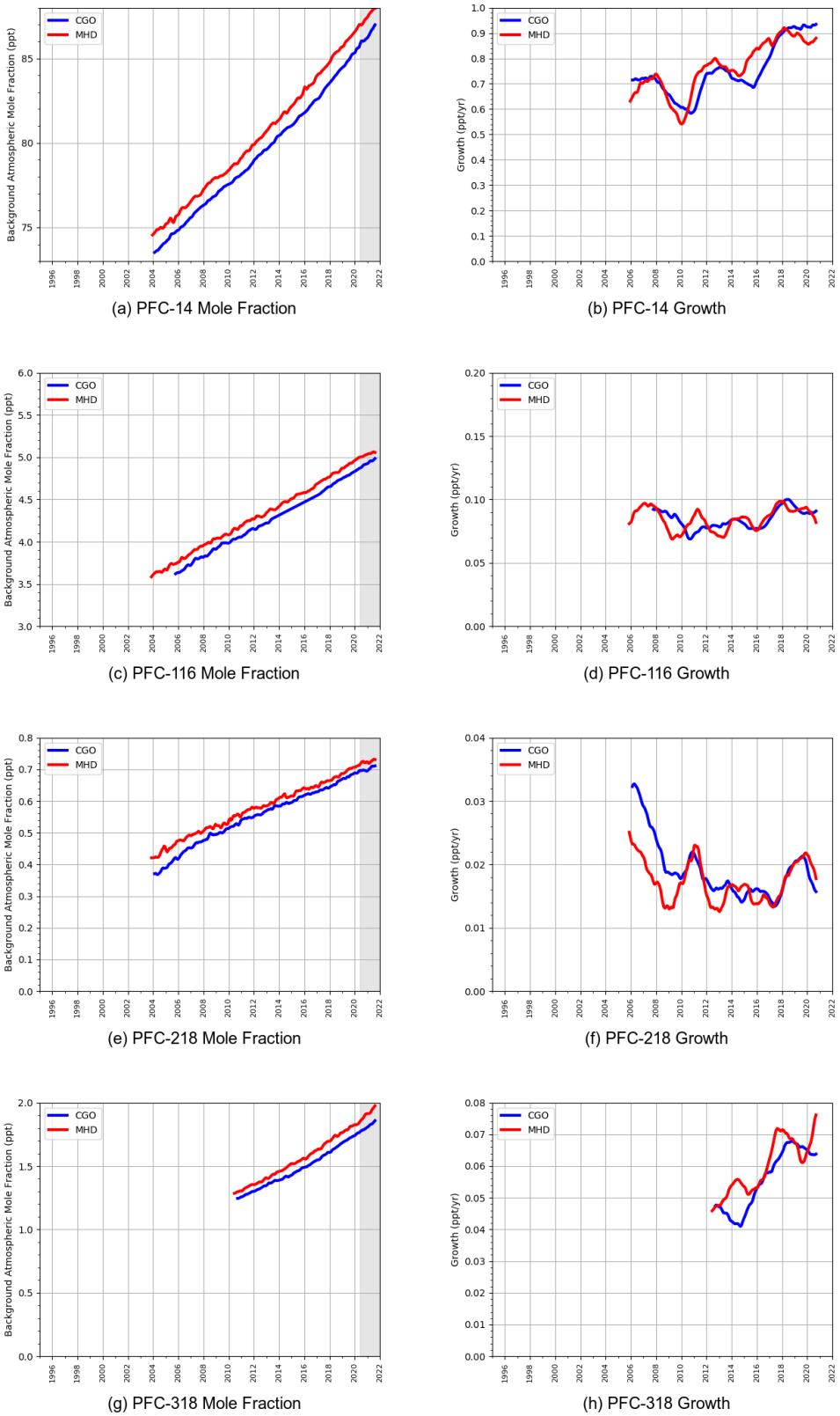

Figure 33: Northern (red) and Southern (blue) Hemisphere atmospheric background levels (left) and rates of increase (right) as observed at the Mace Head, Ireland and Cape Grim, Australia measurement stations. Grey shaded area represents un-ratified provisional data.

Figure 34 shows the UK InTEM and reported GHGI emissions of the PFCs. The emissions of these gases have been quite stable at low levels for the last few years, however there is a slight upturn seen in the 2021 estimates in all four gases, as was seen in the HFCs. As 2021 is incomplete, and the observational data provisional, it is not possible to draw any conclusions from this as yet.

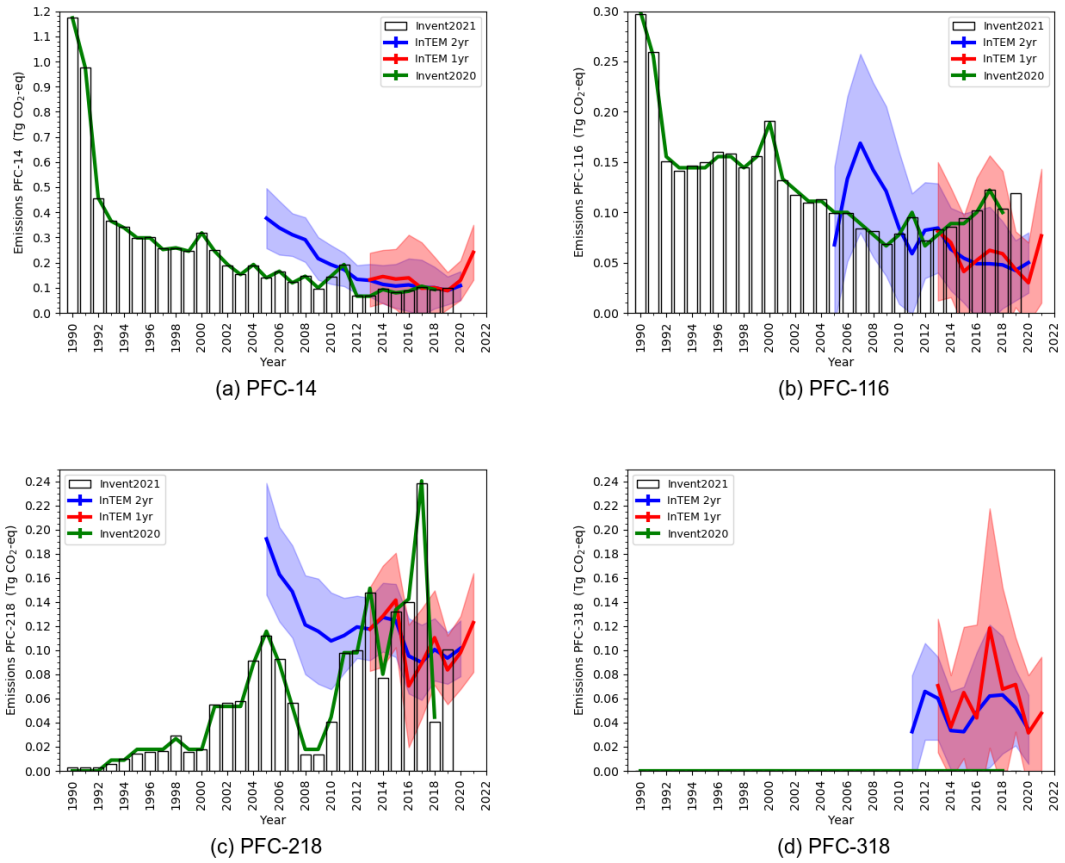

Figure 34: PFC UK emission estimates (Gg yr^{-1} CO_2-eq) from the 2021 UNFCCC inventory (black bars), 2020 UNFCCC inventory (green) and InTEM annualised 2-year inversion (blue) and annual inversion (red). The shading represents 1-σ.

InTEM estimates larger PFC-14 emissions than the GHGI for the UK from 2005-2009, but with reasonable agreement thereafter with the InTEM uncertainty range encompassing the reported GHGI value. Both InTEM and UK GHGI show largely flat UK emissions of PFC-14 in the last few years, however InTEM results show a slight increase in 2020. The PFC-116 InTEM uncertainties encapsulate UK GHGI estimates in all reporting years except for the most recently reported year, 2019. InTEM shows a decline in UK emissions from 2013 that is not seen in the reported GHGI values which are generally increasing. InTEM PFC-218 estimates significantly larger emissions than the UK GHGI between 2005 - 2010 with reasonable agreement thereafter, however the InTEM estimates remain flatter and do not replicate the very high value reported in 2017, or the very low value in 2018. The InTEM and GHGI values however agree well in 2019. The UK GHGI reports

very low emissions of PFC-318. The InTEM estimates are not statistically greater than zero in most years, i.e. the 1-σ uncertainty reaches to zero.

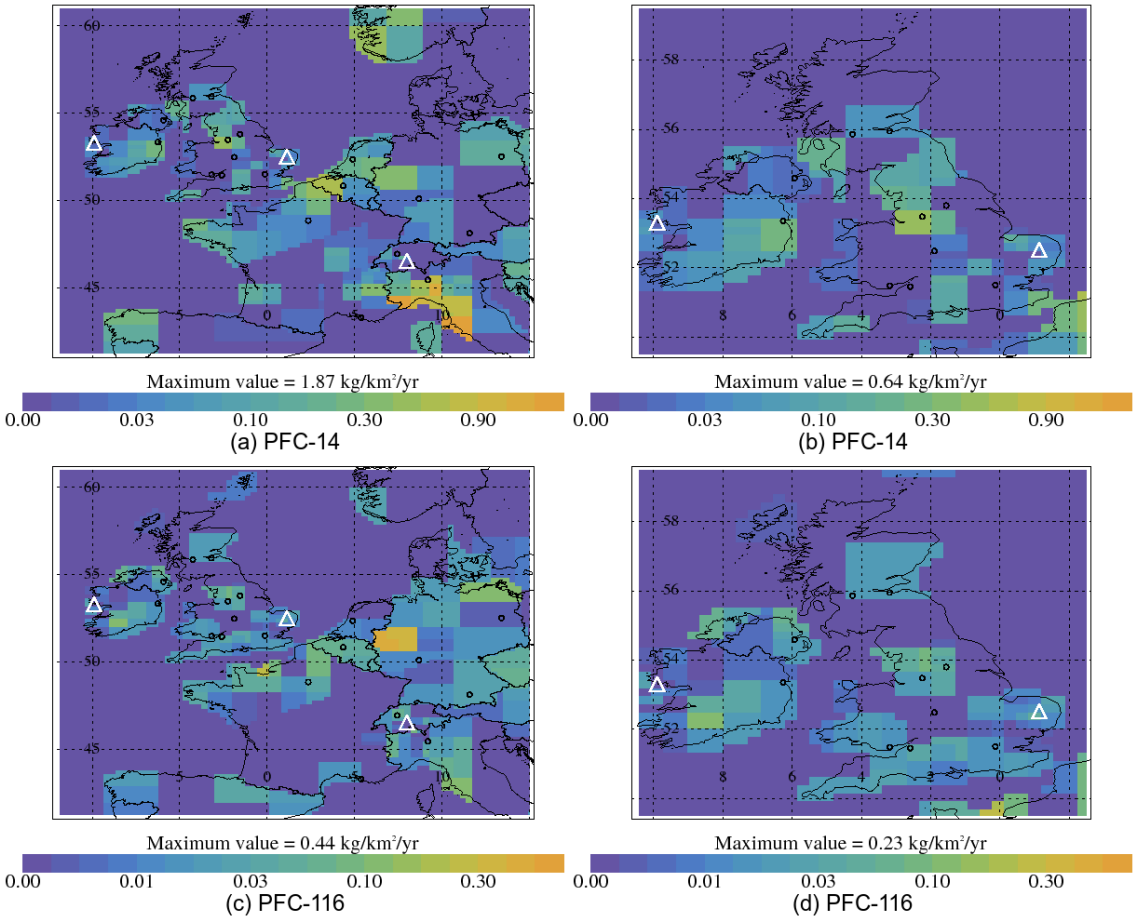

Figure 35: InTEM PFC-14 and PFC-116 emission estimates (kg km^{-2} yr^{-1}). Panels (b) and (d) are panels (a) and (c) respectively zoomed in over the UK. Note each species has its own scale.

Figures 35 and 36 show 4-year average InTEM emission maps (2017-2020) for the four PFCs. Plots on the left-hand panels show the wider European domain and the right-hand plots are zoomed over the UK (same scale). Please note the scale varies between gases. The emission map for PFC-14 shows a strong source from north-west Italy. In the UK the highest emissions are coming from an area in the north-west of England. The emission map for PFC-116 shows elevated emissions from the Ruhr Valley, Germany, as well as a region on the northern French coastline near the port of Le Havre. The main emission of PFC-218 is from the north-west of England and the strongest source of PFC-318 is the Benelux region.

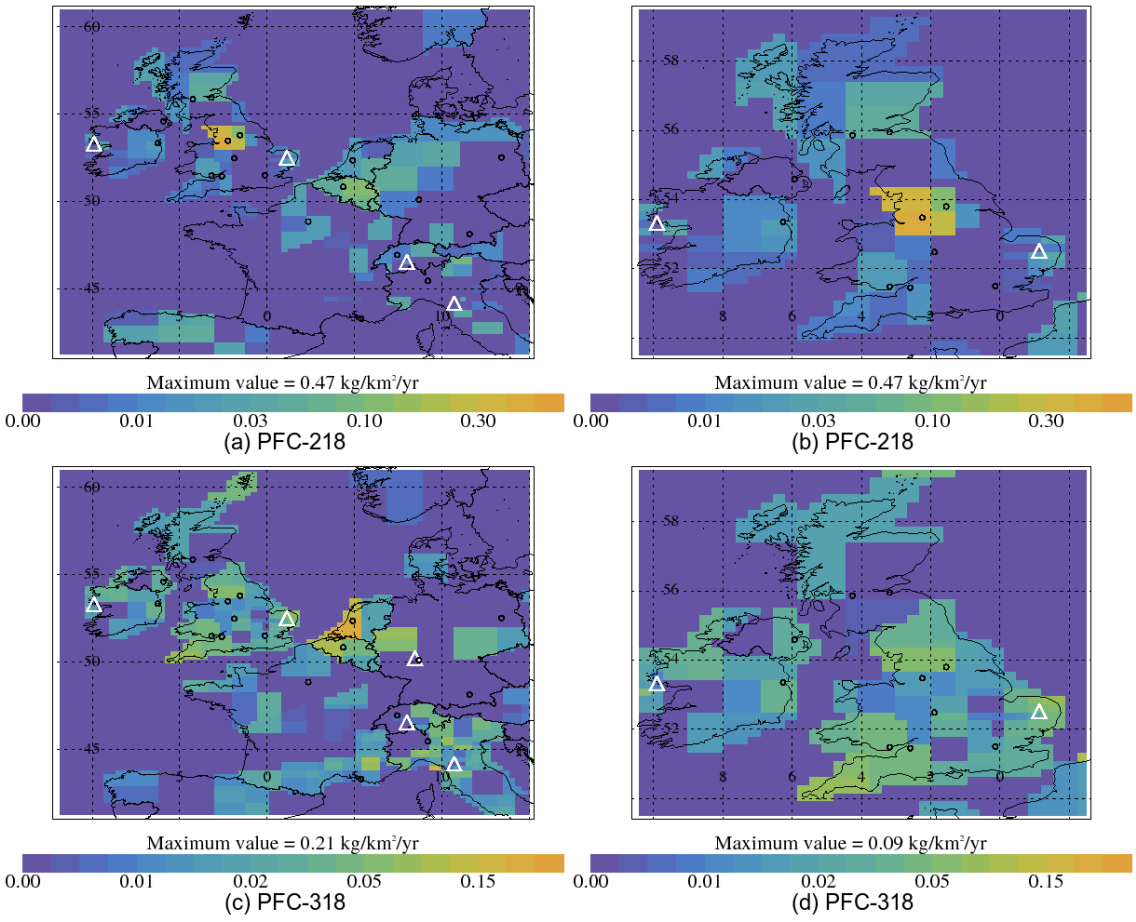

Figure 36: InTEM PFC-218 and PFC-318 emission estimates (kg km^{-2} yr^{-1}). Panels (b) and (d) are panels (a) and (c) respectively zoomed in over the UK. Note each species has its own scale.

All of the PFCs, weighted by their GWP_{100} values, have been combined to estimate a total UK PFC emission estimate in Tg CO_2-eq yr^{-1} which is shown in Figure 37. The InTEM estimates are initially higher than the reported GHGI values (2005-2010) but in more recent years the total PFC estimates have compared well and are largely level.

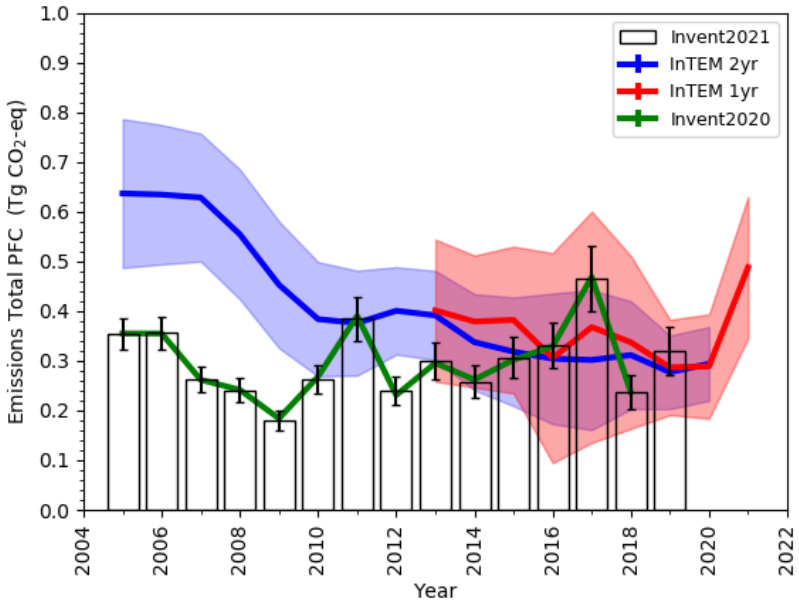

Figure 37: Total UK PFC emission estimates (PFC-14, PFC-116, PFC-218 and PFC-318) in Tg CO_2-eq yr^{-1} from the UK inventory submitted to the UNFCCC in 2021 (black), 2020 UNFCCC inventory (green), InTEM annualised 2-year inversion (blue) and InTEM 1-year inversion (red). The uncertainty shown represents 1 σ.

6.10 Nitrogen trifluoride (NF_3)

NF_3 is used in the manufacture of semiconductors, flat panel displays and photovoltaic cells. Although the current contribution of NF_3 to radiative forcing is small, its potential to impact the climate is significant (see Table 5). NF_3 is steadily increasing in the atmosphere (Figure 38). UK emissions reported in the GHGI are very small and this is in line with what is observed in the atmosphere. The InTEM results for the UK are very small and uncertain (Figure 39).

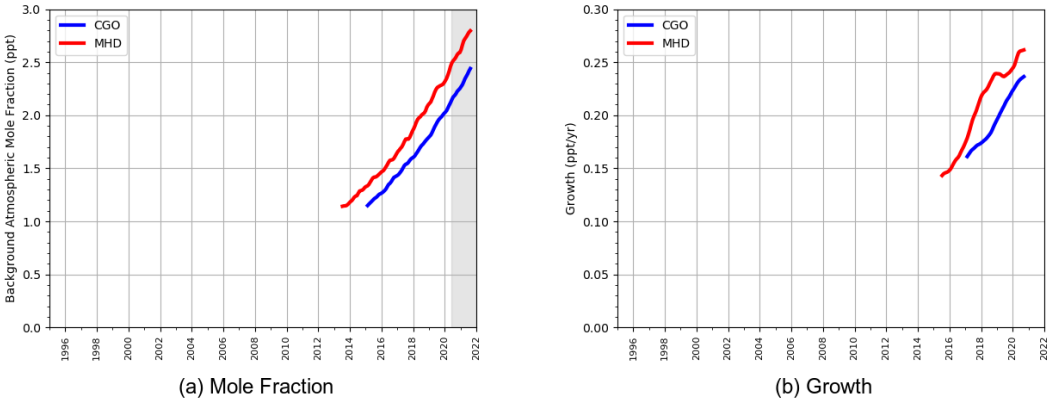

Figure 38: Northern (red) and Southern (blue) Hemisphere atmospheric background levels (left) and rates of increase (right) as observed at the Mace Head, Ireland and Cape Grim, Australia measurement stations. Grey shaded area represents un-ratified provisional data.

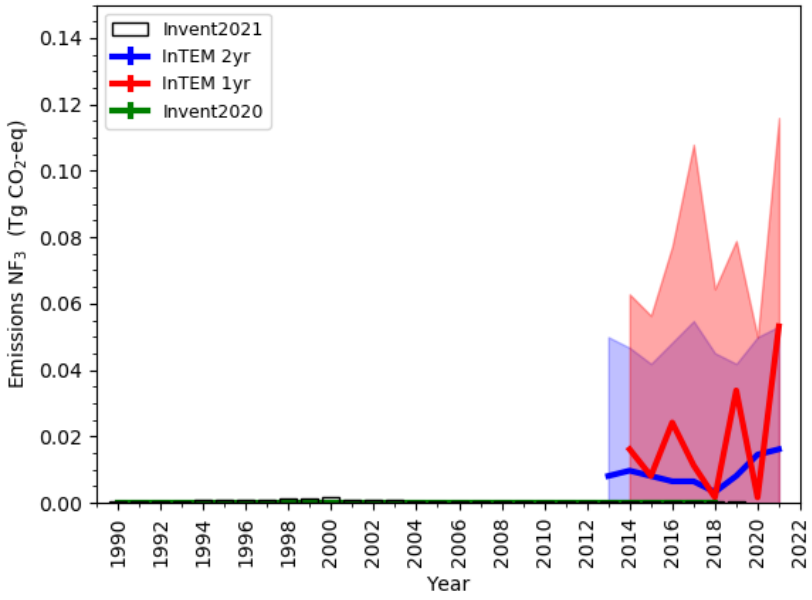

Figure 39: NF_3 UK emission estimates (Gg yr^{-1} CO_2-eq) from the 2021 UNFCCC inventory (black bars), 2020 UNFCCC inventory (green) and InTEM annualised 2-year inversion (blue) and annual inversion (red). The shading represents 1-σ.

6.11 Hydrogen (H_2)

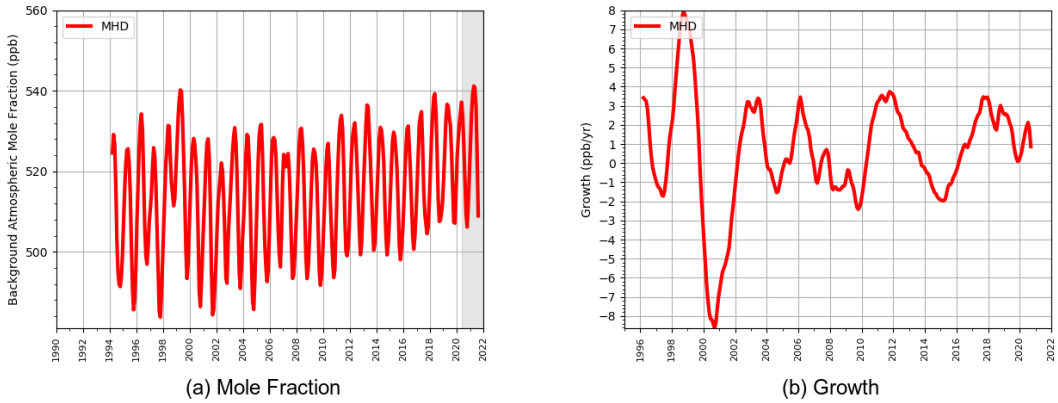

Figure 40: Northern (red) Hemisphere atmospheric background levels (left) and rates of increase (right) as observed at the Mace Head, Ireland measurement station. Grey shaded area represents un-ratified provisional data.

Hydrogen mole fractions have gradually increasing in the NH atmosphere over the last two decades. There are however strong year to year variations in growth. The large growth in the late 1990s is related to the huge fires in Indonesia in 1998 and 1999.

6.12 Chlorofluorocarbons (CFCs)

The global atmospheric mole fractions of CFC-11, CFC-12 and CFC-113 (Figure 41) are continuing to fall. The inter-hemispheric gradient of CFC-11, that widened 2013-2018, has now virtually disappeared, one of the indications that the extra emissions of CFC-11, 40-60% of which were identified as emanating from Eastern China, have ceased (Montzka et al. 2021; Park et al. 2021). CFC-114 and CFC-115 (Figure 42) have global mole fractions that are flat and growing respectively. Figure 43 shows the InTEM emissions estimates for CFC-11 and CFC-12, left-hand plots from 1990 and right-hand plots from 2000.

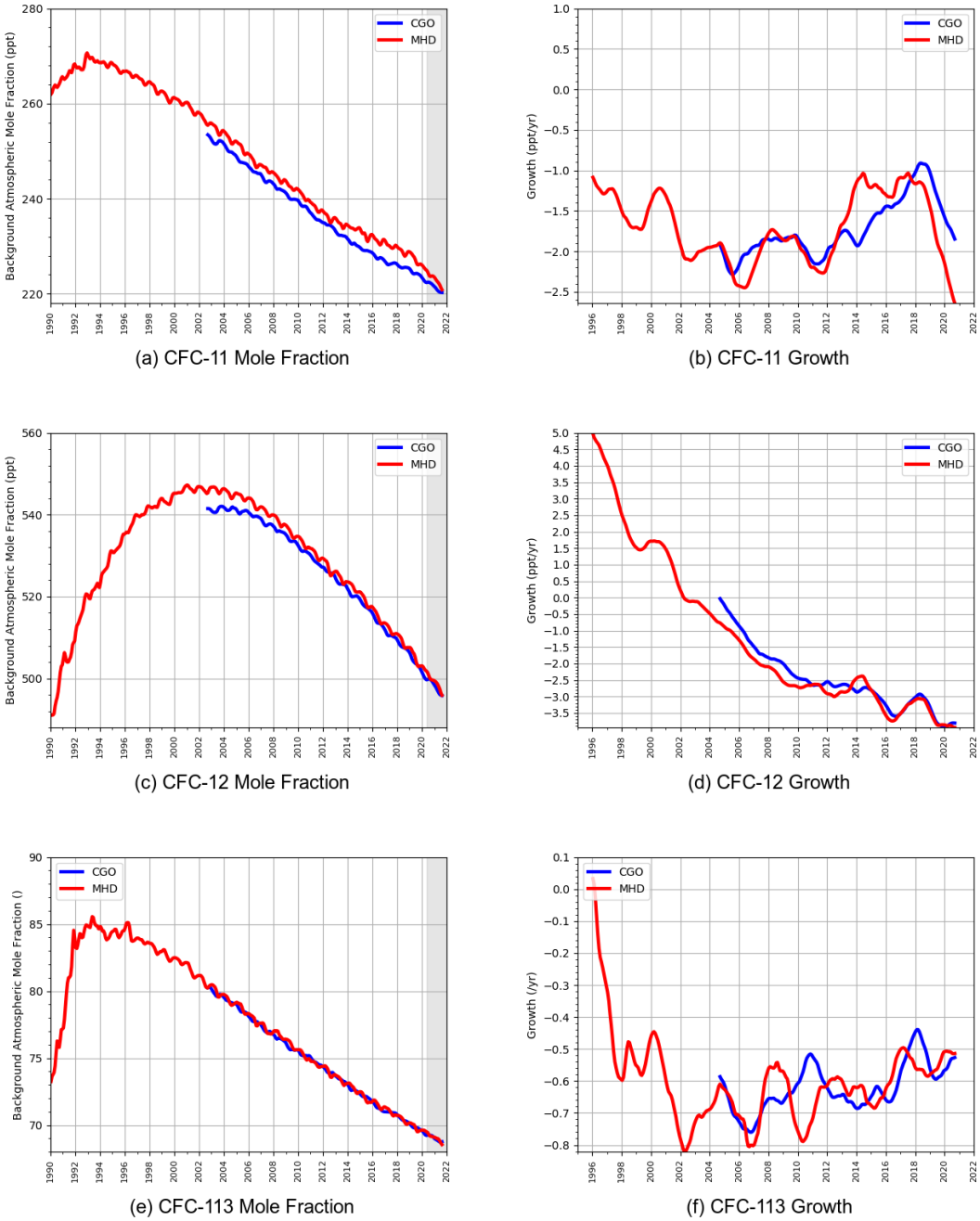

Figure 41: Northern (red) and Southern (blue) Hemisphere atmospheric background levels (left) and rates of increase (right) as observed at the Mace Head, Ireland and Cape Grim, Australia measurement stations. Grey shaded area represents un-ratified provisional data.

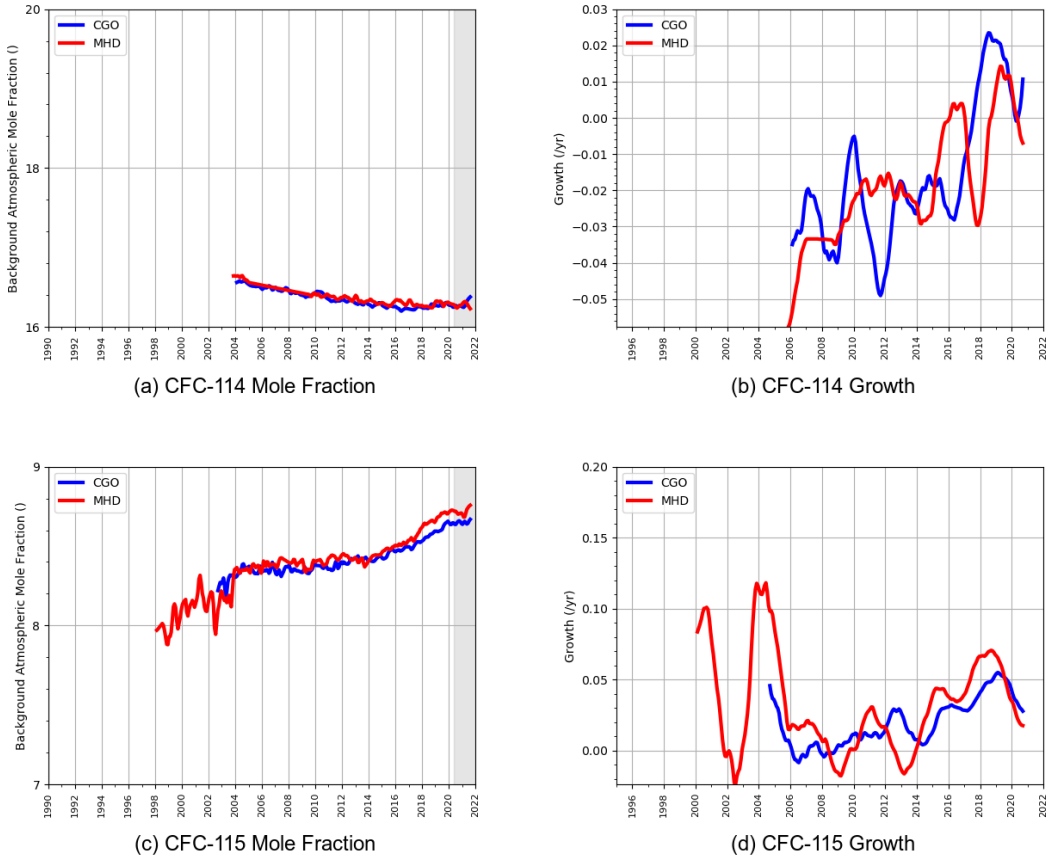

Figure 42: Northern (red) and Southern (blue) Hemisphere atmospheric background levels (left) and rates of increase (right) as observed at the Mace Head, Ireland and Cape Grim, Australia measurement stations. Grey shaded area represents un-ratified provisional data.

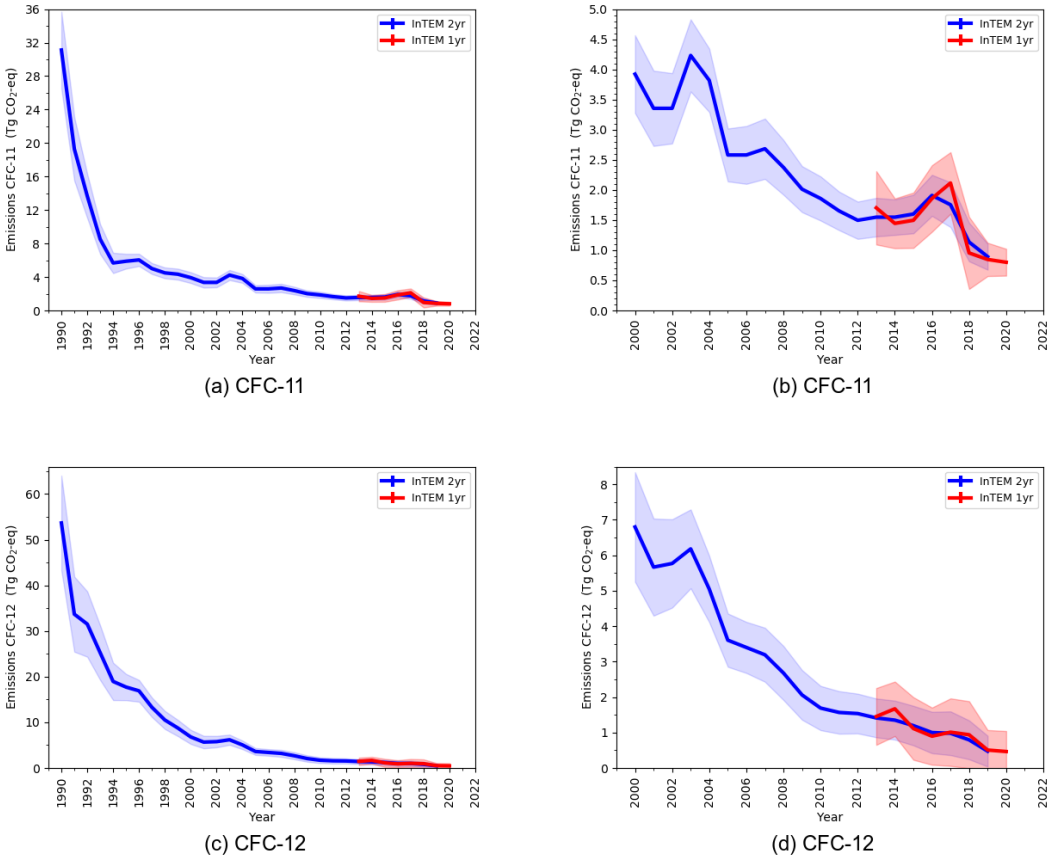

Figure 43: CFC UK emission estimates (Gg yr^{-1} CO_2-eq) from InTEM annualised 2-year inversion (blue) and annual inversion (red). The shading represents 1-σ. Left plot 1990-2021 and the right expanded x-axis, 2000-2021

6.13 Hydrochlorofluorocarbons (HCFCs)

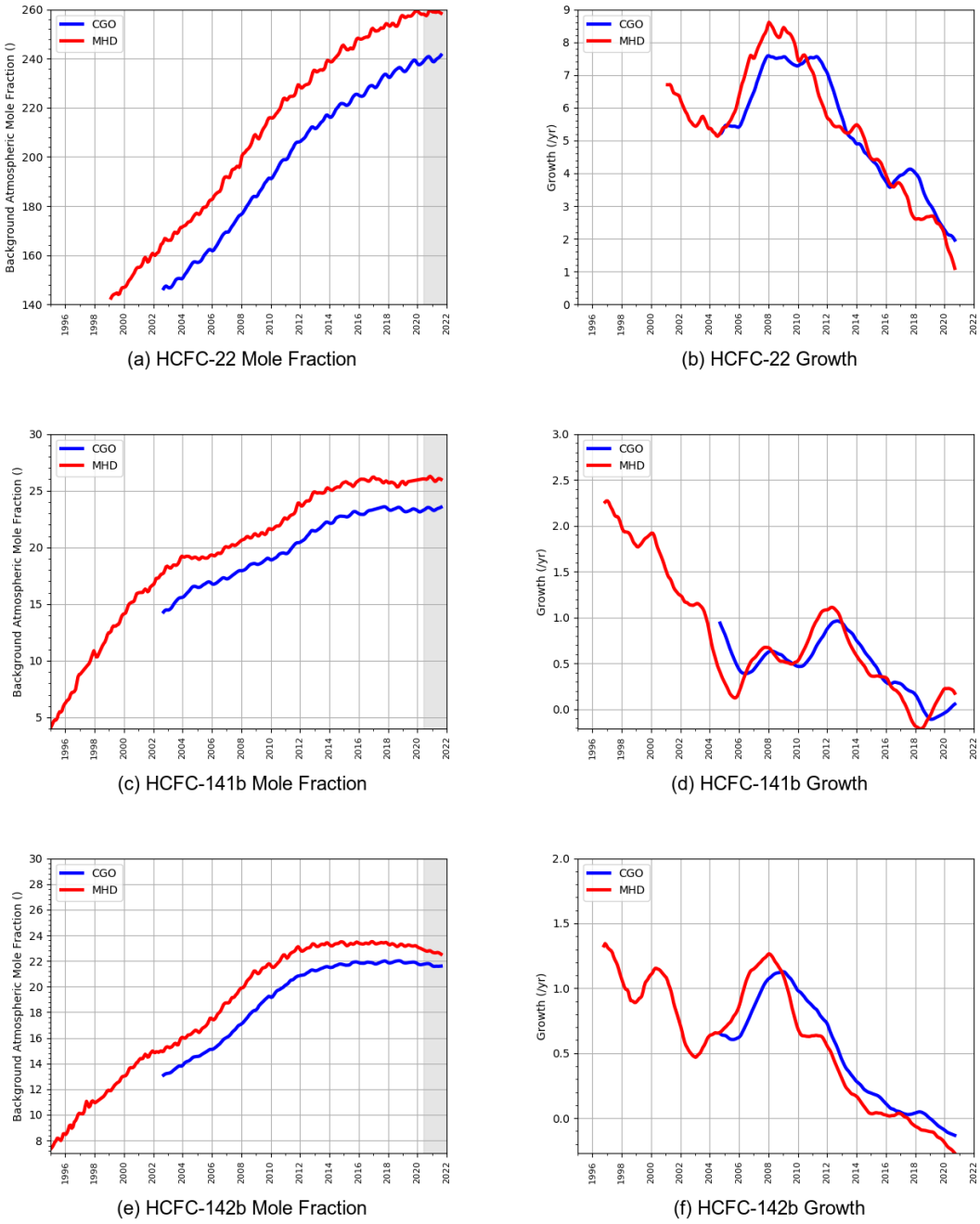

Figure 44: Northern (red) and Southern (blue) Hemisphere atmospheric background levels (left) and rates of increase (right) as observed at the Mace Head, Ireland and Cape Grim, Australia measurement stations. Grey shaded area represents un-ratified provisional data.

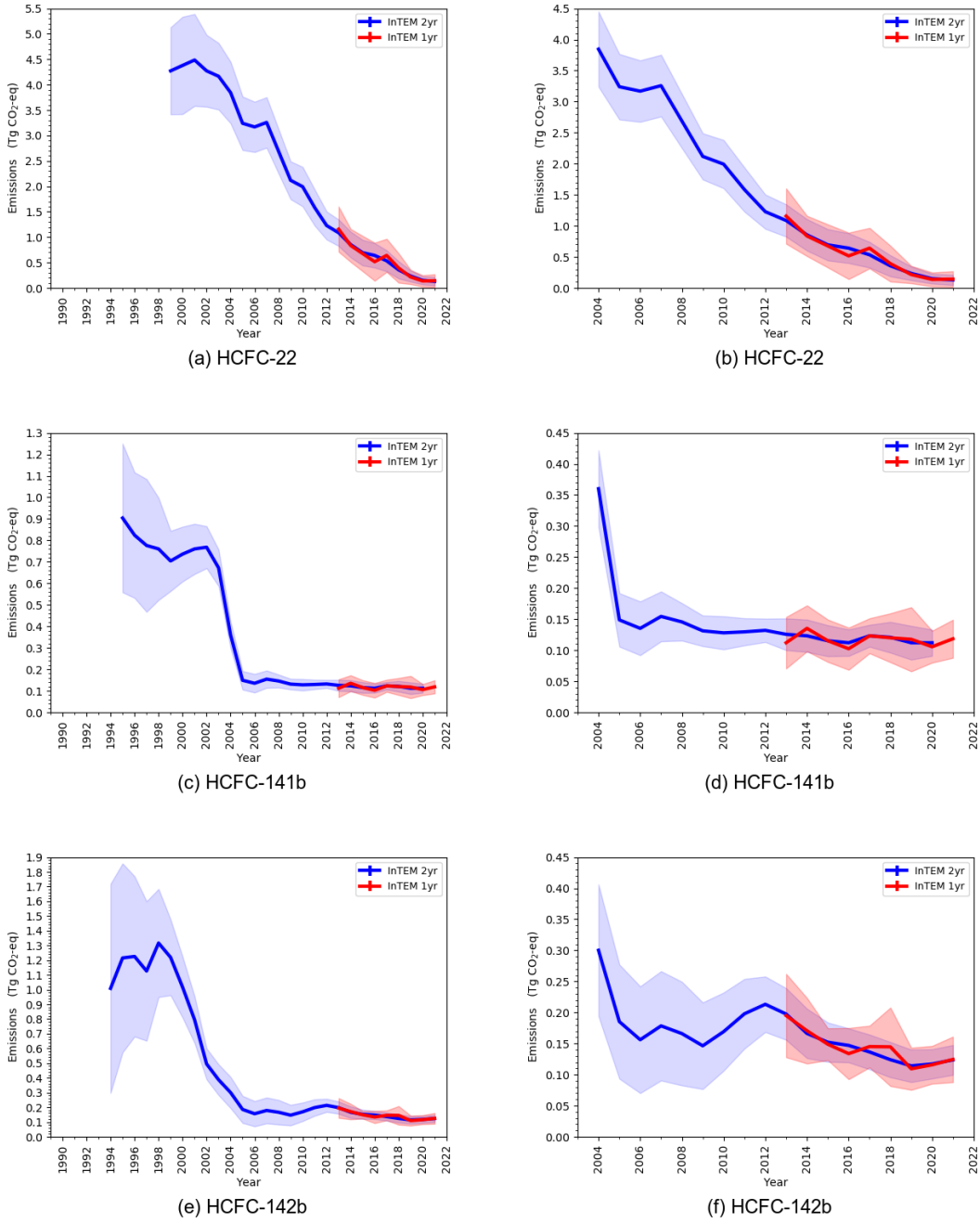

Figure 45: HCFC UK emission estimates (Gg yr^{-1} CO_2-eq) from InTEM annualised 2-year inversion (blue) and annual inversion (red). The shading represents 1-σ. Left plot 1990-2021 and the right expanded x-axis, 2004-2021

Figure 44 shows the global atmospheric mole fractions of HCFC-22, HCFC-141b and HCFC-142b (left-hand plots) and their respective growths (right-hand plots). HCFC-22 is still growing in the atmosphere however HCFC-141b has levelled off and HCFC-142b has started to decline. InTEM UK emission estimates (Figure 45) show that UK HCFC-22 emissions have decreased steadily since

2000, and that UK HCFC-142b emissions rapidily declined 1999-2005, then plateaued, and then slowly declined from 2012. UK HCFC-141b emissions fell very sharply 2002-2005 but have since largely remained constant.

6.14 Chlorocarbons

Global mole fractions of carbon tetrachloride (CCl_4) and methyl chloroform (CH_3CCl_3), both strong ozone-depleting gases, are continuing to decrease in the atmosphere, as seen in Figure 46. The mole fraction of CH_3CCl_3 is now nearly negligible. Figure 47 shows the UK InTEM emissions estimates of each gas, both show sharp declines in the 1990s followed by continuing modest declines in the last two decades.

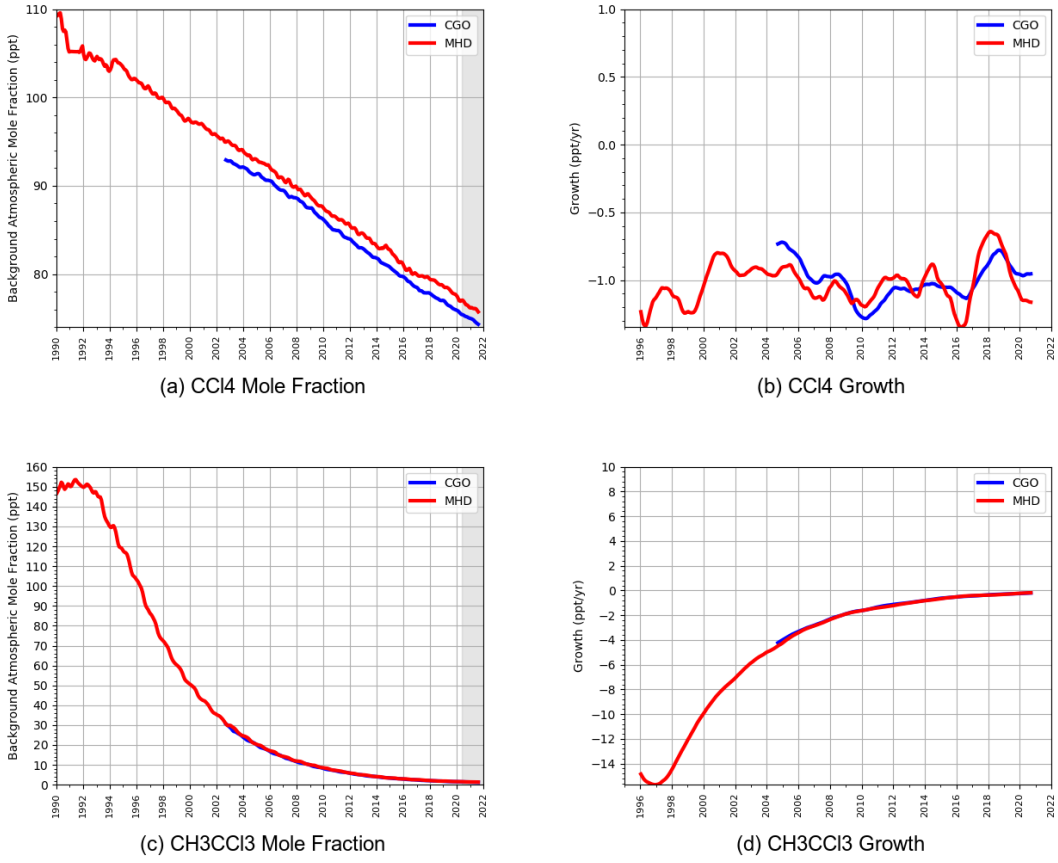

Figure 46: Northern (red) and Southern (blue) Hemisphere atmospheric background levels (left) and rates of increase (right) as observed at the Mace Head, Ireland and Cape Grim, Australia measurement stations. Grey shaded area represents un-ratified provisional data.

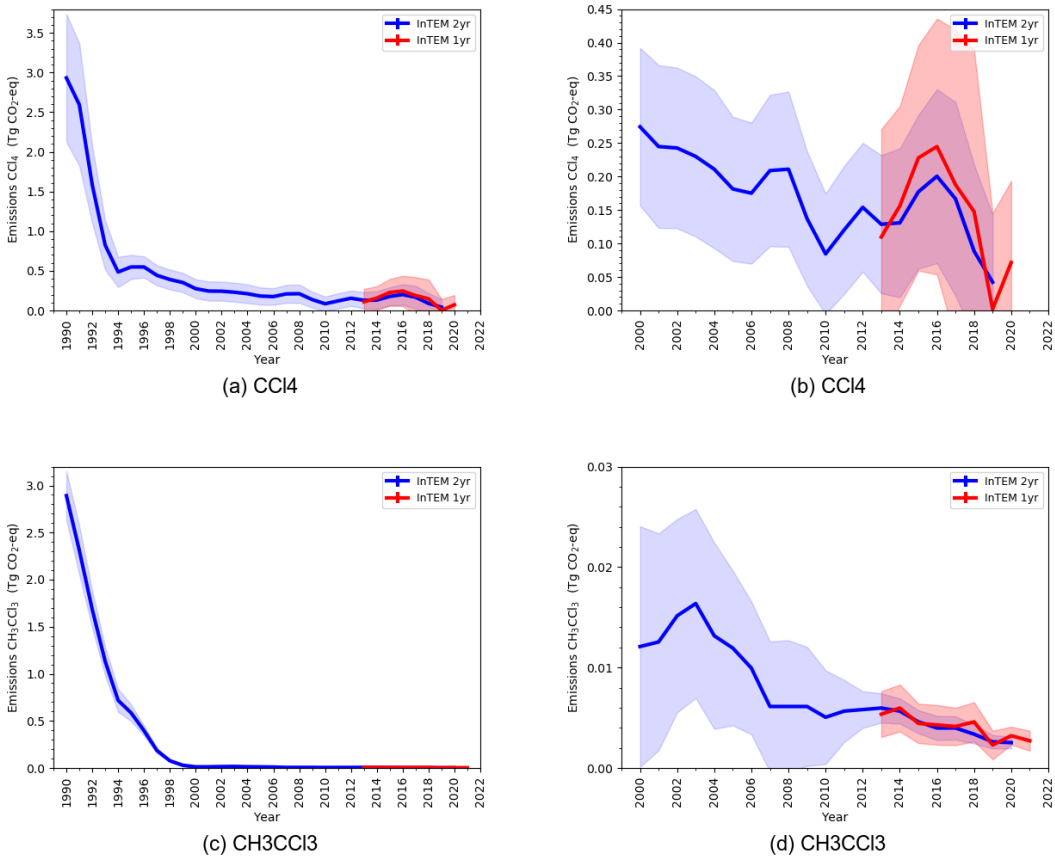

Figure 47: Carbon tetrachloride and methyl chloroform UK emission estimates (Gg yr^{-1} CO_2-eq) from InTEM annualised 2-year inversion (blue) and annual inversion (red). The shading represents 1-σ. Left plot 1990-2021 and the right expanded x-axis, 2000-2021

6.15 Halons

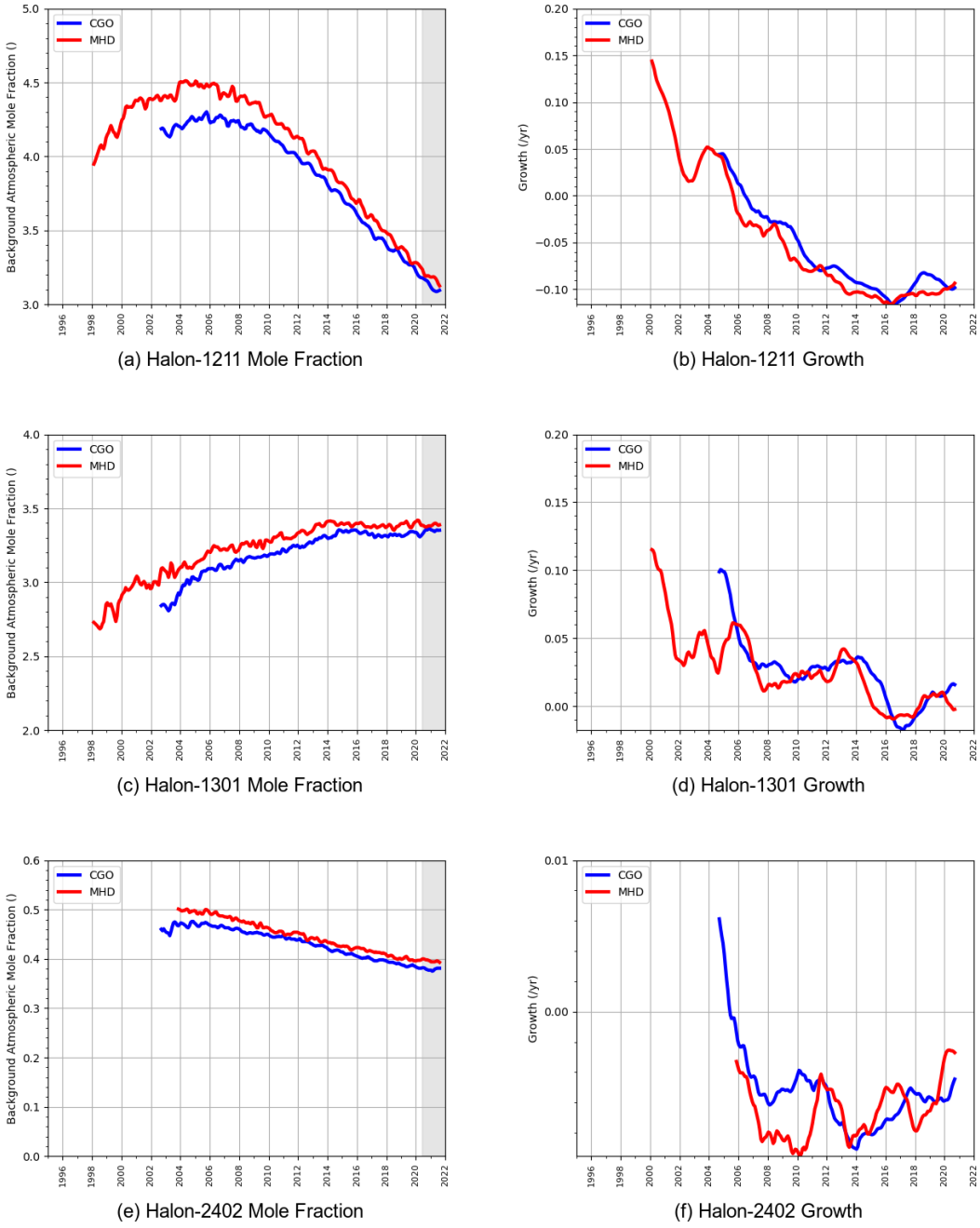

Figure 48: Northern (red) and Southern (blue) Hemisphere atmospheric background levels (left) and rates of increase (right) as observed at the Mace Head, Ireland and Cape Grim, Australia measurement stations. Grey shaded area represents un-ratified provisional data.

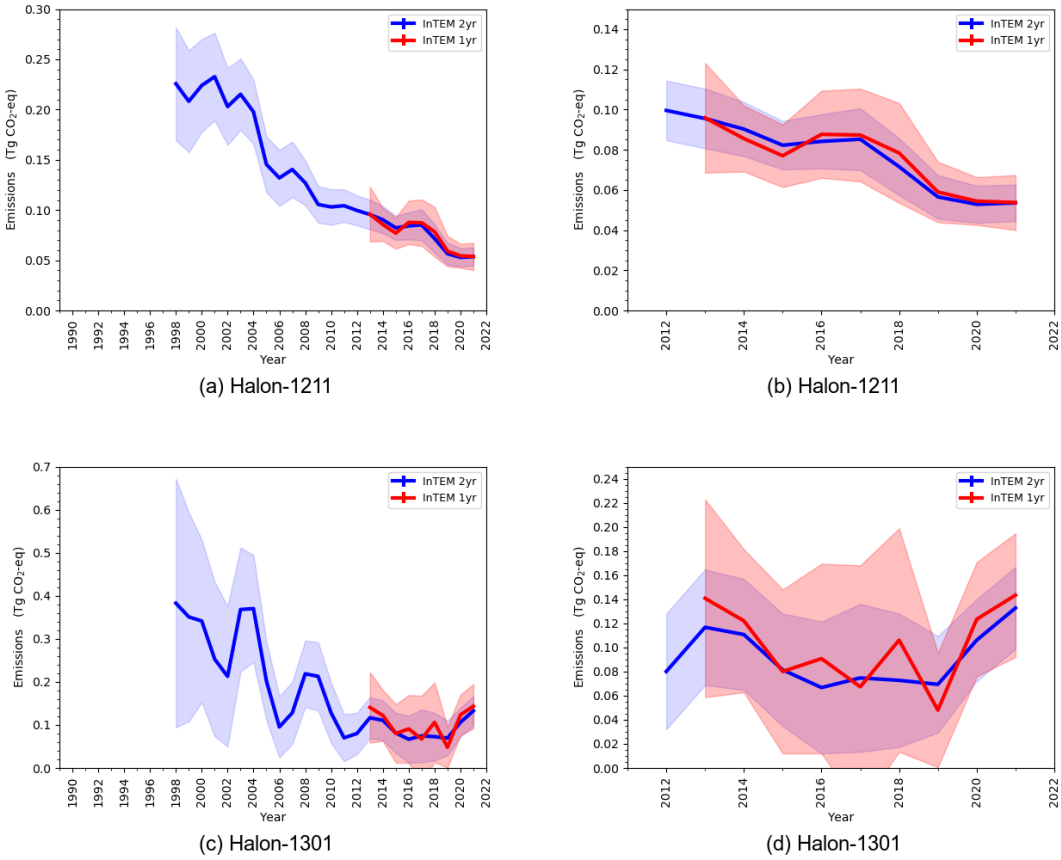

Figure 49: Halon UK emission estimates (Gg yr^{-1} CO_2-eq) from InTEM annualised 2-year inversion (blue) and annual inversion (red). The shading represents 1-σ. Left plot 1990-2021 and the right expanded x-axis, 2012-2021

Figure 48 shows the atmospheric mole fractions for Halon-1211, Halon-1301 and Halon-2402. Halon-1211 and Halon-2402 are decreasing globally. Since 2014, Halon-1301 has had negligible growth but has yet to start declining. Figure 49 shows the InTEM estimates for the UK emissions of Halon-1211 and Halon-1301. UK Halon-1211 emissions have declined steadily since the late 1990s, the picture for UK Halon-1301 emissions is more mixed, overall it declined 1998-2011 but has since remained constant within the uncertainty estimates.

6.16 Hydrofluoroolefins (HFOs) and Hydrochlorofluoroolefins (HCFOs)

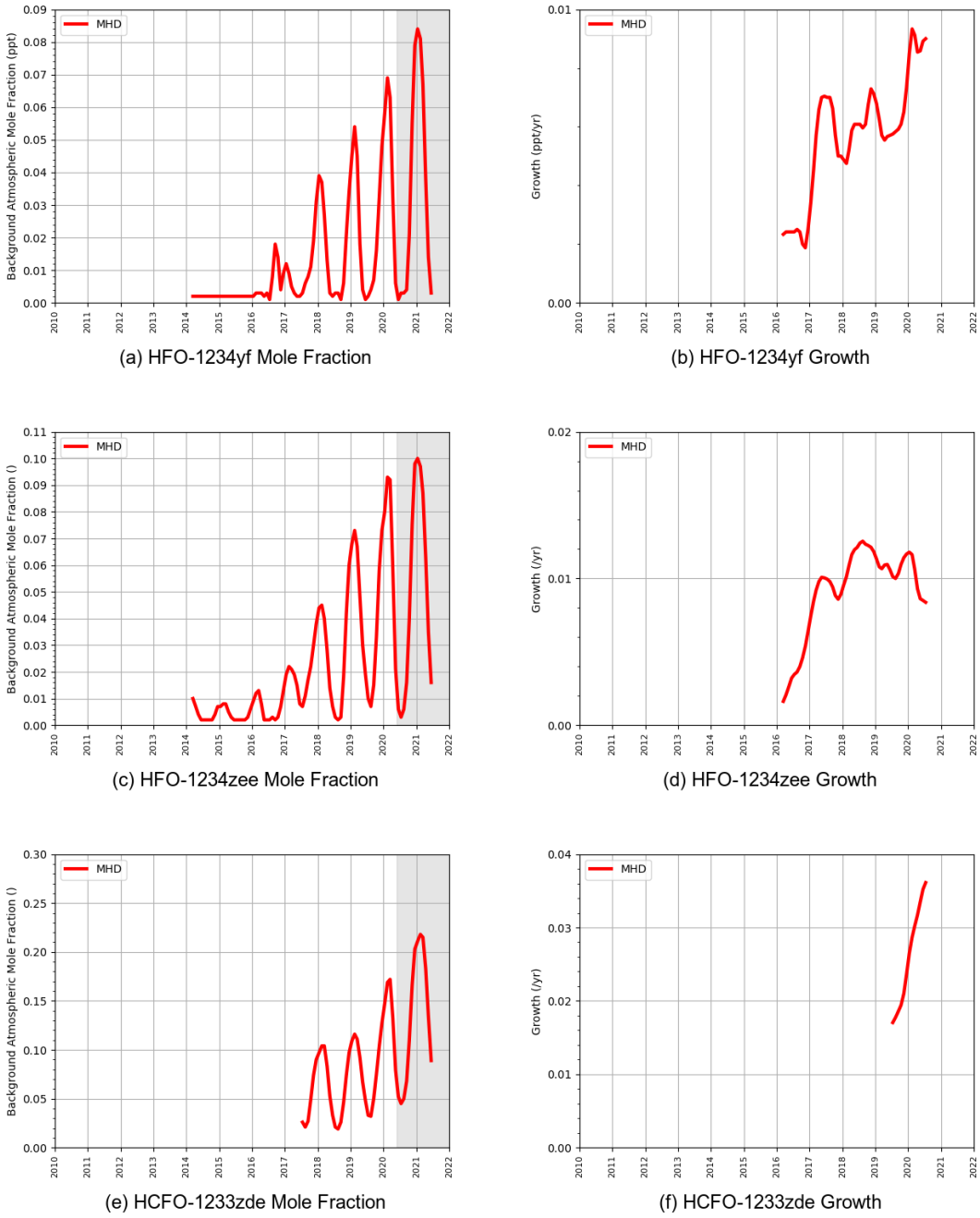

Figure 50: Northern (red) Hemisphere atmospheric background levels (left) and rates of increase (right) as observed at the Mace Head, Ireland measurement station. Grey shaded area represents un-ratified provisional data.

Figure 50 shows the background atmospheric mole fraction of HFO-1234yf, HFO-1234ze(E) and HCFO-1233zd(E) at Mace Head. HFOs and HCFOs are unsaturated organic compounds and as

such have short atmospheric lifetimes as they decompose quickly in the atmosphere. Currently these gases are growing the atmosphere.

HFOs and HCFOs are rapidly replacing hydrofluorocarbons as refrigerant gases due to their short atmospheric lifetimes and low global warming potentials (GWP). Atmospheric measurements of these gases at Mace Head and Tacolneston observatories show that emissions of these gases to the atmosphere are increasing. Two potential by-products of HFO degradation are of environmental concern, Trifluoroacetic acid (TFA) and HFC-23.

Trifluoroacetic acid (TFA), a mildly phytotoxic by-product, is produced by all HFOs in varying molar yields. TFA is rapidly deposited to the land and sea, leading to highly persistent terrestrial and aqueous contamination.

Photolysis of trifluoroacetaldehyde (CH_3CFO), an intermediary in the atmospheric decay of some HFOs/HCFOs, e.g. HFO-1234ze(E) and HCFO-1233zd(E), has been reported to form trifluoromethane (CHF_3, HFC-23) as a minor by-product (Campbell et al. 2021). They proposed that this reaction pathway could account for the fate $11.0 \pm 5.5\%$ of atmospheric CF_3CFO. HFC-23 is an extremely potent greenhouse gas, whose atmospheric abundance continues to rise despite regulation designed to reduce emissions. Production of HFC-23 via this route would lead to a higher 'effective GWP' for these HFO/HCFOs. Campbell et al. (2021) have stressed the need for further work to confirm the results of their study. Reaction mechanisms observed in the laboratory do not necessarily mimic those observed in the atmosphere, and the analogous photo-chemistry of CF_3CHO and CH_3CHO has not been conclusively proven. Furthermore, conclusions from Campbell et al. (2021) are in direct contrast with previous studies. Chiappero et al. (2006) conducted photolysis experiments in a reaction chamber near to atmospheric pressure and concluded that the production of HFC-23 from CF_3CHO was of 'no significance'.

7 Recent Publications

A list of current publications and presentations resulting from AGAGE and other research are summarized below.

Derwent, R., D. Parrish, P. G. Simmonds, S. J. O'Doherty, and T. G. Spain (2020). "Seasonal Cycles in Baseline Mixing Ratios of a Large Number of Trace Gases at the Mace Head, Ireland Atmospheric Research Station". In: *Atmospheric Environment* 233, p. 117531. ISSN: 13522310. DOI: 10.1016/j.atmosenv.2020.117531.

A flexible approach for quantifying average long-term changes and seasonal cycles has been applied to the baseline mixing ratios of thirty-two trace gases monitored at the Atmospheric Research Station located at Mace Head, Ireland on the Atlantic Ocean coastline of Europe. Almost all these trace gases exhibit minima in their baseline seasonal cycles during a two-month period from mid-July to the end of September and maxima during a six-month period between November and May. Relative seasonal cycle amplitudes are largest for those trace gases with the shortest atmospheric lifetimes and smallest for the longest. Robust relationships were found between the timings of the seasonal maxima and minima and their relative amplitudes with the atmospheric lifetimes of the trace gases. These relationships provide a basis for understanding the reasons that the seasonal cycles of a few species (that is, H_2, CCl_4 and the longest-lived gases) deviate significantly; they also have excellent potential as tools to assess global chemistry-transport model performance.

Droste, E. S., K. E. Adcock, M. J. Ashfold, C. Chou, Z. Fleming, P. J. Fraser, L. J. Gooch, A. J. Hind, R. L. Langenfelds, E. Leedham Elvidge, N. Mohd Hanif, S. O'Doherty, D. E. Oram, C.-F. Ou-Yang, M. Panagi, C. E. Reeves, W. T. Sturges, and J. C. Laube (2020). "Trends and Emissions of Six Perfluorocarbons in the Northern Hemisphere and Southern Hemisphere". In: *Atmospheric Chemistry and Physics* 20.8, pp. 4787–4807. ISSN: 1680-7324. DOI: 10.5194/acp-20-4787-2020.

Perfluorocarbons (PFCs) are potent greenhouse gases with global warming potentials up to several thousand times greater than CO_2 on a 100-year time horizon. The lack of any significant sinks for PFCs means that they have long atmospheric lifetimes of the order of thousands of years. Anthropogenic production is thought to be the only source for most PFCs. Here we report an update on the global atmospheric abundances of the following PFCs, most of which have for the first time been analytically separated according to their isomers: c-octafluorobutane (c-C_4F_8), n-decafluorobutane (n-C_4F_{10}), n-dodecafluoropentane (n-C_5F_{12}), n-tetradecafluorohexane (n-C_6F_{14}), and n-hexadecafluoroheptane (n-C_7F_{16}). Additionally, we report the first data set on the atmospheric mixing ratios of perfluoro-2-methylpentane (i-C_6F_{14}). The existence and significance of PFC isomers have not been reported before, due to the analytical challenges of separating them. The time series spans a period from 1978 to the present. Several data sets are used to investigate temporal and spatial trends of these PFCs: time series of air samples collected at Cape Grim, Australia, from 1978 to the start of 2018; a time series of air samples collected

between July 2015 and April 2017 at Tacolneston, UK; and intensive campaign-based sampling collections from Taiwan. Although the remote "background" Southern Hemispheric Cape Grim time series indicates that recent growth rates of most of these PFCs are lower than in the 1990s, we continue to see significantly increasing mixing ratios that are between 6 % and 27 % higher by the end of 2017 compared to abundances measured in 2010. Air samples from Tacolneston show a positive offset in PFC mixing ratios compared to the Southern Hemisphere baseline. The highest mixing ratios and variability are seen in air samples from Taiwan, which is therefore likely situated much closer to PFC sources, confirming predominantly Northern Hemispheric emissions for most PFCs. Even though these PFCs occur in the atmosphere at levels of parts per trillion molar or less, their total cumulative global emissions translate into 833 million metric tonnes of CO_2 equivalent by the end of 2017, 23 % of which has been emitted since 2010. Almost two-thirds of the CO_2 equivalent emissions within the last decade are attributable to c-C_4F_8, which currently also has the highest emission rates that continue to grow. Sources of all PFCs covered in this work remain poorly constrained and reported emissions in global databases do not account for the abundances found in the atmosphere.

Fraser, P. J., B. L. Dunse, P. B. Krummel, L. P. Steele, N. Derek, B. Mitrevski, C. E. Allison, Z. Loh, A. J. Manning, A. Redington, and M. Rigby (2020). "Australian chlorofluorocarbon (CFC) emissions: 1960-2017". In: *Environmental Chemistry* 17, pp. 525–544. DOI: https://doi.org/10.1071/EN19322.

Australian emissions of chlorofluorocarbons (CFCs) have been estimated from atmospheric CFC observations by both inverse modelling and interspecies correlation techniques, and from CFC production, import and consumption data compiled by industry and government. Australian and global CFC emissions show similar temporal behaviour, with emissions peaking in the late-1980s and then declining by ∼10% per year through to the present. Australian CFC emissions since 1978 account for less than 1% of global emissions and therefore make a correspondingly small contribution to stratospheric ozone depletion. The current CFC emissions in Australia are likely from banks of closed-cell foams, and refrigeration air conditioning equipment now more than 20 years old. There is no evidence of renewed consumption or emissions of CFCs in Australia. The reduction in CFC emissions has made a significant contribution to reducing Australian greenhouse gas emissions.

Ganesan, A. L., M. Manizza, E. J. Morgan, C. M. Harth, E. Kozlova, T. Lueker, A. J. Manning, M. F. Lunt, J. Mühle, J. V. Lavric, M. Heimann, R. F. Weiss, and M. Rigby (2020). "Marine Nitrous Oxide Emissions From Three Eastern Boundary Upwelling Systems Inferred From Atmospheric Observations". In: *Geophysical Research Letters* 47.14. e2020GL087822 2020GL087822, e2020GL087822. DOI: https://doi.org/10.1029/2020GL087822. eprint: https://agupubs.onlinelibrary.wiley.com/doi/pdf/10.1029/2020GL087822.

Eastern Boundary Upwelling Systems (EBUSs) are coastal hotspots of the potent greenhouse gas nitrous oxide (N_2O). However, estimates of their emissions suffer from large uncertainties due to their significant spatial and temporal heterogeneity. Here, we derive the first multiyear, monthly resolution N_2O emissions from three of

the four major EBUSs using high-frequency coastal atmospheric measurements and an inverse method. We find average combined N_2O emissions from the northern California, Benguela, and southern Canary upwelling systems to be 57.7 (51.4–63.9) Gg-N yr^{-1}. We also find an offshore region near the Benguela EBUS that exhibits large pulses of emissions with emissions that reach 677 Gg-N yr^{-1} in 1 month. Our findings highlight that atmospheric measurements coupled with inverse modeling can capture the large variability in EBUS emissions by quantifying emissions over large spatial distances and over long time periods compared to previous methods using traditional oceanographic measurements.

Gill-Olivas, B., J. Telling, M. Tranter, M. Skidmore, B. Christner, S. O'Doherty, and J. Priscu (2021). "Subglacial Erosion Has the Potential to Sustain Microbial Processes in Subglacial Lake Whillans, Antarctica". In: *Communications Earth & Environment* 2.1, p. 134. ISSN: 2662-4435. DOI: 10.1038/s43247-021-00202-x.

Subglacial Lake Whillans lies below around 800 m of Antarctic ice and is isolated from fresh sources of photosynthetic organic matter to sustain life. The diverse microbial ecosystems within the lake and underlying sediments are therefore dependent on a combination of relict, overridden, marine-derived organic matter and mineral-derived energy. Here, we conduct experiments to replicate subglacial erosion involving both gentle and high-energy crushing of Subglacial Lake Whillans sediments and the subsequent addition of anoxic water. We find that substantial quantities of reduced species, including hydrogen, methane, acetate and ammonium and oxidised species such as hydrogen peroxide, sulfate and carbon dioxide are released. We propose that the concomitant presence of both hydrogen and hydrogen peroxide, alongside high concentrations of mineral surface radicals, suggests that the splitting of water on freshly abraded mineral surfaces increases the concentrations of redox pairs from rock-water reactions and could provide a mechanism to augment the energy available to microbial ecosystems.

Gressent, A., M. Rigby, A. L. Ganesan, R. G. Prinn, A. J. Manning, J. Mühle, P. K. Salameh, P. B. Krummel, P. J. Fraser, L. P. Steele, B. Mitrevski, R. F. Weiss, C. M. Harth, R. H. Wang, S. O'Doherty, D. Young, S. Park, S. Li, B. Yao, S. Reimann, M. K. Vollmer, M. Maione, J. Arduini, and C. R. Lunder (2021). "Growing Atmospheric Emissions of Sulfuryl Fluoride". In: *Journal of Geophysical Research: Atmospheres*. ISSN: 2169-897X, 2169-8996. DOI: 10.1029/2020JD034327.

The potent greenhouse gas sulfuryl fluoride (SO_2F_2) is increasingly used as a fumigant, replacing methyl bromide, whose structural and soil fumigation uses have been phased out under the Montreal Protocol. We use measurements on archived air samples and in situ observations from the Advanced Global Atmospheric Gases Experiment (AGAGE) and a box model of the global atmosphere to show a global increase of SO_2F_2 mole fraction from 0.3 ± 0.02 to 2.5 ± 0.08 ppt along with a global increase in emissions from 0.5 ± 0.4 Gg yr^{-1} to 2.9 ± 0.4 Gg yr^{-1} from 1978 to 2019. Based on a hybrid model incorporating bottom-up industry data and a top-down downscaling approach, we estimate the spatial distribution and trend in SO_2F_2 regional emissions between 2000 and 2019 and propose that the global emissions increase is driven by the growing use of SO_2F_2 in

structural fumigation in North America and in postharvest treatment of grains and other agricultural products worldwide.

Lickley, M., S. Solomon, D. Kinnison, P. Krummel, J. Mühle, S. O'Doherty, R. Prinn, M. Rigby, K. A. Stone, P. Wang, R. Weiss, and D. Young (2021). "Quantifying the Imprints of Stratospheric Contributions to Interhemispheric Differences in Tropospheric CFC-11, CFC-12, and N_2O Abundances". In: *Geophysical Research Letters* 48.15. ISSN: 0094-8276, 1944-8007. DOI: 10.1029/2021GL093700.

For trace gases destroyed in the stratosphere, mass flux across the tropopause can substantially influence observed surface hemispheric differences (NH-SH). Here, we quantify associations between observed stratospheric and tropospheric NH-SH growth rate anomalies of CFC-11, CFC-12, and N2O. We employ a chemistry climate model along with satellite and global surface station observations. Our model explains 60% of observed N2O NH-SH growth rate variability from 2005 to 2019, compared to 30% for CFC-11% and 40% for CFC-12, supporting evidence that unexpected anthropogenic emissions caused sustained positive NH-SH anomalies in these CFCs from 2012 to 2017. Between 2012 and 2015, the observed CFC-11 NH-SH difference grew by 1.7 ppt; our model explains 0.5 $\pm$ 0.1 ppt of this growth, but not the duration. Our model suggests that in the absence of further emission anomalies, new NH-SH positive tracer anomalies should have occurred in 2020, and predicts small negative anomalies in 2021.

Manning, A. J., A. L. Redington, D. Say, S. O'Doherty, D. Young, P. G. Simmonds, M. K. Vollmer, J. Mühle, J. Arduini, G. Spain, A. Wisher, M. Maione, T. J. Schuck, K. Stanley, S. Reimann, A. Engel, P. B. Krummel, P. J. Fraser, C. M. Harth, P. K. Salameh, R. F. Weiss, R. Gluckman, P. N. Brown, J. D. Watterson, and T. Arnold (2021). "Evidence of a recent decline in UK emissions of hydrofluorocarbons determined by the InTEM inverse model and atmospheric measurements". In: *Atmospheric Chemistry and Physics* 21.16, pp. 12739–12755. DOI: 10.5194/acp-21-12739-2021.

National Greenhouse Gas Inventories (GHGI) are submitted annually to the United Nations Framework Convention on Climate Change (UNFCCC). They are estimated in compliance with Intergovernmental Panel on Climate Change (IPCC) methodological guidance using activity data, emission factors and facility-level measurements. For some sources, the outputs from these calculations are very uncertain. Inverse modelling techniques that use high-quality, long-term measurements of atmospheric gases have been developed to provide independent verification of national GHGI. This is considered good practice by the IPCC as it helps national inventory compilers to verify reported emissions and to reduce emission uncertainty. Emission estimates from the InTEM (Inversion Technique for Emissions Modelling) model are presented for the UK for the hydrofluorocarbons (HFCs) reported to the UNFCCC (HFC-125, HFC-134a, HFC-143a, HFC-152a, HFC-23, HFC-32, HFC-227ea, HFC-245fa, HFC-43-10mee and HFC-365mfc). These HFCs have high Global Warming Potentials (GWPs) and the global background mole fractions of all but two are increasing, thus highlighting their relevance to the climate and a

need for increasing the accuracy of emission estimation for regulatory purposes. This study presents evidence that the long-term annual increase in growth of HFC-134a has stopped and is now decreasing. For HFC-32 there is an early indication its rapid global growth period has ended, and there is evidence that the annual increase in global growth for HFC-125 has slowed from 2018. The inverse modelling results indicate that the UK implementation of European Union regulation of HFC emissions has been successful in initiating a decline in UK emissions from 2018. Comparison of the total InTEM UK HFC emissions in 2020 with the average from 2009–2012 shows a drop of 35%, indicating progress toward the target of a 79% decrease in sales by 2030. The total InTEM HFC emission estimates (2008–2018) are on average 73 (62–83)% of, or 4.3 (2.7–5.9) Tg CO_2-eq yr^{-1} lower than, the total HFC emission estimates from the UK GHGI inventory. There are also significant discrepancies between the two estimates for the individual HFCs.

Monteil, G., G. Broquet, M. Scholze, M. Lang, U. Karstens, C. Gerbig, F.-T. Koch, N. E. Smith, R. L. Thompson, I. T. Luijkx, E. White, A. Meesters, P. Ciais, A. L. Ganesan, A. Manning, M. Mischurow, W. Peters, P. Peylin, J. Tarniewicz, M. Rigby, C. Rödenbeck, A. Vermeulen, and E. M. Walton (2020). "The regional European atmospheric transport inversion comparison, EUROCOM: first results on European-wide terrestrial carbon fluxes for the period 2006–2015". In: *Atmospheric Chemistry and Physics* 20.20, pp. 12063–12091. DOI: 10.5194/acp-20-12063-2020.

Atmospheric inversions have been used for the past two decades to derive large-scale constraints on the sources and sinks of CO_2 into the atmosphere. The development of dense in situ surface observation networks, such as ICOS in Europe, enables in theory inversions at a resolution close to the country scale in Europe. This has led to the development of many regional inversion systems capable of assimilating these high-resolution data, in Europe and elsewhere. The EUROCOM (European atmospheric transport inversion comparison) project is a collaboration between seven European research institutes, which aims at producing a collective assessment of the net carbon flux between the terrestrial ecosystems and the atmosphere in Europe for the period 2006-2015. It aims in particular at investigating the capacity of the inversions to deliver consistent flux estimates from the country scale up to the continental scale. The project participants were provided with a common database of in situ-observed CO_2 concentrations (including the observation sites that are now part of the ICOS network) and were tasked with providing their best estimate of the net terrestrial carbon flux for that period, and for a large domain covering the entire European Union. The inversion systems differ by the transport model, the inversion approach, and the choice of observation and prior constraints, enabling us to widely explore the space of uncertainties. This paper describes the inter-comparison protocol and the participating systems, and it presents the first results from a reference set of inversions, at the continental scale and in four large regions. At the continental scale, the regional inversions support the assumption that European ecosystems are a relatively small sink (-0.21±0.2 $PgCyr^{-1}$). We find that the convergence of the regional inversions at this scale is not better than that obtained in state-of-the-art global inversions. However, more robust results are obtained for sub-regions within Europe, and

in these areas with dense observational coverage, the objective of delivering robust country-scale flux estimates appears achievable in the near future.

Montzka, S. A., G. S. Dutton, R. W. Portmann, M. P. Chipperfield, S. Davis, W. Feng, A. J. Manning, E. Ray, M. Rigby, B. D. Hall, C. Siso, J. D. Nance, P. B. Krummel, J. Mühle, D. Young, S. O'Doherty, P. K. Salameh, C. M. Harth, R. G. Prinn, R. F. Weiss, J. W. Elkins, H. Walter-Terrinoni, and C. Theodoridi (2021). "A Decline in Global CFC-11 Emissions during 2018-2019". In: *Nature*. ISSN: 0028-0836, 1476-4687. DOI: 10.1038/s41586-021-03260-5.

The atmospheric concentration of trichlorofluoromethane (CFC-11) has been in decline since the production of ozone-depleting substances was phased out under the Montreal Protocol1,2. Since 2013, the concentration decline of CFC-11 slowed unexpectedly owing to increasing emissions, probably from unreported production, which, if sustained, would delay the recovery of the stratospheric ozone layer. Here we report an accelerated decline in the global mean CFC-11 concentration during 2019 and 2020, derived from atmospheric concentration measurements at remote sites around the world. We find that global CFC-11 emissions decreased by 18 ± 6 gigagrams per year (26 ± 9 per cent; one standard deviation) from 2018 to 2019, to a 2019 value (52 ± 10 gigagrams per year) that is similar to the 2008-2012 mean. The decline in global emissions suggests a substantial decrease in unreported CFC-11 production. If the sharp decline in unexpected global emissions and unreported production is sustained, any associated future ozone depletion is likely to be limited, despite an increase in the CFC-11 bank (the amount of CFC-11 produced, but not yet emitted) by 90 to 725 gigagrams by the beginning of 2020.

Park, S., L. M. Western, T. Saito, A. L. Redington, S. Henne, X. Fang, R. G. Prinn, A. J. Manning, S. A. Montzka, P. J. Fraser, A. L. Ganesan, C. M. Harth, J. Kim, P. B. Krummel, Q. Liang, J. Mühle, S. O'Doherty, H. Park, M.-K. Park, S. Reimann, P. K. Salameh, R. F. Weiss, and M. Rigby (2021). "A Decline in Emissions of CFC-11 and Related Chemicals from Eastern China". In: *Nature* 590.7846, pp. 433–437. ISSN: 0028-0836, 1476-4687. DOI: 10.1038/s41586-021-03277-w.

Emissions of ozone-depleting substances, including trichlorofluoromethane (CFC-11), have decreased since the mid-1980s in response to the Montreal Protocol. In recent years, an unexpected increase in CFC-11 emissions beginning in 2013 has been reported, with much of the global rise attributed to emissions from eastern China. Here we use high-frequency atmospheric mole fraction observations from Gosan, South Korea and Hateruma, Japan, together with atmospheric chemical transport-model simulations, to investigate regional CFC-11 emissions from eastern China. We find that CFC-11 emissions returned to pre-2013 levels in 2019 (5.0 ± 1.0 gigagrams per year in 2019, compared to 7.2 ± 1.5 gigagrams per year for 2008–2012, ±1 standard deviation), decreasing by 10 ± 3 gigagrams per year since 2014–2017. Furthermore, we find that in this region, carbon tetrachloride (CCl_4) and dichlorodifluoromethane (CFC-12) emissions—potentially associated with CFC-11 production—were higher than expected after 2013 and then declined one to two years before the CFC-11 emissions reduction. This suggests that CFC-11 production occurred in eastern China after the mandated global phase-out, and that

there was a subsequent decline in production during 2017–2018. We estimate that the amount of the CFC-11 bank (the amount of CFC-11 produced, but not yet emitted) in eastern China is up to 112 gigagrams larger in 2019 compared to pre-2013 levels, probably as a result of recent production. Nevertheless, it seems that any substantial delay in ozone-layer recovery has been avoided, perhaps owing to timely reporting and subsequent action by industry and government in China.

Patra, P. K., M. C. Krol, R. G. Prinn, M. Takigawa, J. Mühle, S. A. Montzka, S. Lal, Y. Yamashita, S. Naus, N. Chandra, R. F. Weiss, P. B. Krummel, P. J. Fraser, S. O'Doherty, and J. W. Elkins (2021). "Methyl Chloroform Continues to Constrain the Hydroxyl (OH) Variability in the Troposphere". In: *Journal of Geophysical Research: Atmospheres* 126.4. ISSN: 2169-897X, 2169-8996. DOI: 10.1029/2020JD033862.

Trends and variability in tropospheric hydroxyl (OH) radicals influence budgets of many greenhouse gases, air pollutant species, and ozone depleting substances. Estimations of tropospheric OH trends and variability based on budget analysis of methyl chloroform (CH_3CCl_3) and process-based chemistry transport models often produce conflicting results. Here we use a previously tested transport model to simulate atmospheric CH_3CCl_3 for the period 1985–2018. Based on mismatches between model output and observations, we derive consistent anomalies in the inverse lifetime of CH_3CCl_3 (KG) using measurements from two independent observational networks (National Oceanic and Atmospheric Administration and Advanced Global Atmospheric Gases Experiment). Our method allows a separation between "physical" (transport, temperature) and "chemical" (i.e., abundance) influences on OH + CH_3CCl_3 reaction rate in the atmosphere. Small increases in KG due to "physical" influences are mostly driven by increases in the temperature-dependent reaction between OH and CH_3CCl_3 and resulted in a smoothly varying increase of 0.80% decade^{-1}. Chemical effects on KG, linked to global changes in OH sources and sinks, show larger year-to-year variations (∼2%–3%), and have a negative correlation with the El Niño Southern Oscillation. A significant positive trend in KG can be derived after 2001, but it persists only through 2015 and only if we assume that CH_3CCl_3 emissions decayed more slowly over time than our best estimate suggests. If global CH_3CCl_3 emissions dropped below 3 Gg year^{-1} after 2015, recent CH_3CCl_3 measurements indicate that the 2015–2018 loss rate of CH_3CCl_3 due to reaction with OH is comparable to its value 2 decades ago.

Petrescu, A. M. R., C. Qiu, P. Ciais, R. L. Thompson, P. Peylin, M. J. McGrath, E. Solazzo, G. Janssens-Maenhout, F. N. Tubiello, P. Bergamaschi, D. Brunner, G. P. Peters, L. Höglund-Isaksson, P. Regnier, R. Lauerwald, D. Bastviken, A. Tsuruta, W. Winiwarter, P. K. Patra, M. Kuhnert, G. D. Oreggioni, M. Crippa, M. Saunois, L. Perugini, T. Markkanen, T. Aalto, C. D. Groot Zwaaftink, H. Tian, Y. Yao, C. Wilson, G. Conchedda, D. Günther, A. Leip, P. Smith, J.-M. Haussaire, A. Leppänen, A. J. Manning, J. McNorton, P. Brockmann, and A. J. Dolman (2021). "The consolidated European synthesis of CH_4 and N_2O emissions for the European

Union and United Kingdom: 1990-2017". In: *Earth System Science Data* 13.5, pp. 2307–2362. DOI: 10.5194/essd-13-2307-2021.

Reliable quantification of the sources and sinks of greenhouse gases, together with trends and uncertainties, is essential to monitoring the progress in mitigating anthropogenic emissions under the Paris Agreement. This study provides a consolidated synthesis of CH_4 and N_2O emissions with consistently derived state-of-the-art bottom-up (BU) and top-down (TD) data sources for the European Union and UK (EU27 + UK). We integrate recent emission inventory data, ecosystem process-based model results and inverse modeling estimates over the period 1990-2017. BU and TD products are compared with European national greenhouse gas inventories (NGHGIs) reported to the UN climate convention UNFCCC secretariat in 2019. For uncertainties, we used for NGHGIs the standard deviation obtained by varying parameters of inventory calculations, reported by the member states (MSs) following the recommendations of the IPCC Guidelines. For atmospheric inversion models (TD) or other inventory datasets (BU), we defined uncertainties from the spread between different model estimates or model-specific uncertainties when reported. In comparing NGHGIs with other approaches, a key source of bias is the activities included, e.g., anthropogenic versus anthropogenic plus natural fluxes. In inversions, the separation between anthropogenic and natural emissions is sensitive to the geospatial prior distribution of emissions. Over the 2011-2015 period, which is the common denominator of data availability between all sources, the anthropogenic BU approaches are directly comparable, reporting mean emissions of 20.8 Tg CH_4 yr^{-1} (EDGAR v5.0) and 19.0 Tg CH_4 yr^{-1} (GAINS), consistent with the NGHGI estimates of 18.9 $\pm$ 1.7 Tg CH_4 yr^{-1}. The estimates of TD total inversions give higher emission estimates, as they also include natural emissions. Over the same period regional TD inversions with higher-resolution atmospheric transport models give a mean emission of 28.8 Tg CH_4 yr^{-1}. Coarser-resolution global TD inversions are consistent with regional TD inversions, for global inversions with GOSAT satellite data (23.3 Tg CH_4 yr^{-1}) and surface network (24.4 Tg CH_4 yr^{-1}). The magnitude of natural peatland emissions from the JSBACH-HIMMELI model, natural rivers and lakes emissions, and geological sources together account for the gap between NGHGIs and inversions and account for 5.2 Tg CH_4 yr^{-1}. For N_2O emissions, over the 2011-2015 period, both BU approaches (EDGAR v5.0 and GAINS) give a mean value of anthropogenic emissions of 0.8 and 0.9 Tg N_2O yr^{-1}, respectively, agreeing with the NGHGI data (0.9 $\pm$ 0.6 Tg N_2O yr^{-1}). Over the same period, the average of the three total TD global and regional inversions was 1.3 $\pm$ 0.4 and 1.3 $\pm$ 0.1 Tg N_2O yr^{-1}, respectively. The TD and BU comparison method defined in this study can be operationalized for future yearly updates for the calculation of CH_4 and N_2O budgets both at the EU+UK scale and at the national scale. The referenced datasets related to figures are visualized at https://doi.org/10.5281/zenodo.4590875 (Petrescu et al., 2020b).

Ramonet, M., P. Ciais, F. Apadula, J. Bartyzel, A. Bastos, P. Bergamaschi, P. E. Blanc, D. Brunner, L. Caracciolo di Torchiarolo, F. Calzolari, H. Chen, L. Chmura, A. Colomb, S. Conil, P. Cristofanelli, E. Cuevas, R. Curcoll, M. Delmotte, A. di Sarra, L. Emmenegger, G. Forster, A. Frumau, C. Gerbig, F. Gheusi, S. Hammer, L. Haszpra, J. Hatakka, L. Hazan, M. Heliasz, S. Henne, A. Hensen, O. Hermansen, P. Keronen, R. Kivi, K. Komínková, D. Kubistin, O. Laurent,

T. Laurila, J. V. Lavric, I. Lehner, K. E. J. Lehtinen, A. Leskinen, M. Leuenberger, I. Levin, M. Lindauer, M. Lopez, C. L. Myhre, I. Mammarella, G. Manca, A. Manning, M. V. Marek, P. Marklund, D. Martin, F. Meinhardt, N. Mihalopoulos, M. Mölder, J. A. Morgui, J. Necki, S. O'Doherty, C. O'Dowd, M. Ottosson, C. Philippon, S. Piacentino, J. M. Pichon, C. Plass-Duelmer, A. Resovsky, L. Rivier, X. Rodó, M. K. Sha, H. A. Scheeren, D. Sferlazzo, T. G. Spain, K. M. Stanley, M. Steinbacher, P. Trisolino, A. Vermeulen, G. Vítková, D. Weyrauch, I. Xueref-Remy, K. Yala, and C. Yver Kwok (2020). "The Fingerprint of the Summer 2018 Drought in Europe on Ground-Based Atmospheric CO $_2$ Measurements". In: *Philosophical Transactions of the Royal Society B: Biological Sciences* 375.1810, p. 20190513. ISSN: 0962-8436, 1471-2970. DOI: 10.1098/rstb.2019.0513.

During the summer of 2018, a widespread drought developed over Northern and Central Europe. The increase in temperature and the reduction of soil moisture have influenced carbon dioxide (CO_2) exchange between the atmosphere and terrestrial ecosystems in various ways, such as a reduction of photosynthesis, changes in ecosystem respiration, or allowing more frequent fires. In this study, we characterize the resulting perturbation of the atmospheric CO_2 seasonal cycles. 2018 has a good coverage of European regions affected by drought, allowing the investigation of how ecosystem flux anomalies impacted spatial CO_2 gradients between stations. This density of stations is unprecedented compared to previous drought events in 2003 and 2015, particularly thanks to the deployment of the Integrated Carbon Observation System (ICOS) network of atmospheric greenhouse gas monitoring stations in recent years. Seasonal CO_2 cycles from 48 European stations were available for 2017 and 2018. Earlier data were retrieved for comparison from international databases or national networks. Here, we show that the usual summer minimum in CO_2 due to the surface carbon uptake was reduced by 1.4 ppm in 2018 for the 10 stations located in the area most affected by the temperature anomaly, mostly in Northern Europe. Notwithstanding, the CO_2 transition phases before and after July were slower in 2018 compared to 2017, suggesting an extension of the growing season, with either continued CO_2 uptake by photosynthesis and/or a reduction in respiration driven by the depletion of substrate for respiration inherited from the previous months due to the drought. For stations with sufficiently long time series, the CO_2 anomaly observed in 2018 was compared to previous European droughts in 2003 and 2015. Considering the areas most affected by the temperature anomalies, we found a higher CO_2 anomaly in 2003 (+3 ppm averaged over 4 sites), and a smaller anomaly in 2015 (+1 ppm averaged over 11 sites) compared to 2018. This article is part of the theme issue 'Impacts of the 2018 severe drought and heatwave in Europe: from site to continental scale'.

Saunois, M., A. R. Stavert, B. Poulter, P. Bousquet, J. G. Canadell, R. B. Jackson, P. A. Raymond, E. J. Dlugokencky, S. Houweling, P. K. Patra, P. Ciais, V. K. Arora, D. Bastviken, P. Bergamaschi, D. R. Blake, G. Brailsford, L. Bruhwiler, K. M. Carlson, M. Carrol, S. Castaldi, N. Chandra, C. Crevoisier, P. M. Crill, K. Covey, C. L. Curry, G. Etiope, C. Frankenberg, N. Gedney, M. I. Hegglin, L. Höglund-Isaksson, G. Hugelius, M. Ishizawa, A. Ito, G. Janssens-Maenhout, K. M. Jensen, F. Joos, T. Kleinen, P. B. Krummel, R. L. Langenfelds, G. G. Laruelle,

L. Liu, T. Machida, S. Maksyutov, K. C. McDonald, J. McNorton, P. A. Miller, J. R. Melton, I. Morino, J. Müller, F. Murguia-Flores, V. Naik, Y. Niwa, S. Noce, S. O'Doherty, R. J. Parker, C. Peng, S. Peng, G. P. Peters, C. Prigent, R. Prinn, M. Ramonet, P. Regnier, W. J. Riley, J. A. Rosentreter, A. Segers, I. J. Simpson, H. Shi, S. J. Smith, L. P. Steele, B. F. Thornton, H. Tian, Y. Tohjima, F. N. Tubiello, A. Tsuruta, N. Viovy, A. Voulgarakis, T. S. Weber, M. van Weele, G. R. van der Werf, R. F. Weiss, D. Worthy, D. Wunch, Y. Yin, Y. Yoshida, W. Zhang, Z. Zhang, Y. Zhao, B. Zheng, Q. Zhu, Q. Zhu, and Q. Zhuang (2020). "The Global Methane Budget 2000–2017". In: *Earth System Science Data* 12.3, pp. 1561–1623. ISSN: 1866-3516. DOI: 10.5194/essd-12-1561-2020.

Understanding and quantifying the global methane (CH_4) budget is important for assessing realistic pathways to mitigate climate change. Atmospheric emissions and concentrations of CH_4 continue to increase, making CH_4 the second most important human-influenced greenhouse gas in terms of climate forcing, after carbon dioxide (CO_2). The relative importance of CH_4 compared to CO_2 depends on its shorter atmospheric lifetime, stronger warming potential, and variations in atmospheric growth rate over the past decade, the causes of which are still debated. Two major challenges in reducing uncertainties in the atmospheric growth rate arise from the variety of geographically overlapping CH_4 sources and from the destruction of CH_4 by short-lived hydroxyl radicals (OH). To address these challenges, we have established a consortium of multidisciplinary scientists under the umbrella of the Global Carbon Project to synthesize and stimulate new research aimed at improving and regularly updating the global methane budget. Following Saunois et al. (2016), we present here the second version of the living review paper dedicated to the decadal methane budget, integrating results of top-down studies (atmospheric observations within an atmospheric inverse-modelling framework) and bottom-up estimates (including process-based models for estimating land surface emissions and atmospheric chemistry, inventories of anthropogenic emissions, and data-driven extrapolations). For the 2008–2017 decade, global methane emissions are estimated by atmospheric inversions (a top-down approach) to be 576 $\mathrm{Tg\,CH_4\,yr^{-1}}$ (range 550–594, corresponding to the minimum and maximum estimates of the model ensemble). Of this total, 359 $\mathrm{Tg\,CH_4\,yr^{-1}}$ or $\sim$60 % is attributed to anthropogenic sources, that is emissions caused by direct human activity (i.e. anthropogenic emissions; range 336–376 $\mathrm{Tg\,CH_4\,yr^{-1}}$ or 50 %–65 %). The mean annual total emission for the new decade (2008–2017) is 29 $\mathrm{Tg\,CH_4\,yr^{-1}}$ larger than our estimate for the previous decade (2000–2009), and 24 $\mathrm{Tg\,CH_4\,yr^{-1}}$ larger than the one reported in the previous budget for 2003–2012 (Saunois et al., 2016). Since 2012, global CH_4 emissions have been tracking the warmest scenarios assessed by the Intergovernmental Panel on Climate Change. Bottom-up methods suggest almost 30 % larger global emissions (737 $\mathrm{Tg\,CH_4\,yr^{-1}}$, range 594–881) than top-down inversion methods. Indeed, bottom-up estimates for natural sources such as natural wetlands, other inland water systems, and geological sources are higher than top-down estimates. The atmospheric constraints on the top-down budget suggest that at least some of these bottom-up emissions are overestimated. The latitudinal distribution of atmospheric observation-based emissions indicates a predominance of tropical emissions ($\sim$65 % of the global budget, $<$30°N) compared to mid-latitudes ($\sim$30 %, 30–60°N) and high northern latitudes ($\sim$4 %, 60–90°N). The most important source of uncertainty in the methane budget is attributable to natural emissions,

especially those from wetlands and other inland waters. Some of our global source estimates are smaller than those in previously published budgets (Saunois et al., 2016; Kirschke et al., 2013). In particular wetland emissions are about 35 Tg CH_4 yr^{-1} lower due to improved partition wetlands and other inland waters. Emissions from geological sources and wild animals are also found to be smaller by 7 Tg CH_4 yr^{-1} by 8 Tg CH_4 yr^{-1}, respectively. However, the overall discrepancy between bottom-up and top-down estimates has been reduced by only 5 % compared to Saunois et al. (2016), due to a higher estimate of emissions from inland waters, highlighting the need for more detailed research on emissions factors. Priorities for improving the methane budget include (i) a global, high-resolution map of water-saturated soils and inundated areas emitting methane based on a robust classification of different types of emitting habitats; (ii) further development of process-based models for inland-water emissions; (iii) intensification of methane observations at local scales (e.g., FLUXNET-CH_4 measurements) and urban-scale monitoring to constrain bottom-up land surface models, and at regional scales (surface networks and satellites) to constrain atmospheric inversions; (iv) improvements of transport models and the representation of photochemical sinks in top-down inversions; and (v) development of a 3D variational inversion system using isotopic and/or co-emitted species such as ethane to improve source partitioning. The data presented here can be downloaded from https://doi.org/10.18160/GCP-CH4-2019 (Saunois et al., 2020) and from the Global Carbon Project.

Say, D., B. Kuyper, L. Western, M. A. H. Khan, T. Lesch, C. Labuschagne, D. Martin, D. Young, A. J. Manning, S. O'Doherty, M. Rigby, P. B. Krummel, M. T. Davies-Coleman, A. L. Ganesan, and D. E. Shallcross (2020). "Emissions and Marine Boundary Layer Concentrations of Unregulated Chlorocarbons Measured at Cape Point, South Africa". In: *Environmental Science & Technology* 54.17, pp. 10514–10523. ISSN: 0013-936X, 1520-5851. DOI: 10.1021/acs.est.0c02057.

Unregulated chlorocarbons, here defined as dichloromethane (CH_2Cl_2), perchloroethene (C_2Cl_4), chloroform ($CHCl_3$), and methyl chloride (CH_3Cl), are gases not regulated by the Montreal Protocol. While CH_3Cl is the largest contributor of atmospheric chlorine, recent studies have shown that growth in emissions of the less abundant chlorocarbons could pose a significant threat to the recovery of the ozone layer. Despite this, there remain many regions for which no atmospheric monitoring exists, leaving gaps in our understanding of global emissions. Here, we report on a new time series of chlorocarbon measurements from Cape Point, South Africa for 2017, which represent the first published high-frequency measurements of these gases from Africa. For CH_2Cl_2 and C_2Cl_4, the majority of mole fraction enhancements were observed from the north, consistent with anthropogenically modified air from Cape Town, while for $CHCl_3$ and CH_3Cl, we found evidence for both oceanic and terrestrial sources. Using an inverse method, we estimated emissions for south-western South Africa (SWSA). For each chlorocarbon, SWSA accounted for less than 1% of global emissions. For CH_2Cl_2 and C_2Cl_4, we extrapolated using population statistics and found South African emissions of 8.9 (7.4-10.4) Gg yr^{-1} and 0.80 (0.64-1.04) Gg yr^{-1}, respectively.

Say, D., A. J. Manning, L. M. Western, D. Young, A. Wisher, M. Rigby, S. Reimann, M. K. Vollmer,

M. Maione, J. Arduini, P. B. Krummel, J. Mühle, C. M. Harth, B. Evans, R. F. Weiss, R. G. Prinn, and S. O'Doherty (2021). "Global Trends and European Emissions of Tetrafluoromethane (CF_4), Hexafluoroethane (C_2F_6 and Octafluoropropane (C_3F_8)". In: *Atmospheric Chemistry and Physics* 21.3, pp. 2149–2164. ISSN: 1680-7324. DOI: 10.5194/acp-21-2149-2021.

Perfluorocarbons (PFCs) are amongst the most potent greenhouse gases listed under the United Nations Framework Convention on Climate Change (UNFCCC). With atmospheric lifetimes on the order of thousands to tens of thousands of years, PFC emissions represent a permanent alteration to the global atmosphere on human timescales. While the industries responsible for the vast majority of these emissions – aluminium smelting and semi-conductor manufacturing – have made efficiency improvements and introduced abatement measures, the global mean mole fractions of three PFCs, namely tetrafluoromethane (CF_4, PFC-14), hexafluoroethane (C_2F_6, PFC-116) and octafluoropropane (C_3F_8, PFC-218), continue to grow. In this study, we update baseline growth rates using in situ high-frequency measurements from the Advanced Global Atmospheric Gases Experiment (AGAGE) and, using data from four European stations, estimate PFC emissions for northwest Europe. The global growth rate of CF_4 decreased from 1.3 ppt yr^{-1} in 1979 to 0.6 ppt yr^{-1} around 2010 followed by a renewed steady increase to 0.9 ppt yr^{-1} in 2019. For C_2F_6, the growth rate grew to a maximum of 0.125 ppt yr^{-1} around 1999, followed by a decline to a minimum of 0.075 ppt yr^{-1} in 2009, followed by weak growth thereafter. The C_3F_8 growth rate was around 0.007 ppt yr^{-1} until the early 1990s and then quickly grew to a maximum of 0.03 ppt yr^{-1} in 2003–2004. Following a period of decline until 2012 to 0.015 ppt yr^{-1}, the growth rate slowly increased again to $\sim$0.017 ppt yr^{-1} in 2019. We used an inverse modelling framework to infer PFC emissions for northwest Europe. No statistically significant trend in regional emissions was observed for any of the PFCs assessed. For CF_4, European emissions in early years were linked predominantly to the aluminium industry. However, we link large emissions in recent years to a chemical manufacturer in northwest Italy. Emissions of C_2F_6 are linked to a range of sources, including a semi-conductor manufacturer in Ireland and a cluster of smelters in Germany's Ruhr valley. In contrast, northwest European emissions of C_3F_8 are dominated by a single source in northwest England, raising the possibility of using emissions from this site for a tracer release experiment.

Simmonds, P. G., M. Rigby, A. J. Manning, S. Park, K. M. Stanley, A. McCulloch, S. Henne, F. Graziosi, M. Maione, J. Arduini, S. Reimann, M. K. Vollmer, J. Mühle, S. O'Doherty, D. Young, P. B. Krummel, P. J. Fraser, R. F. Weiss, P. K. Salameh, C. M. Harth, M.-K. Park, H. Park, T. Arnold, C. Rennick, L. P. Steele, B. Mitrevski, R. H. J. Wang, and R. G. Prinn (2020). "The increasing atmospheric burden of the greenhouse gas sulfur hexafluoride (SF_6)". In: *Atmospheric Chemistry and Physics* 20.12, pp. 7271–7290. DOI: 10.5194/acp-20-7271-2020.

We report a 40-year history of SF_6 atmospheric mole fractions measured at the Advanced Global Atmospheric Gases Experiment (AGAGE) monitoring sites, combined with archived air samples, to determine emission estimates from 1978 to 2018. Previously we reported a global emission rate of 7.3 $\pm$ 0.6 Gg yr^{-1} in 2008 and over the past decade emissions have continued to increase by about 24% to 9.04 $\pm$ 0.35 Gg yr^{-1} in 2018. We show that changing patterns in SF_6 consumption from developed (Kyoto Protocol Annex-1) to developing countries

(non-Annex-1) and the rapid global expansion of the electric power industry, mainly in Asia, have increased the demand for SF_6-insulated switchgear, circuit breakers, and transformers. The large bank of SF_6 sequestered in this electrical equipment provides a substantial source of emissions from maintenance, replacement, and continuous leakage. Other emissive sources of SF_6 occur from the magnesium, aluminium, and electronics industries as well as more minor industrial applications. More recently, reported emissions, including those from electrical equipment and metal industries, primarily in the Annex-1 countries, have declined steadily through substitution of alternative blanketing gases and technological improvements in less emissive equipment and more efficient industrial practices. Nevertheless, there are still demands for SF_6 in Annex-1 countries due to economic growth, as well as continuing emissions from older equipment and additional emissions from newly installed SF_6-insulated electrical equipment, although at low emission rates. In addition, in the non-Annex-1 countries, SF_6 emissions have increased due to an expansion in the growth of the electrical power, metal, and electronics industries to support their continuing development. There is an annual difference of 2.5-5 Gg yr^{-1} (1990-2018) between our modelled top-down emissions and the UNFCCC-reported bottom-up emissions (United Nations Framework Convention on Climate Change), which we attempt to reconcile through analysis of the potential contribution of emissions from the various industrial applications which use SF_6. We also investigate regional emissions in East Asia (China, S. Korea) and western Europe and their respective contributions to the global atmospheric SF_6 inventory. On an average annual basis, our estimated emissions from the whole of China are approximately 10 times greater than emissions from western Europe. In 2018, our modelled Chinese and western European emissions accounted for ∼36% and 3.1%, respectively, of our global SF_6 emissions estimate.

Simmonds, P., P. Palmer, M. Rigby, A. McCulloch, S. O'Doherty, and A. Manning (2021). "Tracers for Evaluating Computational Models of Atmospheric Transport and Oxidation at Regional to Global Scales". In: *Atmospheric Environment* 246, p. 118074. ISSN: 13522310. DOI: 10.1016/j.atmosenv.2020.118074.

Atmospheric tracers are effective tools for characterizing dispersion and for testing computational models of atmospheric transport. Atmospheric trace gas measurements are now used widely to infer geographical surface flux distributions. However, robust flux estimates critically rely on well-validated knowledge of atmospheric chemistry, loss processes and transport, without which we are not fully realizing the potential of atmospheric measurements collected on the ground, or from aircraft and satellites. This challenge has taken on renewed importance in the shadow of the Paris Agreement that will likely take advantage of atmospheric trace gas measurements to help improve national and global greenhouse gas emission budgets. We describe a wide range of existing and new potential atmospheric tracers for improving our understanding of atmospheric dispersion. We consider the investigation of atmospheric transport over two scales: (1) short-to-medium length scale (on the order of 1–1000 km) to improve our understanding of convection and boundary layer transport processes, and (2) hemisphere-to-global length scale (on the order of 1000–10,000 km), where large-scale mixing, cross hemisphere transport and stratosphere-troposphere exchange are important. Although we note the possibility of using "tracers of opportunity," our primary focus is on deliberate-release tracers, and we explore the use

of cyclic perfluorocarbons, hydrofluorocarbons, hydrochlorofluorocarbons, hydrofluoroethers and novel tracers of deuterium-substituted halocarbons. We examine how we might exploit existing instrumentation already deployed at remote global monitoring sites as well as requirements for new instrumentation. To guide the discussion, we provide example scenarios for how experiments might be set up, covering regional to global spatial scales for the evaluation and improvement of atmospheric transport models. However, we stress that appropriate three-dimensional modelling studies and preliminary experiments would need to be carried out to determine the specific details of any real-world experiment.

Tham, Y. J., X.-C. He, Q. Li, C. A. Cuevas, J. Shen, J. Kalliokoski, C. Yan, S. Iyer, T. Lehmusjärvi, S. Jang, R. C. Thakur, L. Beck, D. Kemppainen, M. Olin, N. Sarnela, J. Mikkilä, J. Hakala, M. Marbouti, L. Yao, H. Li, W. Huang, Y. Wang, D. Wimmer, Q. Zha, J. Virkanen, T. G. Spain, S. O'Doherty, T. Jokinen, F. Bianchi, T. Petäjä, D. R. Worsnop, R. L. Mauldin, J. Ovadnevaite, D. Ceburnis, N. M. Maier, M. Kulmala, C. O'Dowd, M. Dal Maso, A. Saiz-Lopez, and M. Sipilä (2021). "Direct Field Evidence of Autocatalytic Iodine Release from Atmospheric Aerosol". In: *Proceedings of the National Academy of Sciences* 118.4, e2009951118. ISSN: 0027-8424, 1091-6490. DOI: 10.1073/pnas.2009951118.

Reactive iodine plays a key role in determining the oxidation capacity, or cleansing capacity, of the atmosphere in addition to being implicated in the formation of new particles in the marine boundary layer. The postulation that heterogeneous cycling of reactive iodine on aerosols may significantly influence the lifetime of ozone in the troposphere not only remains poorly understood but also heretofore has never been observed or quantified in the field. Here, we report direct ambient observations of hypoiodous acid (HOI) and heterogeneous recycling of interhalogen product species (i.e., iodine monochloride [ICl] and iodine monobromide [IBr]) in a midlatitude coastal environment. Significant levels of ICl and IBr with mean daily maxima of 4.3 and 3.0 parts per trillion by volume (1-min average), respectively, have been observed throughout the campaign. We show that the heterogeneous reaction of HOI on marine aerosol and subsequent production of iodine interhalogens are much faster than previously thought. These results indicate that the fast formation of iodine interhalogens, together with their rapid photolysis, results in more efficient recycling of atomic iodine than currently considered in models. Photolysis of the observed ICl and IBr leads to a 32% increase in the daytime average of atomic iodine production rate, thereby enhancing the average daytime iodine-catalyzed ozone loss rate by 10 to 20%. Our findings provide direct field evidence that the autocatalytic mechanism of iodine release from marine aerosol is important in the atmosphere and can have significant impacts on atmospheric oxidation capacity.

Tunnicliffe, R. L., A. L. Ganesan, R. J. Parker, H. Boesch, N. Gedney, B. Poulter, Z. Zhang, J. V. Lavrič, D. Walter, M. Rigby, S. Henne, D. Young, and S. O'Doherty (2020). "Quantifying Sources of Brazil's CH_4 Emissions between 2010 and 2018 from Satellite Data". In: *Atmospheric Chemistry and Physics* 20.21, pp. 13041–13067. ISSN: 1680-7324. DOI: 10.5194/acp-20-13041-2020.

Brazil's CH_4 emissions over the period 2010–2018 were derived for the three main sectors of activity: anthropogenic, wetland and biomass burning. Our inverse modelling estimates were derived from GOSAT (Greenhouse gases Observing SATellite) satellite measurements of XCH_4 combined with surface data from Ragged Point, Barbados, and the high-resolution regional atmospheric transport model NAME (Numerical Atmospheric-dispersion Modelling Environment). We find that Brazil's mean emissions over 2010–2018 are 33.6 ± 3.6 Tg yr^{-1}, which are comprised of 19.0 ± 2.6 Tg yr^{-1} from anthropogenic (primarily related to agriculture and waste), 13.0 ± 1.9 Tg yr^{-1} from wetlands and 1.7 ± 0.3 Tg yr^{-1} from biomass burning sources. In addition, between the 2011–2013 and 2014–2018 periods, Brazil's mean emissions rose by 6.9 ± 5.3 Tg yr^{-1} and this increase may have contributed to the accelerated global methane growth rate observed during the latter period. We find that wetland emissions from the western Amazon increased during the start of the 2015–2016 El Niño by 3.7 ± 2.7 Tg yr^{-1} and this is likely driven by increased surface temperatures. We also find that our estimates of anthropogenic emissions are consistent with those reported by Brazil to the United Framework Convention on Climate Change. We show that satellite data are beneficial for constraining national-scale CH_4 emissions, and, through a series of sensitivity studies and validation experiments using data not assimilated in the inversion, we demonstrate that (a) calibrated ground-based data are important to include alongside satellite data in a regional inversion and that (b) inversions must account for any offsets between the two data streams and their representations by models.

Vollmer, M. K., J. Mühle, S. Henne, D. Young, M. Rigby, B. Mitrevski, S. Park, C. R. Lunder, T. S. Rhee, C. M. Harth, M. Hill, R. L. Langenfelds, M. Guillevic, P. M. Schlauri, O. Hermansen, J. Arduini, R. H. J. Wang, P. K. Salameh, M. Maione, P. B. Krummel, S. Reimann, S. O'Doherty, P. G. Simmonds, P. J. Fraser, R. G. Prinn, R. F. Weiss, and L. P. Steele (2021). "Unexpected Nascent Atmospheric Emissions of Three Ozone-Depleting Hydrochlorofluorocarbons". In: *Proceedings of the National Academy of Sciences* 118.5, e2010914118. ISSN: 0027-8424, 1091-6490. DOI: 10.1073/pnas.2010914118.

Global and regional atmospheric measurements and modeling can play key roles in discovering and quantifying unexpected nascent emissions of environmentally important substances. We focus here on three hydrochlorofluorocarbons (HCFCs) that are restricted by the Montreal Protocol because of their roles in stratospheric ozone depletion. Based on measurements of archived air samples and on in situ measurements at stations of the Advanced Global Atmospheric Gases Experiment (AGAGE) network, we report global abundances, trends, and regional enhancements for HCFC-132b ($CH_2ClCClF_2$), which is newly discovered in the atmosphere, and updated results for HCFC-133a (CH_2ClCF_3) and HCFC-31 (CH_2ClF). No purposeful end-use is known for any of these compounds. We find that HCFC-132b appeared in the atmosphere 20 y ago and that its global emissions increased to 1.1 Gg·y^{-1} by 2019. Regional top-down emission estimates for East Asia, based on high-frequency measurements for 2016–2019, account for ∼95% of the global HCFC-132b emissions and for ∼80% of the global HCFC-133a emissions of 2.3 Gg·y^{-1} during this period. Global emissions of HCFC-31 for the same period are 0.71 Gg·y^{-1}. Small European emissions of HCFC-132b and HCFC-133a, found in southeastern France, ceased in early 2017 when a fluorocarbon production facility in that area closed. Although unreported emissive end-uses

cannot be ruled out, all three compounds are most likely emitted as intermediate by-products in chemical production pathways. Identification of harmful emissions to the atmosphere at an early stage can guide the effective development of global and regional environmental policy.

Western, L. M., Z. Sha, M. Rigby, A. L. Ganesan, A. J. Manning, K. M. Stanley, S. J. O'Doherty, D. Young, and J. Rougier (2020). "Bayesian spatio-temporal inference of trace gas emissions using an integrated nested Laplacian approximation and Gaussian Markov random fields". In: *Geoscientific Model Development* 13.4, pp. 2095–2107. DOI: 10.5194/gmd-13-2095-2020.

We present a method to infer spatially and spatio-temporally correlated emissions of greenhouse gases from atmospheric measurements and a chemical transport model. The method allows fast computation of spatial emissions using a hierarchical Bayesian framework as an alternative to Markov chain Monte Carlo algorithms. The spatial emissions follow a Gaussian process with a Matérn correlation structure which can be represented by a Gaussian Markov random field through a stochastic partial differential equation approach. The inference is based on an integrated nested Laplacian approximation (INLA) for hierarchical models with Gaussian latent fields. Combining an autoregressive temporal correlation and the Matérn field provides a full spatio-temporal correlation structure. We first demonstrate the method on a synthetic data example and follow this using a well-studied test case of inferring UK methane emissions from tall tower measurements of atmospheric mole fraction. Results from these two test cases show that this method can accurately estimate regional greenhouse gas emissions, accounting for spatio-temporal uncertainties that have traditionally been neglected in atmospheric inverse modelling.

Yu, D., B. Yao, W. Lin, M. K. Vollmer, B. Ge, G. Zhang, Y. Li, H. Xu, S. O'Doherty, L. Chen, and S. Reimann (2020). "Atmospheric CH_3CCl_3 Observations in China: Historical Trends and Implications". In: *Atmospheric Research* 231, p. 104658. ISSN: 01698095. DOI: 10.1016/j.atmosres.2019.104658.

Although CH_3CCl_3 is an important ozone-depleting substance regulated by the Montreal Protocol on Substances that Deplete the Ozone Layer and its Amendments, the levels of atmospheric CH_3CCl_3 mixing ratios in China are poorly understood. Long-term in-situ measurements by GC-ECD have been conducted at the Shangdianzi Station in northern China since October 2006. In addition, air samples have been collected daily/weekly at seven sta- tions and analyzed by GC/MS system since 2010. The two methods show comparable precisions at around 1% and all the measurements were calibrated by standards linked to the Advanced Global Atmospheric Gases Experiment (AGAGE) reference scale Scripps Institution of Oceanography (SIO)-05. Mixing ratios for both "background" and "polluted" conditions are reported. The atmospheric CH_3CCl_3 mixing ratios during back- ground conditions showed a significant and consistent decreasing trend with a decline rate from 1.9 ppt/yr (October 2006 to December 2007) to 0.3 ppt/yr (November 2015 to December 2017) at the Shangdianzi Station. Measured background mixing ratios increased from 41% in 2007 to 95% in 2017. The mean mixing ratios and their enhancement of polluted conditions have decreased from 15.1 and 2.0 ppt in 2007 to 2.7 and 0.3 ppt in

2017 at Shangdianzi. The mixing ratios in air at background conditions at the seven stations in China agree well with each other and all decrease gradually. The percentage of pollution events to the total number of measurements (POL/SUM) at Lin'an has decreased significantly from 2010 to 2017, especially after 2013. In 2017, POL/SUMs of all stations were $< 8\%$ and the enhancements above background were < 0.7 ppt. Both mixing ratios and enhancements have decreased by one or two orders of magnitude when comparing the results from previous studies, in the early 2000s, with the results in 2017 from this study. Chinese emissions of CH_3CCl_3, which were estimated by a tracer-ratio method, have decreased from 1.6 kt/yr in 2007 to 0.3 kt/yr in 2013, indicating that CH_3CCl_3 has been phased-out in China in accordance with the Montreal Protocol.

8 Bibliography

Arnold, T., A. J. Manning, J. Kim, S. Li, H. Webster, D. Thomson, J. Mühle, R. F. Weiss, S. Park, and S. O'Doherty (2018). "Inverse Modelling of CF_4 and NF_3 Emissions in East Asia". In: *Atmospheric Chemistry and Physics* 18.18, pp. 13305–13320. ISSN: 1680-7324. DOI: 10.5194/acp-18-13305-2018 (cit. on p. 33).

Behringer, D., F. Heydel, B. Gschrey, S. Osterheld, W. Schwarz, K. Warncke, F. Freeling, K. Nödler, S. Henne, S. Reimann, M. Blepp, W. Jörß, R. Liu, S. Ludig, I. Rüdenauer, and S. Gartiser (2021). *Persistent degradation products of halogenated refrigerants and blowing agents in the environment: type, environmental concentrations, and fate with particular regard to new halogenated substitutes with low global warming potential*. en. Tech. rep. (cit. on p. 6).

Campbell, J. S., S. H. Kable, and C. S. Hansen (2021). "Photodissociation of CF_3CHO provides a new source of CHF_3 (HFC-23) in the atmosphere: implications for new refrigerants". In: DOI: 10.21203/rs.3.rs-199769/v1 (cit. on pp. 6, 77).

Chiappero, M. S., F. E. Malanca, G. A. Argüello, S. T. Wooldridge, M. D. Hurley, J. C. Ball, T. J. Wallington, R. L. Waterland, and R. C. Buck (2006). "Atmospheric Chemistry of Perfluoroaldehydes (C x F_2 x+ 1CHO) and Fluorotelomer Aldehydes (C x F_2 x+ $1CH_2CHO$): Quantification of the Important Role of Photolysis". In: *The Journal of Physical Chemistry A* 110.43, pp. 11944–11953 (cit. on p. 77).

Ciais, P., C. Sabine, G. Bala, L. Bopp, V. Brovkin, J. Canadell, A. Chhabra, R. DeFries, J. Galloway, M. Heimann, C. Jones, C. Le Quéré, R. B. Myneni, S. Piao, and P. Thornton (2013). "Carbon and Other Biogeochemical Cycles". In: *Climate Change 2013 - The Physical Science Basis*.

Cambridge: Cambridge University Press, pp. 465–570. ISBN: 978-1-107-41532-4. DOI: 10.1017/CBO9781107415324.015 (cit. on pp. 37, 40).

Crutzen, P. J. (1970). "The Influence of Nitrogen Oxides on the Atmospheric Ozone Content". In: *Quarterly Journal of the Royal Meteorological Society* 96.408, pp. 320–325. ISSN: 00359009, 1477870X. DOI: 10.1002/qj.49709640815 (cit. on p. 40).

Cunnold, D. M., L. P. Steele, P. J. Fraser, P. G. Simmonds, R. G. Prinn, R. F. Weiss, L. W. Porter, S. O'Doherty, R. L. Langenfelds, P. B. Krummel, H. J. Wang, L. Emmons, X. X. Tie, and E. J. Dlugokencky (2002). "In Situ Measurements of Atmospheric Methane at GAGE/AGAGE Sites during 1985–2000 and Resulting Source Inferences". In: *Journal of Geophysical Research* 107.D14. ISSN: 0148-0227. DOI: 10.1029/2001JD001226 (cit. on p. 37).

Dlugokencky, E. J., L. Bruhwiler, J. W. C. White, L. K. Emmons, P. C. Novelli, S. A. Montzka, K. A. Masarie, P. M. Lang, A. M. Crotwell, J. B. Miller, and L. V. Gatti (2009). "Observational Constraints on Recent Increases in the Atmospheric CH_4 Burden". In: *Geophysical Research Letters* 36.18. ISSN: 0094-8276. DOI: 10.1029/2009GL039780 (cit. on p. 37).

Dlugokencky, E. J., S. Houweling, L. Bruhwiler, K. A. Masarie, P. M. Lang, J. B. Miller, and P. P. Tans (2003). "Atmospheric Methane Levels off: Temporary Pause or a New Steady-State?" In: *Geophysical Research Letters* 30.19, p. 1992. ISSN: 0094-8276. DOI: 10.1029/2003GL018126 (cit. on p. 37).

Frankenberg, C., I. Aben, P. Bergamaschi, E. J. Dlugokencky, R. van Hees, S. Houweling, P. van der Meer, R. Snel, and P. Tol (2011). "Global Column-Averaged Methane Mixing Ratios from 2003 to 2009 as Derived from SCIAMACHY: Trends and Variability". In: *Journal of Geophysical Research* 116.D4, p. D04302. ISSN: 0148-0227. DOI: 10.1029/2010JD014849 (cit. on p. 37).

Ganesan, A. L., S. Schwietzke, B. Poulter, T. Arnold, X. Lan, M. Rigby, F. R. Vogel, G. R. Werf, G. Janssens-Maenhout, H. Boesch, S. Pandey, A. J. Manning, R. B. Jackson, E. G. Nisbet, and M. R. Manning (2019). "Advancing Scientific Understanding of the Global Methane Budget in Support of the Paris Agreement". In: *Global Biogeochemical Cycles* 33.12, pp. 1475–1512. ISSN: 0886-6236, 1944-9224. DOI: 10.1029/2018GB006065 (cit. on p. 37).

Griffis, T. J., X. Lee, J. M. Baker, M. P. Russelle, X. Zhang, R. Venterea, and D. B. Millet (2013). "Reconciling the Differences between Top-down and Bottom-up Estimates of Nitrous Oxide

Emissions for the U.S. Corn Belt". In: *Global Biogeochemical Cycles* 27.3, pp. 746–754. ISSN: 08866236. DOI: 10.1002/gbc.20066 (cit. on p. 40).

Hmiel, B., V. V. Petrenko, M. N. Dyonisius, C. Buizert, A. M. Smith, P. F. Place, C. Harth, R. Beaudette, Q. Hua, B. Yang, I. Vimont, S. E. Michel, J. P. Severinghaus, D. Etheridge, T. Bromley, J. Schmitt, X. Faïn, R. F. Weiss, and E. Dlugokencky (2020). "Preindustrial $^{14}CH_4$ Indicates Greater Anthropogenic Fossil CH_4 Emissions". In: *Nature* 578.7795, pp. 409–412. ISSN: 0028-0836, 1476-4687. DOI: 10.1038/s41586-020-1991-8 (cit. on p. 37).

Hoare, D., R. Jones, N. R. Harris, V. Ferracci, D. Carruthers, A. Stidworthy, E. Forsyth, and M. Rigby (2020). "Development of an urban greenhouse gas modelling system to support a London monitoring network". In: *Weather* 75.11, pp. 353–359 (cit. on p. 21).

Lunt, M., A. Manning, G. Allen, T. Arnold, S. Bauguitte, H. Boesch, A. Ganesan, A. Grant, C. Helfter, E. Nemitz, et al. (2021). "Atmospheric observations consistent with reported decline in the UK's methane emissions, 2013–2020". In: *Atmospheric Chemistry and Physics Discussions*, pp. 1–30 (cit. on pp. 4, 35, 37, 39).

Manning, A. J., S. O'Doherty, A. R. Jones, P. G. Simmonds, and R. G. Derwent (2011). "Estimating UK Methane and Nitrous Oxide Emissions from 1990 to 2007 Using an Inversion Modeling Approach". In: *Journal of Geophysical Research: Atmospheres* 116.D2, p. D02305. ISSN: 2156-2202. DOI: 10.1029/2010JD014763 (cit. on p. 33).

Manning, A. J., A. L. Redington, D. Say, S. O'Doherty, D. Young, P. G. Simmonds, M. K. Vollmer, J. Mühle, J. Arduini, G. Spain, A. Wisher, M. Maione, T. J. Schuck, K. Stanley, S. Reimann, A. Engel, P. B. Krummel, P. J. Fraser, C. M. Harth, P. K. Salameh, R. F. Weiss, R. Gluckman, P. N. Brown, J. D. Watterson, and T. Arnold (2021). "Evidence of a recent decline in UK emissions of hydrofluorocarbons determined by the InTEM inverse model and atmospheric measurements". In: *Atmospheric Chemistry and Physics* 21.16, pp. 12739–12755. DOI: 10.5194/acp-21-12739-2021 (cit. on pp. 5, 9, 30, 33, 35, 53).

McNorton, J., C. Wilson, M. Gloor, R. J. Parker, H. Boesch, W. Feng, R. Hossaini, and M. P. Chipperfield (2018). "Attribution of Recent Increases in Atmospheric Methane through 3-D Inverse Modelling". In: *Atmospheric Chemistry and Physics* 18.24, pp. 18149–18168. ISSN: 1680-7324. DOI: 10.5194/acp-18-18149-2018 (cit. on p. 37).

Monteil, G., S. Houweling, E. J. Dlugockenky, G. Maenhout, B. H. Vaughn, J. W. C. White, and T. Rockmann (2011). "Interpreting Methane Variations in the Past Two Decades Using Measurements of CH_4 Mixing Ratio and Isotopic Composition". In: *Atmospheric Chemistry and Physics* 11.17, pp. 9141–9153. ISSN: 1680-7324. DOI: 10.5194/acp-11-9141-2011 (cit. on p. 37).

Montzka, S. A., G. J. M. Velders, P. B. Krummel, J. Mühle, V. L. Orkin, S. Park, N. Shah, and H. Walter-Terrinoni (2018). "Hydrofluorocarbons (HFC's) Chapter 2 in Scientific Assessment of Ozone Depletion: 2018". In: *Global Ozone Research and Monitoring Project Report No. 58, World Meteorological Organization, Geneva, Switzerland* (cit. on p. 36).

Montzka, S. A., G. S. Dutton, R. W. Portmann, M. P. Chipperfield, S. Davis, W. Feng, A. J. Manning, E. Ray, M. Rigby, B. D. Hall, C. Siso, J. D. Nance, P. B. Krummel, J. Mühle, D. Young, S. O'Doherty, P. K. Salameh, C. M. Harth, R. G. Prinn, R. F. Weiss, J. W. Elkins, H. Walter-Terrinoni, and C. Theodoridi (2021). "A Decline in Global CFC-11 Emissions during 2018-2019". In: *Nature*. ISSN: 0028-0836, 1476-4687. DOI: 10.1038/s41586-021-03260-5 (cit. on p. 66).

Myhre, G., D. T. Shindell, F.-M. Bréon, W. Collins, J. Fuglestvedt, J. Huang, D. Koch, J.-F. Lamarque, D. Lee, B. Mendoza, T. Nakajima, A. Robock, G. Stephens, T. Takemura, and H. Zhang (2013). "Anthropogenic and Natural Radiative Forcing". In: *Climate Change 2013 - The Physical Science Basis. Contribution of Working Group I to the Fifth Assessment Report of the Intergovernmental Panel on Climate Change*. Cambridge: Cambridge University Press, pp. 659–740. ISBN: 978-1-107-41532-4. DOI: 10.1017/CBO9781107415324.018 (cit. on pp. 36, 37).

Nisbet, E. G., E. J. Dlugokencky, M. R. Manning, D. Lowry, R. E. Fisher, J. L. France, S. E. Michel, J. B. Miller, J. W. C. White, B. Vaughn, P. Bousquet, J. A. Pyle, N. J. Warwick, M. Cain, R. Brownlow, G. Zazzeri, M. Lanoisellé, A. C. Manning, E. Gloor, D. E. J. Worthy, E.-G. Brunke, C. Labuschagne, E. W. Wolff, and A. L. Ganesan (2016). "Rising Atmospheric Methane: 2007-2014 Growth and Isotopic Shift". In: *Global Biogeochemical Cycles* 30.9, pp. 1356–1370. ISSN: 08866236. DOI: 10.1002/2016GB005406 (cit. on p. 37).

Nisbet, E. G., R. E. Fisher, D. Lowry, J. L. France, G. Allen, S. Bakkaloglu, T. J. Broderick, M. Cain, M. Coleman, J. Fernandez, G. Forster, P. T. Griffiths, C. P. Iverach, B. F. J. Kelly, M. R. Manning, P. B. R. Nisbet-Jones, J. A. Pyle, A. Townsend-Small, A. al-Shalaan, N. Warwick, and G. Zazzeri (2020). "Methane Mitigation: Methods to Reduce Emissions, on the Path to the

Paris Agreement". In: *Reviews of Geophysics* 58.1. ISSN: 8755-1209, 1944-9208. DOI: 10.1029/2019RG000675 (cit. on p. 37).

Nisbet, E. G., M. R. Manning, E. J. Dlugokencky, R. E. Fisher, D. Lowry, S. E. Michel, C. L. Myhre, S. M. Platt, G. Allen, P. Bousquet, R. Brownlow, M. Cain, J. L. France, O. Hermansen, R. Hossaini, A. E. Jones, I. Levin, A. C. Manning, G. Myhre, J. A. Pyle, B. H. Vaughn, N. J. Warwick, and J. W. C. White (2019). "Very Strong Atmospheric Methane Growth in the 4 Years 2014–2017: Implications for the Paris Agreement". In: *Global Biogeochemical Cycles* 33.3, pp. 318–342. ISSN: 0886-6236, 1944-9224. DOI: 10.1029/2018GB006009 (cit. on p. 37).

Park, S., L. M. Western, T. Saito, A. L. Redington, S. Henne, X. Fang, R. G. Prinn, A. J. Manning, S. A. Montzka, P. J. Fraser, A. L. Ganesan, C. M. Harth, J. Kim, P. B. Krummel, Q. Liang, J. Mühle, S. O'Doherty, H. Park, M.-K. Park, S. Reimann, P. K. Salameh, R. F. Weiss, and M. Rigby (2021). "A Decline in Emissions of CFC-11 and Related Chemicals from Eastern China". In: *Nature* 590.7846, pp. 433–437. ISSN: 0028-0836, 1476-4687. DOI: 10.1038/s41586-021-03277-w (cit. on p. 66).

Prather, M. J., J. Hsu, N. M. DeLuca, C. H. Jackman, L. D. Oman, A. R. Douglass, E. L. Fleming, S. E. Strahan, S. D. Steenrod, O. Amund Søvde, I. S. A. Isaksen, L. Froidevaux, and B. Funke (2015). "Measuring and Modeling the Lifetime of Nitrous Oxide Including Its Variability". In: *Journal of Geophysical Research: Atmospheres*, 2015JD023267. ISSN: 2169-8996. DOI: 10.1002/2015JD023267 (cit. on p. 40).

Ravishankara, A. R., J. S. Daniel, and R. W. Portmann (2009). "Nitrous Oxide (N_2O): The Dominant Ozone-Depleting Substance Emitted in the 21st Century". In: *Science* 326.5949, pp. 123–125. ISSN: 0036-8075, 1095-9203. DOI: 10.1126/science.1176985 (cit. on p. 40).

Rigby, M., R. G. Prinn, P. J. Fraser, P. G. Simmonds, R. L. Langenfelds, J. Huang, D. M. Cunnold, L. P. Steele, P. B. Krummel, R. F. Weiss, S. O'Doherty, P. K. Salameh, H. J. Wang, C. M. Harth, J. Mühle, and L. W. Porter (2008). "Renewed Growth of Atmospheric Methane". In: *Geophysical Research Letters* 35.22. ISSN: 0094-8276. DOI: 10.1029/2008GL036037 (cit. on p. 37).

Rigby, M., S. A. Montzka, R. G. Prinn, J. W. C. White, D. Young, S. O'Doherty, M. F. Lunt, A. L. Ganesan, A. J. Manning, P. G. Simmonds, P. K. Salameh, C. M. Harth, J. Mühle, R. F. Weiss, P. J. Fraser, L. P. Steele, P. B. Krummel, A. McCulloch, and S. Park (2017). "Role of Atmospheric Oxidation in Recent Methane Growth". In: *Proceedings of the National Academy of Sciences*, p. 201616426. ISSN: 0027-8424. DOI: 10.1073/PNAS.1616426114 (cit. on p. 37).

Saunois, M., A. R. Stavert, B. Poulter, P. Bousquet, J. G. Canadell, R. B. Jackson, P. A. Raymond, E. J. Dlugokencky, S. Houweling, P. K. Patra, P. Ciais, V. K. Arora, D. Bastviken, P. Bergamaschi, D. R. Blake, G. Brailsford, L. Bruhwiler, K. M. Carlson, M. Carrol, S. Castaldi, N. Chandra, C. Crevoisier, P. M. Crill, K. Covey, C. L. Curry, G. Etiope, C. Frankenberg, N. Gedney, M. I. Hegglin, L. Höglund-Isaksson, G. Hugelius, M. Ishizawa, A. Ito, G. Janssens-Maenhout, K. M. Jensen, F. Joos, T. Kleinen, P. B. Krummel, R. L. Langenfelds, G. G. Laruelle, L. Liu, T. Machida, S. Maksyutov, K. C. McDonald, J. McNorton, P. A. Miller, J. R. Melton, I. Morino, J. Müller, F. Murguia-Flores, V. Naik, Y. Niwa, S. Noce, S. O'Doherty, R. J. Parker, C. Peng, S. Peng, G. P. Peters, C. Prigent, R. Prinn, M. Ramonet, P. Regnier, W. J. Riley, J. A. Rosentreter, A. Segers, I. J. Simpson, H. Shi, S. J. Smith, L. P. Steele, B. F. Thornton, H. Tian, Y. Tohjima, F. N. Tubiello, A. Tsuruta, N. Viovy, A. Voulgarakis, T. S. Weber, M. van Weele, G. R. van der Werf, R. F. Weiss, D. Worthy, D. Wunch, Y. Yin, Y. Yoshida, W. Zhang, Z. Zhang, Y. Zhao, B. Zheng, Q. Zhu, Q. Zhu, and Q. Zhuang (2020). "The Global Methane Budget 2000–2017". In: *Earth System Science Data* 12.3, pp. 1561–1623. ISSN: 1866-3516. DOI: 10.5194/essd-12-1561-2020 (cit. on p. 37).

Schaefer, H., S. E. M. Fletcher, C. Veidt, K. R. Lassey, G. W. Brailsford, T. M. Bromley, E. J. Dlugokencky, S. E. Michel, J. B. Miller, I. Levin, D. C. Lowe, R. J. Martin, B. H. Vaughn, and J. W. C. White (2016). "A 21st-Century Shift from Fossil-Fuel to Biogenic Methane Emissions Indicated by $^{13}CH_4$". In: *Science* 352.6281, pp. 80–84. ISSN: 0036-8075, 1095-9203. DOI: 10.1126/science.aad2705 (cit. on p. 37).

Schwietzke, S., O. A. Sherwood, L. M. P. Bruhwiler, J. B. Miller, G. Etiope, E. J. Dlugokencky, S. E. Michel, V. A. Arling, B. H. Vaughn, J. W. C. White, and P. P. Tans (2016). "Upward Revision of Global Fossil Fuel Methane Emissions Based on Isotope Database". In: *Nature* 538.7623, pp. 88–91. ISSN: 0028-0836, 1476-4687. DOI: 10.1038/nature19797 (cit. on p. 37).

Solomon, K. R., G. J. M. Velders, S. R. Wilson, S. Madronich, J. Longstreth, P. J. Aucamp, and J. F. Bornman (2016). "Sources, fates, toxicity, and risks of trifluoroacetic acid and its salts: Relevance to substances regulated under the Montreal and Kyoto Protocols". In: *Journal of Toxicology and Environmental Health, Part B* 19.7, pp. 289–304. ISSN: 1093-7404. DOI: 10.1080/10937404.2016.1175981 (cit. on p. 6).

Tian, H., R. Xu, J. G. Canadell, R. L. Thompson, W. Winiwarter, P. Suntharalingam, E. A. Davidson, P. Ciais, R. B. Jackson, G. Janssens-Maenhout, et al. (2020). "A comprehensive quantification of global nitrous oxide sources and sinks". In: *Nature* 586.7828, pp. 248–256 (cit. on p. 40).

Turner, A. J., C. Frankenberg, and E. A. Kort (2019). "Interpreting Contemporary Trends in Atmospheric Methane". In: *Proceedings of the National Academy of Sciences* 116.8, pp. 2805–2813. ISSN: 0027-8424, 1091-6490. DOI: 10.1073/pnas.1814297116 (cit. on p. 37).

Turner, P. A., T. J. Griffis, X. Lee, J. M. Baker, R. T. Venterea, and J. D. Wood (2015). "Indirect Nitrous Oxide Emissions from Streams within the US Corn Belt Scale with Stream Order". In: *Proceedings of the National Academy of Sciences* 112.32, pp. 9839–9843. ISSN: 0027-8424, 1091-6490. DOI: 10.1073/pnas.1503598112 (cit. on p. 40).

Vollmer, M. K., S. Reimann, M. Hill, and D. Brunner (2015). "First Observations of the Fourth Generation Synthetic Halocarbons HFC-1234yf, HFC-1234ze(E), and HCFC-1233zd(E) in the Atmosphere". In: *Environmental Science Technology* 49.5, pp. 2703–2708. ISSN: 0013-936X. DOI: 10.1021/es505123x (cit. on p. 6).

WMO (2018). *WMO Greenhouse Gas Bulletin: The State of Greenhouse Gases in the Atmosphere Based on Global Observations through 2017*. Tech. rep. 14. https://library.wmo.int/doc_num.php?explnum_id=5455: World Meteorological Organization, Global Atmosphere Watch (cit. on p. 40).

— (2020). *GAW Report No. 255. 20th WMO/IAEA Meeting on Carbon Dioxide, Other Greenhouse Gases and Related Measurement Techniques (GGMT-2019)*. Ed. by A. Crotwell, H. Lee, and M. Steinbacher (cit. on p. 26).

Worden, J. R., A. A. Bloom, S. Pandey, Z. Jiang, H. M. Worden, T. W. Walker, S. Houweling, and T. Röckmann (2017). "Reduced Biomass Burning Emissions Reconcile Conflicting Estimates of the Post-2006 Atmospheric Methane Budget". In: *Nature Communications* 8.1. ISSN: 2041-1723. DOI: 10.1038/s41467-017-02246-0 (cit. on p. 37).

Yver-Kwok, C., C. Philippon, P. Bergamaschi, T. Biermann, F. Calzolari, H. Chen, S. Conil, P. Cristofanelli, M. Delmotte, J. Hatakka, M. Heliasz, O. Hermansen, K. Komínková, D. Kubistin, N. Kumps, O. Laurent, T. Laurila, I. Lehner, J. Levula, M. Lindauer, M. Lopez, I. Mammarella, G. Manca, P. Marklund, J.-M. Metzger, M. Mölder, S. M. Platt, M. Ramonet, L. Rivier, B. Scheeren, M. K. Sha, P. Smith, M. Steinbacher, G. Vítková, and S. Wyss (2021). "Evaluation and optimization of ICOS atmosphere station data as part of the labeling process". In: *Atmospheric Measurement Techniques* 14.1, pp. 89–116. ISSN: 1867-8548. DOI: 10.5194/amt-14-89-2021 (cit. on p. 20).

Zellweger, C., L. Emmenegger, M. Firdaus, J. Hatakka, M. Heimann, E. Kozlova, T. G. Spain, M. Steinbacher, M. V. van der Schoot, and B. Buchmann (2016). "Assessment of Recent Advances in Measurement Techniques for Atmosphericcarbon Dioxide and Methane Observations". In: *Atmospheric Measurement Techniques* 9.9, pp. 4737–4757. ISSN: 1867-8548. DOI: 10.5194/amt-9-4737-2016 (cit. on p. 25).

Zellweger, C., R. Steinbrecher, O. Laurent, H. Lee, S. Kim, L. Emmenegger, M. Steinbacher, and B. Buchmann (2019). "Recent Advances in Measurement Techniques for Atmospheric Carbon Monoxide and Nitrous Oxide Observations". In: *Atmospheric Measurement Techniques* 12.11, pp. 5863–5878. ISSN: 1867-8548. DOI: 10.5194/amt-12-5863-2019 (cit. on p. 25).

9 Acknowledgements

- Empa, Switzerland for the use of Jungfraujoch (JFJ) observations
- ISAC-CNR, Italy for the use of Monte Cimone (CMN) observations
- Irish EPA for the use of Carnsore Point (CSP) observations
- TNO, The Netherlands, for the use of the Cabauw (CBW) CH_4 observations.
- University of East Anglia and NCAS for the use of CH_4 observations from the Weybourne Atmospheric Observatory (WAO).
- University of Frankfurt, Germany, for the use of Taunus (TOB) observations of HFCs and PFCs.
- AGAGE (NASA) for their support of the global atmospheric GHG and O_3-depleting network.
- CSIRO, Australia, for the use of Cape Grim (CGO) observations of all reported gases.

10 Nomenclature

ACTRIS:	Aerosols, Clouds and Trace gases Research Infrastructure
AGAGE:	Advanced Global Atmospheric Gases Experiment
ANSTO:	Australian Nuclear Science and Technology Organisation
BEIS:	Department of Business, Energy and Industrial Strategy, UK
BSD:	Bilsdale tall tower observatory, North Yorkshire, UK
CBW:	Cabauw tall tower observatory, The Netherlands
CFC:	Chlorofluorocarbon
CMN:	Monte Cimone observatory, Italy
CSP:	Carnsore Point observatory, Ireland

DA:	Devolved Administration of the UK
DARE-UK:	Detection and Attribution of Regional greenhouse gas Emissions in the UK
DECC:	Deriving Emissions related to Climate Change Network
ECMWF:	European Centre for Medium-range Weather Forecasting
EDGAR:	Emission Database for Global Atmospheric Research
ERA-5:	ECMWF Re-Analysis meteorology, version 5
ERA-Interim:	ECMWF Re-Analysis meteorology, Interim version
EU:	European Union
GAGE:	Global Atmospheric Gases Experiment
GAUGE:	Greenhouse gAs UK and Global Emissions
GCMD:	Gas Chromatography Multi-Detector
GCMS:	Gas Chromatography Mass Spectrometry
GHG:	GreenHouse Gas
GHGI:	GreenHouse Gas Inventory
GWP_{100}:	Global Warming Potential over a 100 year time-horizon
HCFC:	Hydrochlorofluorocarbon
HFC:	Hydrofluorocarbon
HFD:	Heathfield tall tower observatory, West Sussex, UK
HUGS	HUb for Greenhouse gas data Science
ICOS:	Integrated Carbon Observation System
InTEM:	Inversion Technique for Emission Modelling
IPCC:	Intergovernmental Panel on Climate Change
JFJ:	Jungfraujoch research station, Switzerland
magl:	Metres above ground level
MHD:	Mace Head research station, Ireland
NAEI:	National Atmospheric Emissions Inventory
NAME:	Numerical Atmospheric dispersion Modelling Environment
NASA:	National Aeronautics and Space Administration
NERC:	Natural Environment Research Council
NH:	Northern Hemisphere
NIR:	National Inventory Report
NOAA:	National Oceanic and Atmospheric Administration
NOAA-ESRL:	NOAA Earth System Research Laboratories
NPL:	National Physical Laboratory
NWEU:	North West Europe (IRL,UK,FRA,BEL,NLD,LUX,DEU)
PFC:	Perfluorocarbon
RGL:	Ridge Hill tall tower observatory, Herefordshire, UK

SH:	Southern Hemisphere
TAC:	Tacolneston tall tower observatory, Norfolk, UK
TOB:	Taunus observatory, Germany
TTA:	Angus tall tower observatory, Scotland, UK
UNFCCC:	United Nations Framework Convention on Climate Change
WAO:	Weybourne Atmospheric Observatory, Norfolk, UK

11 Appendix - Tables of UK and NWEU Emissions

Table 6: CH_4 emission (Tg yr^{-1}) estimates with 1-σ uncertainty.

	UK			NWEU		
Years	Inventory	InTEM 2site	InTEM 8site	Inventory	InTEM 2site	InTEM 8site
1990	5.36 ± 0.64	2.22 ± 0.37		15.4 ± 3.86	11.0 ± 0.93	
1991	5.38 ± 0.64	2.21 ± 0.35		15.3 ± 3.82	10.7 ± 0.94	
1992	5.38 ± 0.63	2.00 ± 0.33		15.1 ± 3.77	11.1 ± 0.83	
1993	5.32 ± 0.62	2.05 ± 0.33		15.1 ± 3.76	10.4 ± 0.74	
1994	5.04 ± 0.58	2.29 ± 0.31		14.7 ± 3.67	10.8 ± 0.75	
1995	5.11 ± 0.58	2.12 ± 0.28		14.6 ± 3.66	11.1 ± 0.66	
1996	5.08 ± 0.57	2.58 ± 0.30		14.4 ± 3.61	11.5 ± 0.69	
1997	4.99 ± 0.55	2.23 ± 0.30		14.0 ± 3.51	10.9 ± 0.73	
1998	4.85 ± 0.53	2.38 ± 0.33		13.6 ± 3.41	10.5 ± 0.85	
1999	4.62 ± 0.50	2.23 ± 0.36		13.3 ± 3.32	10.9 ± 0.85	
2000	4.41 ± 0.47	1.86 ± 0.29		12.8 ± 3.21	9.83 ± 0.77	
2001	4.22 ± 0.44	2.19 ± 0.29		12.5 ± 3.11	10.7 ± 0.68	
2002	4.13 ± 0.43	2.04 ± 0.30		12.0 ± 3.01	10.7 ± 0.69	
2003	3.94 ± 0.40	2.24 ± 0.32		11.6 ± 2.91	11.2 ± 0.79	
2004	3.76 ± 0.38	2.12 ± 0.29		11.1 ± 2.78	10.2 ± 0.69	
2005	3.58 ± 0.36	2.13 ± 0.27		10.7 ± 2.67	10.6 ± 0.67	
2006	3.41 ± 0.34	2.09 ± 0.29		10.3 ± 2.58	10.8 ± 0.64	
2007	3.26 ± 0.32	2.17 ± 0.29		10.0 ± 2.51	10.4 ± 0.67	
2008	3.03 ± 0.29	2.05 ± 0.29		9.76 ± 2.44	10.1 ± 0.66	
2009	2.86 ± 0.27	1.83 ± 0.29		9.41 ± 2.35	10.3 ± 0.77	
2010	2.68 ± 0.25	2.09 ± 0.25		9.17 ± 2.29	10.5 ± 0.65	
2011	2.57 ± 0.24	1.73 ± 0.26		8.93 ± 2.23	9.99 ± 0.61	
2012	2.51 ± 0.23	2.50 ± 0.29	2.49 ± 0.15	8.83 ± 2.21	11.4 ± 0.69	11.6 ± 0.42
2013	2.35 ± 0.21	1.99 ± 0.30	2.23 ± 0.13	8.63 ± 2.16	10.6 ± 0.63	11.1 ± 0.38
2014	2.27 ± 0.20	2.18 ± 0.31	2.27 ± 0.10	8.48 ± 2.12	10.8 ± 0.67	10.9 ± 0.34
2015	2.23 ± 0.19	2.20 ± 0.27	2.17 ± 0.10	8.44 ± 2.11	11.6 ± 0.66	11.2 ± 0.35
2016	2.16 ± 0.18	2.15 ± 0.30	2.15 ± 0.11	8.32 ± 2.08	11.2 ± 0.65	10.8 ± 0.35
2017	2.18 ± 0.18	2.05 ± 0.27	2.06 ± 0.10	8.30 ± 2.07	11.1 ± 0.65	10.8 ± 0.35
2018	2.17 ± 0.18	2.22 ± 0.30	2.14 ± 0.11	8.14 ± 2.04	11.3 ± 0.69	10.8 ± 0.36
2019	2.16 ± 0.18	1.90 ± 0.29	2.03 ± 0.10		10.4 ± 0.71	10.7 ± 0.36
2020		2.19 ± 0.31	1.94 ± 0.10		10.7 ± 0.83	10.4 ± 0.36
2021		2.18 ± 0.36	2.01 ± 0.13		10.6 ± 1.04	10.8 ± 0.49

Table 7: N_2O emission (Gg yr^{-1}) estimates with 1-σ uncertainty.

	UK			NWEU		
Years	Inventory	InTEM 1site	InTEM 5site	Inventory	InTEM 1site	InTEM 5site
1990	166. ± 24.6			737. ± 589.5		
1991	167. ± 24.3			731. ± 584.8		
1992	150. ± 21.5			717. ± 573.5		
1993	136. ± 19.1			693. ± 554.4		
1994	138. ± 19.1			700. ± 559.8		
1995	134. ± 18.2	88.8 ± 19.24		701. ± 560.7	513. ± 61.8	
1996	134. ± 17.8	127. ± 19.4		713. ± 570.4	588. ± 63.6	
1997	135. ± 17.6	106. ± 21.9		701. ± 560.8	523. ± 66.3	
1998	135. ± 17.2	126. ± 21.2		635. ± 507.7	575. ± 64.4	
1999	102. ± 12.8	104. ± 22.1		568. ± 454.2	523. ± 62.7	
2000	100. ± 12.3	80.0 ± 17.41		557. ± 445.5	410. ± 65.1	
2001	94.8 ± 11.40	93.1 ± 20.15		548. ± 438.8	518. ± 62.5	
2002	89.3 ± 10.51	86.7 ± 20.38		526. ± 420.5	472. ± 63.6	
2003	87.8 ± 10.12	94.8 ± 19.89		513. ± 410.4	505. ± 62.9	
2004	89.4 ± 10.08	107. ± 19.6		518. ± 414.3	487. ± 60.5	
2005	86.4 ± 9.53	94.3 ± 18.27		503. ± 402.5	532. ± 64.2	
2006	82.5 ± 8.89	80.3 ± 20.70		490. ± 391.6	484. ± 61.8	
2007	82.6 ± 8.69	104. ± 19.4		489. ± 391.1	513. ± 64.5	
2008	80.2 ± 8.24	72.7 ± 18.31		473. ± 378.2	442. ± 61.1	
2009	75.1 ± 7.52	73.0 ± 18.84		459. ± 367.3	418. ± 69.4	
2010	76.5 ± 7.48	76.2 ± 17.85		428. ± 342.4	447. ± 64.0	
2011	73.9 ± 7.03	72.7 ± 20.74		419. ± 335.1	430. ± 66.0	
2012	73.3 ± 6.79	105. ± 19.2	101. ± 11.3	416. ± 332.7	495. ± 66.3	489. ± 38.9
2013	73.1 ± 6.59	94.3 ± 21.51	91.7 ± 9.55	418. ± 334.5	474. ± 59.1	475. ± 34.8
2014	75.4 ± 6.60	91.9 ± 19.39	91.3 ± 7.65	426. ± 341.1	463. ± 62.1	495. ± 32.0
2015	74.0 ± 6.29	89.8 ± 19.75	84.3 ± 7.06	426. ± 341.1	525. ± 66.9	502. ± 32.0
2016	73.2 ± 6.04	85.7 ± 22.25	92.2 ± 7.38	418. ± 334.4	458. ± 67.3	473. ± 31.1
2017	74.7 ± 5.98	75.7 ± 23.28	91.7 ± 7.03	426. ± 340.9	451. ± 69.5	485. ± 33.2
2018	74.0 ± 5.74	96.3 ± 22.78	93.5 ± 7.56	413. ± 330.6	471. ± 67.7	454. ± 32.4
2019	74.6 ± 5.60	79.6 ± 19.85	85.0 ± 6.49		443. ± 60.3	462. ± 28.7
2020		99.0 ± 19.50	83.3 ± 6.79		511. ± 64.5	473. ± 30.9
2021		88.8 ± 22.72	84.3 ± 8.23		470. ± 78.8	472. ± 40.4

Table 8: SF_6 emission (Mg yr^{-1}) estimates with 1-σ uncertainty.

	UK			NWEU		
Years	Inventory	InTEM 3mth	InTEM 1mth	Inventory	InTEM 3mth	InTEM 1mth
2004	50.2 ± 2.66	48.4 ± 27.60		280. ± 28.0	375. ± 313.6	
2005	47.3 ± 2.51	21.5 ± 21.80		267. ± 26.7	230. ± 455.4	
2006	39.6 ± 2.10	43.7 ± 29.40		249. ± 24.9	343. ± 252.4	
2007	37.6 ± 1.99	36.5 ± 70.00		237. ± 23.7	352. ± 382.8	
2008	30.7 ± 1.63	56.1 ± 33.00		223. ± 22.3	238. ± 133.2	
2009	26.8 ± 1.42	50.9 ± 32.40		210. ± 21.0	172. ± 115.0	
2010	31.1 ± 1.65	62.8 ± 23.50		214. ± 21.4	230. ± 80.7	
2011	27.5 ± 1.46	24.7 ± 18.60		202. ± 20.2	154. ± 129.3	
2012	26.7 ± 1.41	44.1 ± 23.90	42.1 ± 56.10	205. ± 20.5	212. ± 61.6	220. ± 134.4
2013	22.9 ± 1.21	41.7 ± 11.70	37.1 ± 26.70	198. ± 19.8	213. ± 45.1	183. ± 108.1
2014	21.9 ± 1.16	26.1 ± 6.90	23.7 ± 8.40	189. ± 18.9	221. ± 39.4	197. ± 65.3
2015	20.9 ± 1.11	26.6 ± 9.40	26.2 ± 8.00	196. ± 19.6	221. ± 50.4	216. ± 132.3
2016	21.9 ± 1.16	24.9 ± 8.10	28.8 ± 14.00	208. ± 20.8	265. ± 69.1	296. ± 83.0
2017	22.4 ± 1.18	26.2 ± 7.60	19.1 ± 9.30	220. ± 22.0	264. ± 85.4	274. ± 118.1
2018	27.0 ± 1.43	28.9 ± 9.50	30.0 ± 12.20	224. ± 22.4	186. ± 53.0	182. ± 78.2
2019	25.9 ± 1.37	26.2 ± 6.10	21.5 ± 6.30		264. ± 48.8	258. ± 75.1
2020		20.5 ± 5.20	16.3 ± 6.10		191. ± 61.0	185. ± 105.2
2021		20.0 ± 7.60	21.3 ± 17.90		182. ± 172.5	151. ± 156.0

Table 9: HFC-134a emission (Gg yr^{-1}) estimates with 1-σ uncertainty.

	UK			NWEU		
Years	Inventory	InTEM 2-yr	InTEM 1-yr	Inventory	InTEM 2-yr	InTEM 1-yr
1995	0.58 ± 0.041	0.55 ± 0.157		3.56 ± 0.356	1.92 ± 0.924	
1996	0.83 ± 0.057	0.87 ± 0.194		5.04 ± 0.504	3.02 ± 1.127	
1997	1.07 ± 0.073	0.87 ± 0.231		6.48 ± 0.648	4.04 ± 1.339	
1998	1.36 ± 0.092	0.98 ± 0.230		7.52 ± 0.752	5.25 ± 1.238	
1999	1.67 ± 0.110	1.07 ± 0.187		7.71 ± 0.771	6.19 ± 1.129	
2000	1.96 ± 0.128	1.19 ± 0.192		8.85 ± 0.885	6.56 ± 1.216	
2001	2.27 ± 0.146	1.48 ± 0.199		10.3 ± 1.03	7.24 ± 1.161	
2002	2.47 ± 0.157	1.74 ± 0.185		11.2 ± 1.12	7.61 ± 0.937	
2003	2.67 ± 0.167	1.98 ± 0.196		12.2 ± 1.22	7.57 ± 0.759	
2004	2.86 ± 0.176	2.01 ± 0.197		12.8 ± 1.28	7.59 ± 0.679	
2005	3.11 ± 0.188	1.89 ± 0.181		13.8 ± 1.38	7.37 ± 0.649	
2006	3.32 ± 0.198	2.08 ± 0.182		14.3 ± 1.43	7.81 ± 0.707	
2007	3.43 ± 0.201	2.53 ± 0.206		14.8 ± 1.48	8.68 ± 0.729	
2008	3.51 ± 0.202	2.61 ± 0.204		15.1 ± 1.51	8.68 ± 0.684	
2009	3.60 ± 0.204	2.53 ± 0.188		15.1 ± 1.51	8.75 ± 0.692	
2010	3.69 ± 0.205	2.82 ± 0.216		15.3 ± 1.53	9.65 ± 0.743	
2011	3.80 ± 0.208	3.05 ± 0.246		15.5 ± 1.55	10.6 ± 0.81	
2012	3.94 ± 0.212	3.10 ± 0.242		15.5 ± 1.55	11.0 ± 0.81	
2013	4.04 ± 0.213	3.09 ± 0.243	3.20 ± 0.390	15.4 ± 1.54	10.4 ± 0.76	10.3 ± 0.99
2014	4.09 ± 0.212	3.00 ± 0.233	2.97 ± 0.310	15.6 ± 1.56	9.88 ± 0.802	9.19 ± 1.000
2015	4.10 ± 0.208	3.00 ± 0.224	2.98 ± 0.295	15.8 ± 1.58	10.5 ± 0.82	11.5 ± 1.24
2016	4.08 ± 0.203	3.25 ± 0.250	3.24 ± 0.350	16.0 ± 1.60	11.0 ± 0.80	10.5 ± 0.93
2017	4.03 ± 0.197	3.47 ± 0.265	3.48 ± 0.408	15.4 ± 1.54	10.8 ± 0.81	11.2 ± 1.21
2018	3.92 ± 0.188	3.11 ± 0.234	3.66 ± 0.342	14.2 ± 1.42	10.1 ± 0.78	10.4 ± 0.98
2019	3.67 ± 0.173	2.47 ± 0.190	2.32 ± 0.252		9.39 ± 0.729	9.24 ± 0.960
2020		2.28 ± 0.181	2.13 ± 0.243		8.73 ± 0.734	8.95 ± 0.912
2021			2.51 ± 0.285			7.85 ± 1.035

Table 10: HFC-125 emission (Gg yr^{-1}) estimates with 1-σ uncertainty.

	UK			NWEU		
Years	Inventory	InTEM 2-yr	InTEM 1-yr	Inventory	InTEM 2-yr	InTEM 1-yr
1999	0.124 ± 0.0082	0.25 ± 0.044		0.75 ± 0.075	0.92 ± 0.206	
2000	0.163 ± 0.0107	0.22 ± 0.052		0.98 ± 0.098	0.90 ± 0.290	
2001	0.22 ± 0.014	0.28 ± 0.058		1.25 ± 0.125	1.10 ± 0.293	
2002	0.26 ± 0.017	0.36 ± 0.047		1.50 ± 0.150	1.33 ± 0.198	
2003	0.32 ± 0.020	0.40 ± 0.047		1.77 ± 0.177	1.30 ± 0.157	
2004	0.39 ± 0.024	0.42 ± 0.048		2.07 ± 0.207	1.39 ± 0.144	
2005	0.45 ± 0.027	0.45 ± 0.045		2.33 ± 0.233	1.53 ± 0.138	
2006	0.57 ± 0.034	0.54 ± 0.049		2.63 ± 0.263	1.78 ± 0.158	
2007	0.61 ± 0.036	0.66 ± 0.057		2.85 ± 0.285	2.09 ± 0.173	
2008	0.67 ± 0.039	0.69 ± 0.055		3.05 ± 0.305	2.22 ± 0.169	
2009	0.73 ± 0.041	0.68 ± 0.054		3.29 ± 0.329	2.44 ± 0.181	
2010	0.81 ± 0.045	0.77 ± 0.066		3.71 ± 0.371	2.85 ± 0.211	
2011	0.90 ± 0.049	0.90 ± 0.077		3.77 ± 0.377	3.09 ± 0.238	
2012	0.97 ± 0.052	0.98 ± 0.081		3.97 ± 0.397	3.25 ± 0.239	
2013	1.03 ± 0.055	0.99 ± 0.092	1.04 ± 0.139	4.05 ± 0.405	3.18 ± 0.235	3.25 ± 0.312
2014	1.07 ± 0.055	0.93 ± 0.093	0.79 ± 0.124	4.13 ± 0.413	3.11 ± 0.250	2.57 ± 0.308
2015	1.08 ± 0.055	0.91 ± 0.084	1.02 ± 0.109	4.22 ± 0.422	3.41 ± 0.256	4.05 ± 0.367
2016	1.11 ± 0.055	0.96 ± 0.087	0.94 ± 0.118	4.18 ± 0.418	3.54 ± 0.250	3.36 ± 0.291
2017	1.13 ± 0.055	1.01 ± 0.094	1.01 ± 0.143	4.08 ± 0.408	3.47 ± 0.255	3.60 ± 0.368
2018	1.11 ± 0.053	0.91 ± 0.087	1.01 ± 0.122	3.93 ± 0.393	3.30 ± 0.246	3.31 ± 0.306
2019	1.08 ± 0.051	0.74 ± 0.071	0.73 ± 0.099		3.06 ± 0.232	3.09 ± 0.306
2020		0.68 ± 0.064	0.64 ± 0.083		2.88 ± 0.232	2.91 ± 0.283
2021			0.71 ± 0.098			2.64 ± 0.347

Table 11: HFC-143a emission (Gg yr^{-1}) estimates with 1-σ uncertainty.

	UK			NWEU		
Years	Inventory	InTEM 2-yr	InTEM 1-yr	Inventory	InTEM 2-yr	InTEM 1-yr
2005	435. ± 26.3	460. ± 49.6		2080 ± 208	1930 ± 221	
2006	481. ± 28.6	537. ± 57.1		2240 ± 224	2190 ± 226	
2007	529. ± 31.0	623. ± 68.3		2400 ± 240	2250 ± 222	
2008	571. ± 32.9	640. ± 70.7		2550 ± 255	1990 ± 191	
2009	610. ± 34.5	632. ± 69.0		2710 ± 271	1880 ± 176	
2010	642. ± 35.8	653. ± 68.8		2840 ± 284	2120 ± 177	
2011	668. ± 36.6	678. ± 65.5		2710 ± 271	2330 ± 183	
2012	684. ± 36.8	683. ± 60.2		2770 ± 277	2510 ± 183	
2013	684. ± 36.1	651. ± 60.3	678. ± 99.5	2720 ± 272	2510 ± 176	2550 ± 237
2014	667. ± 34.6	599. ± 56.7	573. ± 73.0	2660 ± 266	2460 ± 187	2230 ± 233
2015	639. ± 32.5	572. ± 53.4	595. ± 69.9	2570 ± 257	2540 ± 193	2840 ± 276
2016	612. ± 30.5	575. ± 56.5	561. ± 83.4	2330 ± 233	2430 ± 188	2300 ± 229
2017	584. ± 28.6	525. ± 55.7	556. ± 85.1	1980 ± 198	2150 ± 177	2230 ± 255
2018	548. ± 26.3	394. ± 46.1	434. ± 71.6	1640 ± 164	1810 ± 156	1760 ± 197
2019	507. ± 23.8	291. ± 35.4	293. ± 45.9		1530 ± 138	1550 ± 177
2020		263. ± 31.5	243. ± 40.3		1310 ± 133	1280 ± 161
2021			274. ± 48.4			1140 ± 189

Table 12: HFC-32 emission (Mg yr^{-1}) estimates with 1-σ uncertainty.

	UK			NWEU		
Years	Inventory	InTEM 2-yr	InTEM 1-yr	Inventory	InTEM 2-yr	InTEM 1-yr
2005	90.2 ± 5.46	93.4 ± 14.90		410 ± 41	400 ± 116	
2006	114. ± 6.8	119. ± 18.8		510 ± 51	590 ± 130	
2007	142. ± 8.3	164. ± 21.1		610 ± 61	670 ± 111	
2008	171. ± 9.9	196. ± 21.6		720 ± 72	590 ± 81	
2009	199. ± 11.3	203. ± 24.5		830 ± 83	590 ± 81	
2010	231. ± 12.9	217. ± 28.6		960 ± 96	680 ± 95	
2011	263. ± 14.4	241. ± 29.8		1060 ± 106	770 ± 102	
2012	300. ± 16.1	282. ± 31.3		1160 ± 116	880 ± 102	
2013	337. ± 17.8	311. ± 36.9	356. ± 57.7	1280 ± 128	900 ± 102	970 ± 141
2014	368. ± 19.1	300. ± 37.4	244. ± 47.8	1430 ± 143	900 ± 113	750 ± 139
2015	393. ± 20.0	302. ± 33.9	335. ± 45.2	1590 ± 159	990 ± 118	1170 ± 184
2016	431. ± 21.5	336. ± 36.6	320. ± 49.3	1780 ± 178	1100 ± 120	1030 ± 143
2017	472. ± 23.1	402. ± 49.0	427. ± 72.7	2000 ± 200	1240 ± 147	1300 ± 206
2018	505. ± 24.2	422. ± 53.4	532. ± 101.0	2190 ± 219	1380 ± 164	1430 ± 225
2019	534. ± 25.1	384. ± 41.7	380. ± 57.4		1500 ± 156	1550 ± 208
2020		390. ± 35.6	366. ± 45.1		1600 ± 156	1620 ± 190
2021			428. ± 63.8			1590 ± 250

Table 13: HFC-227ea emission (Mg yr^{-1}) estimates with 1-σ uncertainty.

	UK			NWEU		
Years	Inventory	InTEM 2-yr	InTEM 1-yr	Inventory	InTEM 2-yr	InTEM 1-yr
2006	127. ± 7.6	52.4 ± 16.20		206. ± 20.6	144. ± 33.6	
2007	130. ± 7.6	43.7 ± 8.30		218. ± 21.8	165. ± 28.5	
2008	122. ± 7.0	33.5 ± 6.70		210. ± 21.0	138. ± 23.0	
2009	124. ± 7.0	30.1 ± 5.90		213. ± 21.3	128. ± 19.1	
2010	131. ± 7.3	36.5 ± 7.40		229. ± 22.9	147. ± 20.4	
2011	140. ± 7.7	37.3 ± 7.80		249. ± 24.9	178. ± 22.6	
2012	148. ± 8.0	36.0 ± 6.60		257. ± 25.7	194. ± 21.6	
2013	154. ± 8.1	41.4 ± 6.30	34.8 ± 11.40	257. ± 25.7	173. ± 20.3	169. ± 30.1
2014	162. ± 8.4	47.1 ± 6.10	43.6 ± 8.90	269. ± 26.9	158. ± 21.8	139. ± 30.7
2015	168. ± 8.6	52.8 ± 6.40	51.0 ± 9.80	281. ± 28.1	171. ± 23.6	213. ± 44.9
2016	170. ± 8.5	61.1 ± 7.60	61.2 ± 13.40	283. ± 28.3	174. ± 23.6	170. ± 35.5
2017	171. ± 8.4	69.7 ± 8.50	70.3 ± 13.30	285. ± 28.5	177. ± 24.3	166. ± 40.7
2018	170. ± 8.1	68.3 ± 8.20	90.4 ± 17.20	263. ± 26.3	192. ± 24.7	222. ± 39.9
2019	168. ± 7.9	57.1 ± 7.20	56.7 ± 11.10		199. ± 24.3	202. ± 35.7
2020		50.0 ± 6.80	48.4 ± 9.90		189. ± 25.8	208. ± 37.0
2021			57.8 ± 12.40			163. ± 52.2

Table 14: HFC-23 emission (Mg yr^{-1}) estimates with 1-σ uncertainty.

	UK			NWEU		
Years	Inventory	InTEM 2-yr	InTEM 1-yr	Inventory	InTEM 2-yr	InTEM 1-yr
2008	4.70 ± 0.270	15.3 ± 15.3		104 ± 10.4	176 ± 42.3	
2009	3.80 ± 0.210	16.6 ± 14.1		64 ± 6.4	128 ± 36.3	
2010	1.14 ± 0.063	22.0 ± 13.8		89 ± 8.9	136 ± 39.8	
2011	1.01 ± 0.055	20.0 ± 11.7		84 ± 8.4	137 ± 35.9	
2012	0.90 ± 0.049	19.5 ± 10.8		73 ± 7.3	118 ± 30.3	
2013	1.04 ± 0.055	19.2 ± 13.2	18.9 ± 19.7	85 ± 8.5	103 ± 30.1	113 ± 40.1
2014	1.25 ± 0.065	17.4 ± 14.8	22.0 ± 20.3	78 ± 7.8	90 ± 32.3	79 ± 39.1
2015	1.35 ± 0.068	18.5 ± 14.9	19.0 ± 19.1	93 ± 9.3	110 ± 36.7	137 ± 48.7
2016	1.46 ± 0.073	20.0 ± 17.2	28.0 ± 23.5	96 ± 9.6	103 ± 39.9	127 ± 48.6
2017	1.43 ± 0.070	17.4 ± 18.1	14.9 ± 27.9	118 ± 11.8	86 ± 38.9	059 ± 53.4
2018	1.58 ± 0.076	12.4 ± 13.2	11.6 ± 20.1	133 ± 13.3	110 ± 34.1	123 ± 44.2
2019	1.74 ± 0.082	7.7 ± 8.5	12.5 ± 10.0		117 ± 30.1	140 ± 33.3
2020		6.1 ± 8.9	5.5 ± 11.3		97 ± 33.1	76 ± 40.8
2021			19.7 ± 20.2			129 ± 55.4

Table 15: HFC-245fa emission (Mg yr^{-1}) estimates with 1-σ uncertainty.

	UK			NWEU		
Years	Inventory	InTEM 2-yr	InTEM 1-yr	Inventory	InTEM 2-yr	InTEM 1-yr
2008	66.7 ± 3.84	63.3 ± 16.20		165. ± 16.5	138. ± 34.3	
2009	68.0 ± 3.86	54.6 ± 15.50		150. ± 15.0	117. ± 32.6	
2010	69.2 ± 3.85	47.5 ± 15.20		158. ± 15.8	124. ± 32.5	
2011	69.8 ± 3.82	39.4 ± 13.90		173. ± 17.3	170. ± 35.0	
2012	72.1 ± 3.88	33.9 ± 10.80		175. ± 17.5	196. ± 31.5	
2013	74.7 ± 3.95	34.1 ± 10.10	30.5 ± 12.50	202. ± 20.2	189. ± 26.9	175. ± 31.4
2014	79.4 ± 4.11	36.1 ± 9.90	25.9 ± 13.70	224. ± 22.4	212. ± 28.0	189. ± 34.9
2015	84.4 ± 4.29	43.1 ± 9.80	47.9 ± 12.20	288. ± 28.8	265. ± 30.3	283. ± 41.9
2016	89.9 ± 4.49	47.7 ± 11.90	46.0 ± 16.70	338. ± 33.8	314. ± 33.4	306. ± 40.2
2017	95.7 ± 4.68	53.3 ± 13.90	54.4 ± 19.80	400. ± 40.0	341. ± 37.3	393. ± 52.3
2018	98.0 ± 4.70	52.9 ± 13.20	62.5 ± 19.20	421. ± 42.1	311. ± 37.2	335. ± 47.0
2019	98.9 ± 4.65	44.6 ± 11.00	39.9 ± 14.30		235. ± 33.3	234. ± 41.2
2020		46.3 ± 9.60	42.0 ± 11.00		188. ± 32.4	177. ± 37.0
2021			55.5 ± 15.30			184. ± 53.0

Table 16: HFC-365mfc emission (Mg yr^{-1}) estimates with 1-σ uncertainty.

	UK			NWEU		
Years	Inventory	InTEM 2-yr	InTEM 1-yr	Inventory	InTEM 2-yr	InTEM 1-yr
2005	137. ± 8.3	167. ± 18.7		213. ± 21.3	404. ± 41.1	
2006	148. ± 8.8	182. ± 17.6		232. ± 23.2	466. ± 44.0	
2007	158. ± 9.3	167. ± 16.8		333. ± 33.3	442. ± 44.2	
2008	101. ± 5.8	110. ± 12.8		302. ± 30.2	377. ± 37.8	
2009	101. ± 5.7	69.7 ± 10.30		290. ± 29.0	376. ± 33.8	
2010	101. ± 5.6	77.1 ± 12.20		329. ± 32.9	440. ± 36.8	
2011	99.2 ± 5.43	82.8 ± 12.70		338. ± 33.8	520. ± 41.9	
2012	102. ± 5.5	77.9 ± 10.80		318. ± 31.8	570. ± 40.0	
2013	105. ± 5.6	86.2 ± 11.10	78.7 ± 17.10	328. ± 32.8	577. ± 36.6	590. ± 46.9
2014	112. ± 5.8	95.9 ± 11.30	105. ± 15.3	396. ± 39.6	572. ± 40.3	541. ± 51.5
2015	118. ± 6.0	98.3 ± 11.40	96.0 ± 14.90	491. ± 49.1	591. ± 43.2	652. ± 62.2
2016	126. ± 6.3	98.5 ± 12.50	106. ± 19.1	511. ± 51.1	574. ± 42.8	581. ± 52.2
2017	135. ± 6.6	92.9 ± 12.30	74.8 ± 17.00	527. ± 52.7	520. ± 42.3	523. ± 58.7
2018	137. ± 6.6	74.2 ± 10.80	91.2 ± 15.90	445. ± 44.5	491. ± 39.8	497. ± 50.3
2019	138. ± 6.5	56.4 ± 9.30	50.8 ± 12.40		451. ± 35.7	491. ± 45.8
2020		56.4 ± 8.80	54.1 ± 11.90		380. ± 33.4	388. ± 42.8
2021			68.1 ± 12.60			282. ± 44.9

Table 17: HFC-152a emission (Mg yr^{-1}) estimates with 1-σ uncertainty.

	UK			NWEU		
Years	Inventory	InTEM 2-yr	InTEM 1-yr	Inventory	InTEM 2-yr	InTEM 1-yr
1995	10.2 ± 0.72	19.5 ± 29.20		760 ± 191	290 ± 130	
1996	18.9 ± 1.31	30.3 ± 28.20		820 ± 204	340 ± 134	
1997	41.3 ± 2.82	25.0 ± 23.50		850 ± 212	400 ± 137	
1998	65.9 ± 4.44	32.7 ± 24.40		840 ± 210	440 ± 122	
1999	94.8 ± 6.29	37.0 ± 23.10		930 ± 234	520 ± 117	
2000	122. ± 8.0	43.7 ± 22.30		990 ± 248	710 ± 139	
2001	139. ± 8.9	73.9 ± 25.10		2040 ± 509	1000 ± 143	
2002	193. ± 12.2	107. ± 28.4		2350 ± 587	1160 ± 120	
2003	246. ± 15.4	126. ± 33.0		2230 ± 558	1150 ± 102	
2004	217. ± 13.3	103. ± 34.9		2040 ± 511	1040 ± 97	
2005	207. ± 12.5	68.8 ± 34.50		1490 ± 371	850 ± 100	
2006	213. ± 12.7	72.0 ± 37.10		1400 ± 351	800 ± 115	
2007	219. ± 12.8	92.6 ± 39.70		1470 ± 366	890 ± 123	
2008	188. ± 10.9	97.0 ± 35.50		1360 ± 341	900 ± 115	
2009	136. ± 7.7	94.2 ± 31.20		1280 ± 319	850 ± 109	
2010	129. ± 7.2	113. ± 37.6		1250 ± 313	890 ± 120	
2011	188. ± 10.3	130. ± 45.9		1280 ± 319	920 ± 143	
2012	249. ± 13.4	119. ± 41.5		1170 ± 292	920 ± 133	
2013	260. ± 13.7	94.7 ± 36.10	90.2 ± 47.90	1050 ± 261	840 ± 107	880 ± 132
2014	279. ± 14.5	84.8 ± 36.10	73.8 ± 52.20	1020 ± 254	720 ± 105	640 ± 128
2015	299. ± 15.2	89.9 ± 34.00	104. ± 43.4	960 ± 240	690 ± 102	690 ± 146
2016	319. ± 15.9	106. ± 34.8	100. ± 47.5	960 ± 239	700 ± 98	670 ± 117
2017	340. ± 16.6	121. ± 36.3	146. ± 56.9	980 ± 244	650 ± 99	700 ± 148
2018	364. ± 17.5	104. ± 33.2	115. ± 45.5	1030 ± 258	560 ± 94	520 ± 117
2019	384. ± 18.1	74.5 ± 28.10	66.7 ± 39.60		490 ± 87	560 ± 117
2020		57.8 ± 24.30	58.9 ± 29.90		380 ± 85	350 ± 101
2021			54.3 ± 35.80			310 ± 102

Table 18: HFC-43-10mee emission (Mg yr^{-1}) estimates with 1-σ uncertainty.

	UK			NWEU		
Years	Inventory	InTEM 2-yr	InTEM 1-yr	Inventory	InTEM 2-yr	InTEM 1-yr
2011	9.26 ± 0.507	8.4 ± 4.7		9.26 ± 0.926	34.9 ± 8.0	
2012	9.63 ± 0.518	9.3 ± 3.1		9.63 ± 0.963	30.7 ± 6.0	
2013	9.93 ± 0.524	8.6 ± 2.0	8.3 ± 2.9	11.5 ± 1.15	26.6 ± 4.7	26.2 ± 6.4
2014	10.2 ± 0.53	7.4 ± 1.7	6.8 ± 2.3	11.2 ± 1.12	27.1 ± 4.7	23.5 ± 5.7
2015	10.9 ± 0.55	6.9 ± 2.0	7.1 ± 2.5	12.1 ± 1.21	30.7 ± 5.2	36.3 ± 6.7
2016	10.9 ± 0.54	7.4 ± 2.3	6.4 ± 3.1	12.1 ± 1.21	31.1 ± 5.7	29.5 ± 7.0
2017	10.1 ± 0.50	8.2 ± 2.6	9.1 ± 3.4	13.1 ± 1.31	31.2 ± 6.1	35.7 ± 8.3
2018	9.83 ± 0.471	7.9 ± 2.6	7.3 ± 3.4	12.6 ± 1.26	32.5 ± 6.1	31.4 ± 7.4
2019	9.82 ± 0.462	6.5 ± 2.2	7.3 ± 2.9		28.3 ± 5.6	34.1 ± 7.1
2020		5.3 ± 1.9	4.5 ± 2.4		21.7 ± 5.4	19.0 ± 6.6
2021			5.9 ± 2.3			24.4 ± 7.7

Table 19: PFC-14 emission (Mg yr^{-1}) estimates with 1-σ uncertainty.

	UK			NWEU		
Years	Inventory	InTEM 2-yr	InTEM 1-yr	Inventory	InTEM 2-yr	InTEM 1-yr
2005	21.4 ± 1.93	56.8 ± 18.0		230 ± 23	330 ± 237	
2006	24.7 ± 2.33	51.0 ± 16.1		182 ± 18	320 ± 184	
2007	18.5 ± 1.83	46.9 ± 12.8		151 ± 15	250 ± 244	
2008	22.0 ± 2.27	43.9 ± 13.4		119 ± 12	197 ± 354	
2009	14.7 ± 1.58	32.6 ± 12.8		73 ± 7	174 ± 225	
2010	21.6 ± 2.41	28.9 ± 11.6		79 ± 8	164 ± 64	
2011	28.8 ± 3.35	26.0 ± 10.0		87 ± 9	169 ± 57	
2012	10.1 ± 1.22	20.1 ± 8.5		55 ± 6	155 ± 47	
2013	10.4 ± 1.30	19.5 ± 9.8	19.9 ± 16.1	51 ± 5	133 ± 40	150 ± 59
2014	14.3 ± 1.85	17.1 ± 11.5	21.8 ± 15.9	50 ± 5	117 ± 45	108 ± 66
2015	12.2 ± 1.63	16.1 ± 13.2	20.3 ± 18.0	52 ± 5	121 ± 50	150 ± 88
2016	13.5 ± 1.86	16.8 ± 15.8	21.0 ± 25.8	80 ± 8	122 ± 52	128 ± 70
2017	15.7 ± 2.23	15.2 ± 16.6	14.8 ± 27.5	69 ± 7	99 ± 57	61 ± 91
2018	13.8 ± 2.02	15.1 ± 12.5	15.1 ± 18.4	73 ± 7	99 ± 52	91 ± 70
2019	15.1 ± 2.28	13.4 ± 8.4	13.3 ± 11.1		120 ± 45	143 ± 55
2020		16.3 ± 8.6	19.5 ± 11.9		116 ± 57	105 ± 90
2021			36.3 ± 16.5			155 ± 153

Table 20: PFC-116 emission (Mg yr^{-1}) estimates with 1-σ uncertainty.

	UK			NWEU		
Years	Inventory	InTEM 2-yr	InTEM 1-yr	Inventory	InTEM 2-yr	InTEM 1-yr
2005	8.98 ± 0.810	6.1 ± 7.0		80.9 ± 8.09	70.6 ± 94.9	
2006	8.96 ± 0.847	12.0 ± 7.4		71.8 ± 7.18	85.9 ± 74.8	
2007	7.57 ± 0.748	15.2 ± 8.0		57.3 ± 5.73	69.8 ± 49.7	
2008	7.32 ± 0.756	12.8 ± 7.8		40.1 ± 4.01	40.0 ± 22.6	
2009	6.15 ± 0.662	10.9 ± 7.6		26.7 ± 2.67	39.9 ± 18.4	
2010	7.10 ± 0.795	7.6 ± 6.8		25.4 ± 2.54	39.7 ± 18.7	
2011	8.57 ± 0.996	5.3 ± 5.4		25.7 ± 2.57	34.8 ± 17.8	
2012	6.49 ± 0.783	7.4 ± 4.3		20.7 ± 2.07	32.3 ± 14.5	
2013	7.49 ± 0.936	7.6 ± 4.0	7.3 ± 6.2	18.8 ± 1.88	32.7 ± 12.3	30.3 ± 15.4
2014	7.68 ± 0.993	5.7 ± 3.7	6.3 ± 4.9	18.3 ± 1.83	34.5 ± 12.9	35.4 ± 16.3
2015	8.45 ± 1.129	4.9 ± 4.0	3.7 ± 5.0	19.4 ± 1.94	32.8 ± 14.9	36.8 ± 18.4
2016	9.19 ± 1.268	4.4 ± 4.8	4.7 ± 7.4	22.5 ± 2.25	25.1 ± 16.6	24.2 ± 21.2
2017	11.0 ± 1.57	4.4 ± 5.1	5.6 ± 8.5	24.8 ± 2.48	27.8 ± 17.4	32.7 ± 27.7
2018	9.31 ± 1.365	4.3 ± 3.9	5.3 ± 7.4	21.1 ± 2.11	33.8 ± 15.7	39.4 ± 23.2
2019	10.7 ± 1.62	3.8 ± 2.7	3.9 ± 3.4		31.1 ± 12.9	42.9 ± 15.0
2020		4.5 ± 2.7	2.7 ± 3.6		28.9 ± 15.8	22.4 ± 24.0
2021			6.9 ± 6.0			40.6 ± 34.5

Table 21: PFC-218 emission (Mg yr^{-1}) estimates with 1-σ uncertainty.

	UK			NWEU		
Years	Inventory	InTEM 2-yr	InTEM 1-yr	Inventory	InTEM 2-yr	InTEM 1-yr
2005	12.6 ± 1.14	21.6 ± 5.2		33.3 ± 3.33	48.5 ± 61.9	
2006	10.4 ± 0.98	18.3 ± 4.4		30.6 ± 3.06	49.2 ± 41.3	
2007	6.35 ± 0.628	16.7 ± 4.3		25.7 ± 2.57	42.7 ± 27.1	
2008	1.53 ± 0.158	13.6 ± 4.6		15.5 ± 1.55	30.7 ± 11.9	
2009	1.52 ± 0.163	13.0 ± 4.9		10.8 ± 1.08	27.2 ± 11.3	
2010	4.60 ± 0.514	12.1 ± 4.5		12.0 ± 1.20	27.7 ± 10.3	
2011	11.0 ± 1.27	12.6 ± 3.5		16.7 ± 1.67	28.6 ± 9.3	
2012	11.2 ± 1.35	13.4 ± 2.9		14.6 ± 1.46	28.8 ± 8.0	
2013	16.6 ± 2.07	13.2 ± 2.9	13.2 ± 3.9	19.7 ± 1.97	26.1 ± 7.1	30.3 ± 9.3
2014	8.69 ± 1.124	14.3 ± 3.2	14.4 ± 4.7	11.4 ± 1.14	24.0 ± 7.7	22.1 ± 11.4
2015	14.8 ± 1.97	14.0 ± 3.4	15.9 ± 4.4	17.2 ± 1.72	23.9 ± 8.1	31.8 ± 12.8
2016	15.7 ± 2.16	10.7 ± 3.5	7.9 ± 5.7	17.9 ± 1.79	21.6 ± 7.8	19.8 ± 11.8
2017	26.8 ± 3.81	10.1 ± 3.5	10.0 ± 5.1	28.6 ± 2.86	20.9 ± 7.6	24.3 ± 11.3
2018	4.59 ± 0.674	11.3 ± 2.9	12.4 ± 4.4	6.67 ± 0.67	21.8 ± 7.0	19.6 ± 9.7
2019	11.3 ± 1.70	10.5 ± 2.4	9.4 ± 3.2		22.8 ± 6.3	24.2 ± 8.2
2020		11.4 ± 2.6	11.0 ± 3.4		24.2 ± 7.4	24.3 ± 9.8
2021			13.8 ± 4.6			30.9 ± 13.2

Table 22: PFC-318 emission (Mg yr^{-1}) estimates with 1-σ uncertainty.

	UK			NWEU		
Years	Inventory	InTEM 2-yr	InTEM 1-yr	Inventory	InTEM 2-yr	InTEM 1-yr
2011	0.0038 ± 0.00044	3.4 ± 4.9		0.89 ± 0.089	17.5 ± 14.6	
2012	0.0042 ± 0.00050	6.9 ± 4.2		0.78 ± 0.078	21.2 ± 12.2	
2013	0.0045 ± 0.00056	6.3 ± 3.6	7.4 ± 5.8	0.71 ± 0.071	17.3 ± 9.3	18.9 ± 12.7
2014	0.0049 ± 0.00064	3.5 ± 3.4	3.8 ± 4.5	0.57 ± 0.057	12.1 ± 9.8	13.1 ± 14.5
2015	0.0054 ± 0.00072	3.4 ± 3.9	6.8 ± 5.7	0.68 ± 0.068	16.9 ± 12.0	26.6 ± 19.4
2016	0.0058 ± 0.00081	5.1 ± 5.2	4.6 ± 8.1	0.76 ± 0.076	22.6 ± 13.5	25.5 ± 17.9
2017	0.0064 ± 0.00091	6.5 ± 6.2	12.4 ± 10.4	0.72 ± 0.072	22.8 ± 15.5	28.8 ± 23.2
2018	0.0069 ± 0.00101	6.6 ± 5.1	7.1 ± 8.8	0.78 ± 0.078	22.6 ± 14.2	26.2 ± 21.3
2019	0.0075 ± 0.00114	5.5 ± 3.3	7.5 ± 4.1		18.9 ± 10.4	21.4 ± 13.1
2020		3.6 ± 3.0	3.3 ± 5.0		14.5 ± 10.4	14.8 ± 16.5
2021			5.0 ± 4.9			18.6 ± 17.5

Table 23: NF_3 emission (Mg yr^{-1}) estimates with 1-σ uncertainty.

	UK			NWEU		
Years	Inventory	InTEM 2-yr	InTEM 1-yr	Inventory	InTEM 2-yr	InTEM 1-yr
2013	0.021 ± 0.0053	0.5 ± 2.6		1.70 ± 0.170	2.8 ± 7.1	
2014	0.023 ± 0.0058	0.6 ± 2.3	1.0 ± 2.9	1.67 ± 0.167	2.3 ± 6.9	2.7 ± 7.2
2015	0.025 ± 0.0064	0.5 ± 2.1	0.5 ± 3.0	1.18 ± 0.118	2.4 ± 6.8	2.2 ± 9.3
2016	0.028 ± 0.0070	0.4 ± 2.6	1.5 ± 3.3	1.11 ± 0.111	3.3 ± 7.0	6.3 ± 7.9
2017	0.031 ± 0.0077	0.4 ± 3.0	0.7 ± 6.0	1.25 ± 0.125	2.7 ± 8.2	1.7 ± 13.0
2018	0.034 ± 0.0085	0.2 ± 2.6	0.1 ± 3.9	1.54 ± 0.154	3.3 ± 8.6	4.1 ± 11.5
2019	0.037 ± 0.0093	0.5 ± 2.1	2.1 ± 2.8		5.7 ± 8.8	9.7 ± 12.2
2020		0.9 ± 2.2	0.1 ± 3.0		5.2 ± 11.0	3.1 ± 15.6
2021			3.3 ± 3.9			4.3 ± 23.6

Table 24: CFC emission (Gg yr^{-1}) estimates with 1-σ uncertainty.

	UK		NWEU	
Years	InTEM 2-yr	InTEM 1-yr	InTEM 2-yr	InTEM 1-yr
1990	6.03 ± 0.886		22.5 ± 13.61	
1991	3.74 ± 0.735		20.4 ± 8.54	
1992	2.65 ± 0.510		15.9 ± 6.36	
1993	1.65 ± 0.345		8.02 ± 5.311	
1994	1.10 ± 0.235		5.14 ± 3.453	
1995	1.14 ± 0.171		3.92 ± 2.091	
1996	1.17 ± 0.142		3.72 ± 2.023	
1997	0.97 ± 0.126		4.23 ± 2.070	
1998	0.87 ± 0.125		4.28 ± 1.943	
1999	0.84 ± 0.127		3.49 ± 1.542	
2000	0.76 ± 0.125		3.10 ± 1.272	
2001	0.65 ± 0.121		3.31 ± 1.344	
2002	0.65 ± 0.113		3.53 ± 1.218	
2003	0.82 ± 0.116		3.55 ± 1.052	
2004	0.74 ± 0.102		2.90 ± 1.368	
2005	0.50 ± 0.085		2.43 ± 1.407	
2006	0.50 ± 0.093		2.89 ± 1.164	
2007	0.52 ± 0.097		2.83 ± 0.807	
2008	0.46 ± 0.088		2.26 ± 0.407	
2009	0.39 ± 0.074		1.94 ± 0.343	
2010	0.36 ± 0.071		1.77 ± 0.312	
2011	0.32 ± 0.062		1.72 ± 0.298	
2012	0.29 ± 0.060		1.84 ± 0.272	
2013	0.30 ± 0.062	0.33 ± 0.118	1.84 ± 0.253	1.85 ± 0.296
2014	0.30 ± 0.057	0.28 ± 0.080	1.78 ± 0.278	1.83 ± 0.376
2015	0.31 ± 0.062	0.29 ± 0.089	1.74 ± 0.297	1.65 ± 0.484
2016	0.37 ± 0.066	0.36 ± 0.107	1.70 ± 0.275	1.71 ± 0.360
2017	0.34 ± 0.072	0.41 ± 0.099	1.52 ± 0.275	1.52 ± 0.365
2018	0.22 ± 0.062	0.185 ± 0.1159	1.33 ± 0.252	1.28 ± 0.366
2019	0.173 ± 0.0420	0.164 ± 0.0535	1.27 ± 0.221	1.42 ± 0.284
2020	0.171 ± 0.0366	0.155 ± 0.0432	1.26 ± 0.223	1.16 ± 0.234

Table 25: CFC-12 emission (Gg yr^{-1}) estimates with 1-σ uncertainty.

	UK		NWEU	
Years	InTEM 2-yr	InTEM 1-yr	InTEM 2-yr	InTEM 1-yr
1990	5.21 ± 1.007		22.0 ± 11.12	
1991	3.27 ± 0.798		17.5 ± 7.53	
1992	3.06 ± 0.696		13.9 ± 6.77	
1993	2.45 ± 0.580		10.2 ± 6.99	
1994	1.84 ± 0.397		7.48 ± 5.037	
1995	1.72 ± 0.279		6.33 ± 3.087	
1996	1.64 ± 0.231		5.75 ± 2.835	
1997	1.29 ± 0.207		5.39 ± 2.916	
1998	1.02 ± 0.192		4.93 ± 2.693	
1999	0.85 ± 0.173		3.88 ± 1.921	
2000	0.66 ± 0.150		3.17 ± 1.449	
2001	0.55 ± 0.133		3.30 ± 1.533	
2002	0.56 ± 0.121		3.12 ± 1.255	
2003	0.60 ± 0.108		2.66 ± 0.978	
2004	0.49 ± 0.091		2.09 ± 1.283	
2005	0.35 ± 0.073		1.60 ± 1.184	
2006	0.33 ± 0.070		1.57 ± 0.784	
2007	0.31 ± 0.074		1.50 ± 0.551	
2008	0.26 ± 0.074		1.32 ± 0.334	
2009	0.20 ± 0.068		1.13 ± 0.343	
2010	0.164 ± 0.0606		0.99 ± 0.311	
2011	0.152 ± 0.0582		0.95 ± 0.291	
2012	0.149 ± 0.0544		0.81 ± 0.255	
2013	0.137 ± 0.0531	0.141 ± 0.0778	0.69 ± 0.210	0.59 ± 0.241
2014	0.131 ± 0.0534	0.162 ± 0.0746	0.86 ± 0.227	1.19 ± 0.328
2015	0.116 ± 0.0541	0.108 ± 0.0857	0.80 ± 0.247	0.80 ± 0.421
2016	0.097 ± 0.0567	0.087 ± 0.0783	0.55 ± 0.236	0.51 ± 0.285
2017	0.095 ± 0.0599	0.098 ± 0.0925	0.51 ± 0.238	0.46 ± 0.390
2018	0.077 ± 0.0533	0.091 ± 0.0918	0.47 ± 0.219	0.51 ± 0.304
2019	0.046 ± 0.0422	0.049 ± 0.0548	0.43 ± 0.201	0.45 ± 0.269
2020	0.034 ± 0.0391	0.045 ± 0.0562	0.40 ± 0.207	0.35 ± 0.291

Table 26: HCFC-22 emission (Gg yr^{-1}) estimates with 1-σ uncertainty.

	UK		NWEU	
Years	InTEM 2-yr	InTEM 1-yr	InTEM 2-yr	InTEM 1-yr
1999	2.40 ± 0.481		11.6 ± 4.27	
2000	2.46 ± 0.538		12.0 ± 4.84	
2001	2.52 ± 0.508		10.5 ± 4.83	
2002	2.40 ± 0.397		9.31 ± 2.924	
2003	2.34 ± 0.368		10.1 ± 1.54	
2004	2.16 ± 0.340		9.16 ± 1.389	
2005	1.82 ± 0.296		7.56 ± 1.319	
2006	1.78 ± 0.278		6.63 ± 1.350	
2007	1.83 ± 0.279		6.33 ± 1.328	
2008	1.51 ± 0.245		6.37 ± 1.168	
2009	1.19 ± 0.209		5.49 ± 0.912	
2010	1.12 ± 0.218		4.64 ± 0.824	
2011	0.89 ± 0.200		3.83 ± 0.811	
2012	0.69 ± 0.155		2.84 ± 0.607	
2013	0.61 ± 0.146	0.65 ± 0.250	2.43 ± 0.439	2.53 ± 0.577
2014	0.48 ± 0.142	0.47 ± 0.182	1.96 ± 0.461	1.97 ± 0.605
2015	0.39 ± 0.141	0.38 ± 0.195	1.55 ± 0.502	1.57 ± 0.865
2016	0.36 ± 0.135	0.29 ± 0.210	1.27 ± 0.449	1.17 ± 0.488
2017	0.30 ± 0.116	0.36 ± 0.183	0.96 ± 0.379	1.16 ± 0.651
2018	0.20 ± 0.095	0.22 ± 0.162	0.69 ± 0.302	0.71 ± 0.374
2019	0.132 ± 0.0620	0.121 ± 0.0785	0.53 ± 0.211	0.57 ± 0.272
2020	0.084 ± 0.0441	0.077 ± 0.0632	0.51 ± 0.198	0.45 ± 0.233
2021	0.073 ± 0.0459	0.080 ± 0.0711	0.57 ± 0.226	0.77 ± 0.470

Table 27: HCFC-141b emission (Gg yr^{-1}) estimates with 1-σ uncertainty.

	UK		NWEU	
Years	InTEM 2-yr	InTEM 1-yr	InTEM 2-yr	InTEM 1-yr
1994	1.15 ± 0.505		3.49 ± 4.720	
1995	1.13 ± 0.432		4.23 ± 4.403	
1996	1.03 ± 0.365		4.99 ± 4.043	
1997	0.97 ± 0.386		4.62 ± 3.841	
1998	0.95 ± 0.297		4.02 ± 3.086	
1999	0.88 ± 0.175		3.82 ± 2.319	
2000	0.92 ± 0.159		4.33 ± 2.312	
2001	0.95 ± 0.146		4.12 ± 1.972	
2002	0.96 ± 0.122		3.76 ± 1.214	
2003	0.84 ± 0.106		3.59 ± 0.932	
2004	0.45 ± 0.077		2.20 ± 1.024	
2005	0.186 ± 0.0538		1.25 ± 0.874	
2006	0.169 ± 0.0541		1.08 ± 0.621	
2007	0.193 ± 0.0502		0.97 ± 0.462	
2008	0.182 ± 0.0377		0.80 ± 0.232	
2009	0.164 ± 0.0308		0.63 ± 0.169	
2010	0.160 ± 0.0333		0.61 ± 0.166	
2011	0.162 ± 0.0273		0.56 ± 0.125	
2012	0.165 ± 0.0236		0.52 ± 0.081	
2013	0.157 ± 0.0319	0.140 ± 0.0518	0.47 ± 0.083	0.47 ± 0.110
2014	0.154 ± 0.0326	0.169 ± 0.0462	0.38 ± 0.083	0.36 ± 0.110
2015	0.144 ± 0.0312	0.144 ± 0.0426	0.38 ± 0.082	0.38 ± 0.101
2016	0.140 ± 0.0266	0.128 ± 0.0424	0.42 ± 0.074	0.45 ± 0.105
2017	0.154 ± 0.0220	0.154 ± 0.0352	0.42 ± 0.068	0.43 ± 0.107
2018	0.151 ± 0.0309	0.150 ± 0.0492	0.40 ± 0.072	0.38 ± 0.105
2019	0.140 ± 0.0339	0.147 ± 0.0645	0.40 ± 0.073	0.45 ± 0.119
2020	0.140 ± 0.0263	0.132 ± 0.0321	0.43 ± 0.076	0.39 ± 0.086
2021	0.142 ± 0.0243	0.148 ± 0.0383	0.44 ± 0.082	0.47 ± 0.123

Table 28: HCFC-142b emission (Mg yr^{-1}) estimates with 1-σ uncertainty.

	UK		NWEU	
Years	InTEM 2-yr	InTEM 1-yr	InTEM 2-yr	InTEM 1-yr
1994	487. ± 343.3		3760 ± 3702	
1995	587. ± 310.3		3730 ± 3755	
1996	592. ± 263.2		3610 ± 3792	
1997	544. ± 228.9		3820 ± 3126	
1998	636. ± 177.5		3980 ± 2053	
1999	589. ± 124.4		3870 ± 1605	
2000	491. ± 99.9		3500 ± 1457	
2001	384. ± 76.4		2770 ± 1178	
2002	239. ± 50.8		1930 ± 738	
2003	187. ± 50.5		1320 ± 497	
2004	145. ± 51.2		970 ± 754	
2005	89.5 ± 44.4		830 ± 717	
2006	75.4 ± 41.5		820 ± 487	
2007	86.2 ± 42.5		740 ± 878	
2008	80.2 ± 40.3		790 ± 266	
2009	70.7 ± 33.7		750 ± 725	
2010	81.7 ± 30.4		730 ± 157	
2011	95.6 ± 27.1		750 ± 140	
2012	103. ± 21.6		650 ± 105	
2013	95.4 ± 20.1	94.2 ± 32.4	570 ± 73	580 ± 89
2014	80.3 ± 19.2	82.4 ± 25.5	580 ± 80	560 ± 100
2015	73.5 ± 15.3	71.9 ± 12.4	600 ± 79	610 ± 90
2016	71.0 ± 13.2	64.6 ± 19.9	560 ± 67	570 ± 92
2017	65.9 ± 13.5	70.1 ± 16.2	510 ± 66	500 ± 97
2018	59.9 ± 13.7	69.9 ± 30.5	460 ± 68	490 ± 102
2019	55.1 ± 12.6	52.8 ± 16.4	450 ± 69	430 ± 90
2020	56.6 ± 11.4	55.9 ± 14.7	470 ± 74	520 ± 95
2021	59.7 ± 11.6	60.1 ± 17.7	470 ± 81	460 ± 122

Table 29: CCl_4 emission (Gg yr^{-1}) estimates with 1-σ uncertainty.

	UK		NWEU	
Years	InTEM 2-yr	InTEM 1-yr	InTEM 2-yr	InTEM 1-yr
1990	1.39 ± 0.382		3.80 ± 3.303	
1991	1.23 ± 0.366		2.90 ± 2.427	
1992	0.75 ± 0.229		2.13 ± 2.249	
1993	0.39 ± 0.147		1.39 ± 2.043	
1994	0.23 ± 0.090		1.07 ± 1.308	
1995	0.26 ± 0.072		1.06 ± 1.019	
1996	0.26 ± 0.063		1.02 ± 0.960	
1997	0.21 ± 0.060		0.79 ± 0.923	
1998	0.185 ± 0.0592		0.95 ± 0.917	
1999	0.167 ± 0.0577		0.80 ± 0.808	
2000	0.130 ± 0.0558		0.53 ± 0.725	
2001	0.116 ± 0.0576		0.69 ± 0.838	
2002	0.115 ± 0.0568		0.68 ± 0.753	
2003	0.109 ± 0.0567		0.60 ± 0.564	
2004	0.100 ± 0.0560		0.59 ± 0.692	
2005	0.086 ± 0.0510		0.66 ± 0.588	
2006	0.083 ± 0.0499		0.68 ± 0.266	
2007	0.099 ± 0.0536		0.73 ± 0.208	
2008	0.100 ± 0.0549		0.71 ± 0.198	
2009	0.065 ± 0.0475		0.61 ± 0.201	
2010	0.040 ± 0.0427		0.54 ± 0.223	
2011	0.057 ± 0.0453		0.53 ± 0.269	
2012	0.073 ± 0.0456		0.46 ± 0.233	
2013	0.061 ± 0.0489	0.052 ± 0.0764	0.34 ± 0.170	0.32 ± 0.207
2014	0.062 ± 0.0527	0.074 ± 0.0706	0.40 ± 0.183	0.45 ± 0.253
2015	0.084 ± 0.0543	0.108 ± 0.0798	0.54 ± 0.203	0.65 ± 0.343
2016	0.095 ± 0.0616	0.116 ± 0.0905	0.61 ± 0.198	0.64 ± 0.273
2017	0.079 ± 0.0685	0.089 ± 0.1098	0.61 ± 0.197	0.64 ± 0.308
2018	0.042 ± 0.0611	0.070 ± 0.1147	0.51 ± 0.200	0.59 ± 0.280
2019	0.020 ± 0.0477	0.001 ± 0.0676	0.37 ± 0.191	0.26 ± 0.272
2020	0.021 ± 0.0435	0.034 ± 0.0578	0.34 ± 0.184	0.43 ± 0.262

Table 30: CH_3CCl_3 emission (Gg yr^{-1}) estimates with 1-σ uncertainty.

	UK		NWEU	
Years	InTEM 2-yr	InTEM 1-yr	InTEM 2-yr	InTEM 1-yr
1990	18.9 ± 1.69		44.3 ± 21.09	
1991	15.1 ± 1.68		48.8 ± 16.82	
1992	11.0 ± 1.29		39.1 ± 16.41	
1993	7.40 ± 1.000		26.1 ± 13.46	
1994	4.69 ± 0.798		18.2 ± 8.51	
1995	3.83 ± 0.576		12.6 ± 6.42	
1996	2.59 ± 0.351		7.16 ± 5.155	
1997	1.21 ± 0.177		3.19 ± 2.861	
1998	0.50 ± 0.094		1.71 ± 1.216	
1999	0.187 ± 0.0895		1.08 ± 0.971	
2000	0.079 ± 0.0783		0.65 ± 0.828	
2001	0.082 ± 0.0706		0.53 ± 0.908	
2002	0.099 ± 0.0629		0.42 ± 0.527	
2003	0.107 ± 0.0615		0.38 ± 0.162	
2004	0.086 ± 0.0606		0.41 ± 0.181	
2005	0.078 ± 0.0503		0.30 ± 0.132	
2006	0.065 ± 0.0432		0.24 ± 0.093	
2007	0.040 ± 0.0424		0.24 ± 0.087	
2008	0.040 ± 0.0431		0.21 ± 0.089	
2009	0.040 ± 0.0387		0.21 ± 0.088	
2010	0.033 ± 0.0305		0.25 ± 0.082	
2011	0.037 ± 0.0202		0.23 ± 0.061	
2012	0.038 ± 0.0119		0.181 ± 0.0345	
2013	0.039 ± 0.0096	0.035 ± 0.0149	0.180 ± 0.0266	0.189 ± 0.0413
2014	0.037 ± 0.0082	0.039 ± 0.0153	0.178 ± 0.0265	0.21 ± 0.052
2015	0.030 ± 0.0075	0.029 ± 0.0128	0.151 ± 0.0245	0.148 ± 0.0566
2016	0.026 ± 0.0079	0.028 ± 0.0129	0.144 ± 0.0222	0.170 ± 0.0337
2017	0.026 ± 0.0076	0.027 ± 0.0122	0.144 ± 0.0218	0.146 ± 0.0468
2018	0.022 ± 0.0061	0.030 ± 0.0128	0.129 ± 0.0187	0.133 ± 0.0377
2019	0.017 ± 0.0044	0.015 ± 0.0093	0.129 ± 0.0154	0.138 ± 0.0338
2020	0.016 ± 0.0038	0.021 ± 0.0058	0.131 ± 0.0143	0.162 ± 0.0356
2021		0.018 ± 0.0065		0.163 ± 0.0414

Table 31: Halon-1211 emission (Mg yr^{-1}) estimates with 1-σ uncertainty.

	UK		NWEU	
Years	InTEM 2-yr	InTEM 1-yr	InTEM 2-yr	InTEM 1-yr
1998	129. ± 32.1		427. ± 224.6	
1999	119. ± 29.0		430. ± 218.7	
2000	128. ± 26.4		454. ± 206.6	
2001	133. ± 24.9		395. ± 192.4	
2002	116. ± 21.9		296. ± 127.4	
2003	123. ± 20.3		271. ± 64.8	
2004	113. ± 18.3		230. ± 53.6	
2005	83.1 ± 15.9		172. ± 44.7	
2006	75.4 ± 15.9		159. ± 44.5	
2007	80.2 ± 15.8		165. ± 43.5	
2008	72.6 ± 12.7		154. ± 35.1	
2009	60.3 ± 10.4		140. ± 29.0	
2010	58.9 ± 10.1		134. ± 29.6	
2011	59.6 ± 9.3		131. ± 31.4	
2012	56.9 ± 8.5		129. ± 28.8	
2013	54.6 ± 8.5	54.8 ± 15.6	128. ± 27.4	136. ± 33.9
2014	51.6 ± 7.7	48.9 ± 9.4	123. ± 29.8	110. ± 42.5
2015	47.0 ± 6.9	44.0 ± 8.9	113. ± 28.5	124. ± 44.8
2016	48.1 ± 7.7	50.1 ± 12.4	104. ± 25.6	93.8 ± 30.7
2017	48.7 ± 8.8	49.9 ± 13.2	106. ± 27.1	132. ± 45.4
2018	40.9 ± 8.1	44.8 ± 14.2	100. ± 26.4	101. ± 37.1
2019	32.3 ± 6.2	33.7 ± 8.6	89.6 ± 23.4	90.1 ± 29.9
2020	30.2 ± 5.3	31.1 ± 6.8	87.1 ± 22.8	95.2 ± 30.3
2021	30.6 ± 5.2	30.7 ± 7.8	87.4 ± 23.2	79.9 ± 27.0

Table 32: Halon-1301 emission (Mg yr^{-1}) estimates with 1-σ uncertainty.

	UK		NWEU	
Years	InTEM 2-yr	InTEM 1-yr	InTEM 2-yr	InTEM 1-yr
1998	57.4 ± 43.3		237. ± 237.1	
1999	52.6 ± 36.4		230. ± 220.7	
2000	51.2 ± 28.3		200. ± 219.7	
2001	37.9 ± 26.9		173. ± 210.8	
2002	31.9 ± 24.4		152. ± 130.9	
2003	55.2 ± 21.6		144. ± 72.5	
2004	55.5 ± 18.6		148. ± 72.4	
2005	30.3 ± 13.7		122. ± 68.9	
2006	14.3 ± 10.7		91.3 ± 55.9	
2007	19.2 ± 10.8		81.4 ± 42.7	
2008	32.8 ± 11.6		78.4 ± 32.7	
2009	31.9 ± 11.9		63.9 ± 27.1	
2010	19.2 ± 10.5		51.7 ± 24.3	
2011	10.5 ± 8.2		52.4 ± 22.0	
2012	12.0 ± 7.2		61.7 ± 19.8	
2013	17.5 ± 7.2	21.1 ± 12.3	65.0 ± 19.2	76.7 ± 27.4
2014	16.6 ± 6.9	18.3 ± 8.9	56.2 ± 20.0	53.6 ± 25.0
2015	12.2 ± 7.0	12.0 ± 10.2	59.3 ± 21.9	64.5 ± 37.6
2016	10.0 ± 8.2	13.6 ± 11.8	64.6 ± 22.9	71.8 ± 29.3
2017	11.2 ± 9.2	10.1 ± 15.1	60.2 ± 22.9	52.9 ± 36.7
2018	10.9 ± 8.3	15.9 ± 13.9	51.0 ± 20.6	60.1 ± 29.0
2019	10.4 ± 6.0	7.2 ± 7.1	47.6 ± 16.2	42.3 ± 19.8
2020	15.9 ± 5.1	18.5 ± 7.1	58.1 ± 15.8	67.0 ± 22.8
2021	19.9 ± 5.1	21.5 ± 7.7	65.2 ± 17.2	74.6 ± 24.4